University
of Southampton

Reduced Order Modelling and Controller Design for Boundary Element Discretised Flow Around Cylinders

by

Bahri Uzunoğlu

A thesis submitted for the degree of

Doctor of Philosophy

in the

School of Engineering Sciences

Fluid Structure Interactions Research Group

(Department of Ship Science)

Computational Engineering and Design Centre

2001

UNIVERSITY OF SOUTHAMPTON

ABSTRACT

FACULTY OF ENGINEERING AND APPLIED SCIENCES

SCHOOL OF ENGINEERING SCIENCES

Doctor of Philosophy

REDUCED ORDER MODELLING AND CONTROLLER DESIGN FOR BOUNDARY ELEMENT DISCRETIZED FLOW AROUND CYLINDERS

by Bahri Uzunoğlu

The objective of this thesis are to (i) investigate and further validate the Viscous Cell Boundary Element Method for more complex fluid mechanics problems and moving bodies and (ii) to use fundamental ideas of image processing and spectral methods to investigate the ability to inverse model the physical phenomena of data generated by the fluid code or any experimental data and to reduce successfully the system to a much smaller subsitute that encapsulates the main physics of the original system. Lastly we aim to design a controller to use in open-loop flow control coupled with the fluid solver. The controller is designed by reduction of the equations describing the system.

I dedicate this thesis to my mother who has given me and my brother affection and support throughout our education.

I would like to thank my father for his continuos support and for his patience. I am greatly indebted to Kerem and Vicdan for being always there when I needed them. I would also like to thank members of my family in Istanbul and Bartin for their continous support. Lastly, I would like to thank Julia for her affection.

Contents

List of Tables

List of Figures

Acknowledgments

I am indebted to my advisors, Dr.M.Tan and Prof.W.G.Price for their constant support. I would like to thank Mingyi for his valuable discussions and advice. I would like to thank Prof.Price for his support, for his patience and for his trust to provide me with the best facilities available and for the freedom that he gave me to work on different topics. I would like to thank Prof.E.Rogers for his discussions and his enthusiasm about my research. A special thanks goes to Dr.P.Nair who greatly enriched my knowledge with his exceptional insight into many engineering problems. I would also like to thank Dr.K.Djidjeli for his invaluable advice on differential equations.

I would like to thank my good friends at our research group W.L.Yan, A.Nayak, Dr.N.Petruzolli, Tahir, Dr.M.Torbati. Those long nights in CEDC lab will not be forgotten. I would also like to thank S.Ozeren and Dr.A.Taner for their outstanding advice throughout the years. In addition, I must thank Dr.O.Belik, Prof.Y.Odabasi, Prof.Pentschew, Dr.G.Unal, Cetin Aroma, Prof.O.Goren, Dr.A.Kukner, Prof.P.Temarel and Dr.M.French for their valuable contributions throughout my education.

I would also like to acknowledge my comrades K.Yelen, S.Demirtas, H.Perera, Dr.R.Allen and W.Patten.

I am also indebted the fellow graduates before me, Dr.G.Padhi, Dr.D.Anthony, Dr.M.El-Beltagy, Dr.Y.Kahana and Dr.Sandy.

I would also like to thank dept. staff Dr.A.Bhaskar, Dr.N.Bresloff and Prof.A.Keane.

I gratefully acknowledge the experimental data supplied by Dr. Stefan Becker from the study undertaken by Dütsch, Durst, Becker and Lienhart.

Nomenclature

$(')$	Dimensional quantity
π'_{jk}	Shear stress
D	Diameter of oscillating cylinder
ω	Circular frequency
A	Amplitude of the oscillation
KC	Keulegan-Carpenter number
β	Stokes parameter
Re	Reynolds number
C_D	Drag coefficient
C_M	Added mass coefficient
C_I	Added inertia coefficient
F_1	Inline force
F_2	Lift force
$\bar{F}_1$	Time averaged inline force
$\bar{F}_1$	Time averaged lift force
$\boldsymbol{v}$	Velocity vector
$\boldsymbol{R}$	Traction vector
$\hat{v}_j(t)$	Velocity of the body
$\tilde{U}_k$	Relative velocity
p	Pressure
$\boldsymbol{\phi}$	Global basis vector
$\boldsymbol{\alpha}$	Time dependent amplititude vector
λ	Eigenvalue
δ_{sj}	Kronecker function
$\Delta()$	Dirac delta function
$\boldsymbol{\xi}$	Field point

$c_k(t)$	Control input
$f(c_k)$	Full cost function
$m(c_k)$	Reduced cost function

Chapter 1

INTRODUCTION

Fluid-body interaction is one of the fundamental research areas of marine vehicles and aerospace industry. Although the body and the fluid are usually defined independent of each other, there is continuous interaction between them involving many complicated phenomena such as turbulence, resonance etc. There is immense effort to predict fully their behaviour because of technological opportunities. The fluid in many cases, especially in the marine environment can be assumed to be isothermal, incompressible, homogenous and Newtonian.

Bodies in the marine environment are usually of low in aspect ratio as a result fluid flow phenomena of separation, vortex shedding and turbulence can be observed. This makes the engineer vulnerable to many complex design considerations which cannot be fully solved by using theoretical techniques such as potential flow, inviscid flow or boundary layer flow because of the underlying assumptions. In most cases, engineers benefit from their daily experience or by well established empirical methods to solve complex problems. However with the new challenges posed by advanced engineering projects and the need to build better and faster vehicles creates the need for research to develop computationally reliable and practable methods for the industry.

The fundamental equations of fluid mechanics have been well known for many years but they are solvable for only a limited number of flows. The known solutions are extremely useful in limited applications and for idealised geometries but they are not useful in general engineering applications. Most of the time equations are simplified and solved but are rarely used in a full engineering analysis and design. The engineer is traditionally forced to use other approaches.

For many flows, nondimensionalization of the Navier-Stokes equations leaves the

Reynolds number as the only independent parameter. If the body shape is known, equivalent results can be derived from an experiment using a scale of model with the same geometric shape. Such approaches are very valuable in developing every day, practical engineering designs.

However many flows require several dimensionless parameters for their specifications and it may be impossible to set up an experiment which correctly scales the actual flow. In this computer age, it does not take much imagination to see that computers might take the study of fluid flow much further.

1.1 COMPUTATIONAL FLUID DYNAMICS

Flows and related phenomena can be described by partial differential (or integro-differential) equations, which cannot be solved analytically except in special cases. In order to obtain an approximate solution numerically, we have to use a discretization method which approximates the differential equations by a system of algebraic equations, which can then be solved on a computer (see Peric *et al* (1996)). The approximations are applied to small domains in space and/or time so the numerical solution provides results at discrete locations in space and time. The accuracy of numerical solutions is dependent on the quality of the discretization used.

1.1.1 Discretization approaches

Instead of trying to give a complete review of numerical methods used for fluid problems, a brief review on well established and relevant methods to our work in this thesis is presented.

Finite difference (FD) method

This is the oldest method for numerical solution of PDE (see Hirsch (1988)). It is also the easiest method to use for simple geometries.

The starting point is the conservation equation in differential form. The solution domain is covered by a grid. At each grid point, the differential equation is approximated by replacing the partial derivatives by approximations in terms of nodal values of the functions. On structured grids, the FD method is very simple and effective. The disadvantage of FD methods is the restriction to simple geometries in complex flows.

Finite volume (FV) method

A development from the finite difference method is the finite volume method. The FV method uses the integral form of the conservation equations as its starting point. The solution domain is subdivided into a finite number of continuous control volumes. The FV can accommodate any type of grid so is suitable for complex geometries. The grid defines control volume boundaries and need not be related to a coordinate system.

In the finite volume method, integration of the governing equations is carried out over finite control volumes. The finite control volumes are constructed to occupy the global problem domain completely without overlap. This step helps to guarantee, from the outset, conservation of important quantities (such as mass). Two forms of the finite volume method have evolved (see Hirsch (1988)). The first form, based on a structured mesh has great similarity with the finite difference method. Unstructured forms of the finite volume method have been developed later (see Hirsch (1988)). Such formulations have the advantage that mesh generation is more flexible. Many of the discretisation procedures found in the finite element method, discussed below, are applicable to unstructured finite volume methods.

Finite element (FE) method

The FE method is similar to FV method. The domain is broken into a set of discrete volumes or finite elements generally unstructured. The distinguishing feature of FE methods is that the equations are multiplied by a weight function before they are integrated through the whole domain. The solution is approximated by a shape function within each element selected in a way that guarantees the continuity of the solution across element boundaries. Such a function can be constructed from its values at the corner of its elements. An approximation is then substituted into the weighted integral of the conservation law and the equations to be solved are derived by requiring the derivative of the integral with respective to each nodal value to be zero; this corresponds to selecting the best solution within the set of allowed functions. The result is a set of non-linear algebraic equations. The principle advantage of the finite element method arises due to the ability to construct meshes, to describe and solve the global problem, by 'plugging together' elements of arbitrary shape. The method is generally found to cope better with low mesh quality, for example distorted elements or rapid

changes in element sizes.

Boundary element (BEM) method

All of the methods discussed above can be classified as domain methods in that the whole of the fluid domain is discretised. All of them may be used for the solution of linear differential equations which might arise in problems such as incompressible potential flow or Stokes flow (see Brebbia (1978)). However, in these situations a solution achieved in this way can be much less efficient than one obtained through the boundary element method (BEM).

Boundary element is a relatively recent method in computational mathematics for the solution of boundary value problems. There are two types of boundary integral equation methods. One of them, i.e the 'indirect' method, relies on the physical characteristics of the problem. The other type is known as the direct method which is based on Fundamental and Green function solutions of partial differential equations (see Brebbia (1978)). The governing differential equations are reduced to integral equations.

The boundary element method starts from the formation of a weighted residual integral equation which incorporates the linear differential equation to be solved (see Brebbia (1978)). The integral equation is then integrated by parts as many times as is necessary to eliminate the derivatives of the unknown quantity in the original equation. This, of course, results in the weighting function being subject to differentiation of the same order as was present in the original equation. By selecting the weighting function to be the impulse response of the system, known as the fundamental solution, the integral equation can be simplified to an expression involving boundary integrals only. This is possible because the domain integral can be evaluated analytically. The remaining equations can then be discretised to form a set of simultaneous algebraic equations where the coefficients are determined through boundary integration. Solution by this method results in the following benefits:

The dimensionality of the problem is reduced by one which results in a considerable reduction in the problem computation. Mesh generation is simplified as there is no requirement for a mesh throughout the domain. The values of unknown quantities can be calculated at any point in the domain. Problems involving an infinite domain can be dealt with easily.

Although the boundary element method is an elegant and efficient technique for solving linear differential equations, its extension to non-linear problems might not be straight forward because the method is reliant upon the availability of the fundamental solution. In nonlinear problems, the fundamental solution is not generally available and it is necessary to introduce some form of linearisation Tosaka and K. Kakuda (1988). Weakly nonlinear problems can be solved by treating the nonlinear terms in the governing equation as a pseudo body force and then moving them to the right hand side of the equation. An iterative or time stepping procedure can then be applied. When this approach is taken it becomes necessary to evaluate a domain integral in addition to those on the boundaries. Furthermore, as the degree of nonlinearity increases the method may suffer from numerical instability. In incompressible flow, the Reynolds number can be viewed as influencing the level of nonlinearity present in the system. However, the nonlinearity is included as a modification to the standard linear form of the BEM. Because of this, its effect on the solution can be clearly identified, as illustrated by the computations of Price and Tan (1992) and Tan (1994). For strongly nonlinear problems a modified version of the boundary element method has been proposed by Tosaka and K. Kakuda (1988). In this case, the boundary element method is applied to a small subdomain, in which, the nonlinear governing differential equation has been linearised. To do this, the subdomain is described using a single element or cell. To describe the global domain, these subdomains, or cells, are assembled using continuity conditions at their interfaces. The linearisation is based on a local approximation.

1.2 REDUCTION METHODS AND FLOW CONTROL

Optimal control of complex time-dependent physical processes governed by partial differential equations is a computationally expensive problem, particularly when the governing equations are modelled with high-fidelity. As a result, the construction of reduced-order models to design controllers for distributed parameter systems which, in this context, are fluid flows, is of considerable interest.

A flow problem is usually hard to solve because of the high order system that describes the state. The proper orthogonal decomposition (POD) is a reduced order

modelling approach that has been succesfully applied for the simulation of complex systems (see Sirovich (1987)). POD based reduced order models are used to avoid difficulty of dealing with large systems by using global basis functions instead of the local basis functions for the Galerkin projection of the considered PDE. A limited number of these global basis functions might be good enough to obtain a satisfactory level of accuracy. This method has become popular as a means of extracting dominant energy-containing structures from flow field data. Further, using these structures as basis functions, a reduced-order model of the governing equations can be constructed.

The POD method has been applied to fluid problems by Sirovich (1987) and many other researchers Berkooz *et al* (1993) and Dean *et al* (1991) to understand the important dynamical features or coherent structures seen in fluid flows. A reduced basis solution of the flow can be obtained as a linear combination of an optimal set of empirical basis functions using an integral equation method such as the Galerkin projection scheme. The limited number of degrees of freedom in the reduced POD model is its main weakness. The POD model is based on the solution of the partial differential equation for a particular control but it might be a poor model when the controller takes it from its original state towards the optimal state. The reduced order process will not necessarily converge to the optimal control of the original system.

In the structural optimization literature (see Alexandrov *et al*(1997)), this difficulty is tackled by combining approximate analysis models and the high-fidelity solver in the optimization procedure. An important issue in developing such a scheme is to ensure that asymptotic convergence to the high-fidelity optima can be achieved. Alexandrov *et al* (1997) proposed a trust-region framework for interleaving the exact and approximate objective function models in numerical optimization. The trust-region framework can be interpreted as an adaptive method to monitor the amount of optimization done with the approximation model, before the high-fidelity model is run to check the validity of the current iterate. By comparing the approximation model prediction to the exact prediction periodically, useful information about the accuracy of the reduced-order model can be obtained. This information can then be employed to decide the move limits to be enforced in the next optimization iteration, as well to update the approximation model as discussed by Arian *et al* (2000).

1.3 OUTLINE OF THE THESIS

Computational fluid dynamics is becoming a well established discipline in many different research areas. There is a demand for accurate and reliable solvers which can be used in industrial problems such as vortex induced vibration, aeroelasticity etc. Flow control is also another discipline which has emerged during the last years as a result of the new progress in the technology. In this thesis we investigate boundary element discretization for fluid mechanics problems at low-Reynolds number. In the later part of the thesis we propose a methodology for control of fluid flows.

This thesis has the following objectives which follow one another in logical progression. The first objective is to investigate and further validate the Viscous Cell Boundary Element Method which has been developed by the School of Engineering Sciences of Southampton University for more complex fluid mechanics problems and moving bodies. The second aim is to use fundamental ideas of image processing and spectral methods to investigate the ability to inverse model the physical phenomena of the data generated by the fluid code or experimental data and to reduce successfully the system to a much smaller subsitute that will encapsulate the main physics of the original system. Lastly we aim to design an optimal flow controller. The controller might be designed by reduction of equations of the system or directly from the data.

In the second chapter a short review of the equations of fluid flow is presented. The flow solver that has been investigated in the third chapter of this thesis is a hybrid method of boundary element and finite element. This hybrid approach incorporates both boundary element and finite element methods since, in the proposed scheme of study, cell equations based on Navier–Stokes equations are generated using the principles of the boundary element method with global equations applicable over the whole fluid domain derived following the procedures of the finite element method. A primitive-variable formulation with an unstructured fluid domain mesh requirement forms the basis of the hybrid approach. This can be applied to both two-and three-dimensional problems associated with a single cylinder or arbitrary arrangements of circular cylinders or other shaped bodies as discussed by Farrant, Tan & Price (2000) . Flow fields from transversely oscillating circular cylinders in water at rest are studied by numerical solutions of the two-dimensional unsteady incompressible Navier–Stokes equations adopting a primitive-variable formulation. These findings are successfully

compared with experimental observations. In this chapter we concentrate on the oscillations of the cylinder in fluid at rest.

In the fourth chapter reduced modelling techniques, based on a Proper Orthogonal Decomposition (POD) method, are applied to an investigation of the incompressible Navier-Stokes equations with inputs. The basic idea underlying the reduction methods is the compression of a large system (of algebraic and/or differential equations) to a similar (in some sense) much smaller subsitute. Many of the reduction methods can be thought of as two-step hybrid analysis techniques combining a discretization method with a direct variational technique. In the first step a number of global approximation vectors (modes or basis vectors), for approximating the response of the system, are generated using a discretization method in conjunction with another approach and in the second step the amplitudes of the global approximation vectors are determined via a variational technique. The mentioned hybrid analysis techniques combine the modelling variety of contemporary discretization methods (eg. finite elements, boundary elements, finite differences and their combinations) with the reduction in the total number of degrees-of-freedom provided by the variational technique. A circular cylinder in uniform flow with and without inputs is studied. Reduced dynamical models are created by POD and by extended POD (EPOD) approaches for the forced flow which is statistically non-stationary. A direct control action is applied to the flow at particular points and this investigation provides insights into the applications of this approach coupled with a full solver.

A full model of the dynamics of such a system is normally represented by a set of high dimensional nonlinear differential equations which can be solved by numerical methods. In this study a cell viscous boundary element method developed by Tan *et al* (1999) is used to generate the required data for the reduced model. The POD method describes the system behaviour as an attractor which is a point of evolution for the state space in a subspace of higher dimensions. A reduced solution can be obtained as a linear combination of an optimal set of empirical basis functions using an integral equation method such as the Galerkin projection method.

These bases are created by applying a POD method for statistically stationary data. When a fluid flow is subject to a time-dependent control, the statistical properties of the flow are usually non-stationary. In this case, an extended POD method (EPOD) developed by Glezer *et al* (1989) can be adopted. Herein applications of the POD

and EPOD methods are investigated in order to derive a reasonable approximation to time-dependent flows associated with vortex shedding.

In the fifth chapter, methods of control to achieve transition delay, separation postponement, lift enhancement, drag reduction, turbulence augmentation, or noise suppression are reviewed. This chapter mainly concentrates on external flows. Internal flows are also mentioned. The physical aspects of the flow control along with the basics of the flow regime and flow stability classification are reviewed rather than aspects related to mathematical modelling methods of controller design. A brief review of these methods is presented in the following chapter.

Chapter 2

EQUATIONS OF FLUID FLOW

All substances are ultimately made up of atoms and molecules. Fluids like air or water are made up of atoms and molecules. We can perceive the river water as a continous substance flowing smoothly as a result of the macroscopic forces acting on it. Engineers almost always deal with fluid flows which can be studied by modelling the fluid as a continuum governed by a set of macroscopic equations. Most of the elementary fluid mechanics textbooks deal with these equations without bothering with the molecular constitution of fluids (see Batchelor (1967)).

Fluids are a collection of particles. In order to develop theories for the time evolution of a system of N particles, that is their dynamics, different levels of dynamical theory can be investigated. Four different levels of theory are adopted. The following classification can be found in most of the graduate physics books.

At a very fundamental level, all particles obey quantum mechanics. The dynamics of the system at this level are described by N-particle wave functions which evolve in time according to Schrödinger's equation. This equation will not be discussed or included herein but mentioned for the completeness of the discussion. At the next level, the system can be modelled as a collection of N classical particles obeying Newtonian dynamics. If the number of particles are large however then it is not realistic to solve the equations of motion for all the position and velocity coordinates. In the next higher level one can introduce distribution functions describing the particle number density in the six-dimensional space time at a particular time. A dynamical theory at this level requires an equation which tells us how the distribution function changes in time. The time derivative of this distribution function for a fluid is given by the Boltzmann equation. At a higher level we model the system as a continuum. This study described

is on this level.

It might appear that in a dynamical theory, knowing the present state of the system, one can always predict the future. Fluids however can often display turbulence, a state of random and chaotic motions which appear unpredictable. Developing a proper theory of turbulence has remained one of the grand unsolved problems of physics. The question of how turbulence arises in systems governed by predictability of the equations remains unanswered. Even in deterministic systems, unpredictability can be observed.

2.1 MICROSCOPIC LEVEL

This area mainly covers different solution methods of the Boltzmann equation. If the equations for the molecular dynamics of dilute gas is simplified for a continuum, the macroscopic equations of hydrodynamics can be derived. The derivation of these equations is beyond the scope of this research.

2.2 MACROSCOPIC LEVEL

2.2.1 Derivatives of time

Two different kind of time derivatives i.e Eulerian and Lagrangian have evolved to describe fluid variables as discussed by Batchelor (1967) . The Eulerian derivative denoted by $\frac{\partial}{\partial t'}$ implies differentation with respect to time at a fixed point. On the other hand, the time derivative of a moving fluid element is denoted by $\frac{d}{dt'}$ which is called the Lagrangian derivative. A prime ($'$) denotes the variable is a dimensional quantity. If $\boldsymbol{x'}$ and $\boldsymbol{v'}\delta t'$ are the positions of fluid element at times t' and $t' + \delta t'$, then the Lagrangian time derivative of some quantity $Q(\boldsymbol{x'}, t')$ is defined as

$$\frac{dQ}{dt'} = \lim_{\delta t' \to 0} \frac{Q(\boldsymbol{x'} + \boldsymbol{v'}\delta t', t' + \delta t') - Q(\boldsymbol{x'}, t')}{\delta t'} \tag{2.1}$$

Keeping the first-order terms in the Taylor expansion, we have

$$Q(\boldsymbol{x'} + \boldsymbol{v'}\delta t', t' + \delta t') = Q(\boldsymbol{x'}, t') + \delta t' \frac{\partial Q}{\delta t'} + \delta t' \boldsymbol{v'}.\nabla Q \tag{2.2}$$

Putting this in (2.2), the relation between the Lagrangian and Eulerian derivatives is derived:

$$\frac{dQ}{dt'} = \frac{\partial Q}{\delta t'} + \boldsymbol{v}'.\nabla Q \tag{2.3}$$

If we want to formulate an interaction of a structure which is vibrating (flow induced vibration) with a fluid or a moving body in a fluid, we have to reformulate the above derivative and boundary conditions for a mixed coordinate system which is known in the literature as Arbitrary Lagrangian Eulerian (ALE) formulation and a less general formulation for moving solid bodies can be traced back to Batchelor (1967).

2.2.2 Equations of continuity

As a next step, we derive another general result -the continuity equation- which applies to any system that conserves mass. If ρ' is the density of the system in some space, then the mass $\int \rho' d\Omega'$ within a volume can change only due to the mass flux across the surface bounding that volume, i.e.

$$\frac{\partial}{\partial t'} \int \rho' d\Omega' = -\int \rho' \boldsymbol{v}'.d\boldsymbol{\Sigma}' \tag{2.4}$$

Here $\rho' \boldsymbol{v}'.d\boldsymbol{\Sigma}'$ is the outward mass flux through the bounding surface, the negative sign implying that an outward mass flux reduces the mass within the bounded volume. Transforming the surface integral to volume integral by Gauss's theorem, we obtain

$$\int \left[\frac{\partial \rho'}{\partial t'} + \nabla.(\rho' \boldsymbol{v}')\right] d\Omega' = 0 \tag{2.5}$$

Since this must be true for any arbitrary volume, we must have

$$\frac{\partial \rho'}{\partial t'} + \nabla.(\rho' \boldsymbol{v}') = 0 \tag{2.6}$$

which is the continuity equation. If we want to derive the same relationship in terms of the Eulerian derivative of ρ', then using the following relation:

$$\nabla.(\rho' \boldsymbol{v}') = \boldsymbol{v}'.\nabla \rho' + \rho' \nabla.\boldsymbol{v}' \tag{2.7}$$

we can write down the equation of continuity using the Lagrangian derivative for compressible fluid

$$\frac{d\rho'}{dt'} + \rho' \nabla . \boldsymbol{v}' = 0. \tag{2.8}$$

2.2.3 Equations of motion

To find the equation for the velocity, we consider a fluid element of volume $\delta\Omega'$. The mass of this fluid element is $\rho'\delta\Omega'$ and its acceleration is given by the Lagrangian derivative $\frac{d\boldsymbol{v}'}{dt'}$. It follows from Newton's second law of motion that

$$\rho'\delta\Omega'\frac{d\boldsymbol{v}'}{dt'} = \delta\boldsymbol{F}'_{body} + \delta\boldsymbol{R}'_{surface} \tag{2.9}$$

where the force acting on the fluid element is divided into two parts: the body force $\delta\boldsymbol{F}'_{body}$ and the surface force $\delta\boldsymbol{R}'_{surface}$. A body force is something that acts at all points within the body of a fluid. Gravity and electromagnetic forces are examples. The body force is usually denoted as body force per unit mass as $\boldsymbol{F}'$ so that

$$\delta\boldsymbol{F}'_{body} = \rho'\delta\Omega'\boldsymbol{F}' \tag{2.10}$$

The surface force on a fluid element is the force acting on it across the surface bounding the fluid element. Let $d\boldsymbol{\Sigma}'$ be an element of area on the bounding surface. The surface force $d\boldsymbol{R}'_{surface}$ acting across this area is assumed proportional to this area. $d\boldsymbol{\Sigma}'$ and $d\boldsymbol{R}'_{surface}$ are both vectors. They are related to each other by the following relation.

$$(d\boldsymbol{R}'_{surface})_j = -P'_{jk}d\Sigma'_k. \tag{2.11}$$

The total surface force acting on a volume of a fluid is then given by the surface integral

$$(\boldsymbol{R}'_{surface})_j = -\oint P'_{jk}d\Sigma'_k. \tag{2.12}$$

This surface integral can be transformed into a volume integral by the following relationship

$$(\boldsymbol{R}'_{surface})_j = -\int \frac{\partial P'_{jk}}{\partial x'_k} d\Omega'. \tag{2.13}$$

Hence the surface force acting on a small fluid element of volume $\delta\Omega'$ is

$$(\delta\boldsymbol{R}'_{surface})_j = -\frac{\partial P'_{jk}}{\partial x'_k}\delta\Omega'. \tag{2.14}$$

Substituting (2.10) and (2.14) into (2.9), we obtain the following relationship.

$$\rho'\frac{dv'_j}{dt'} = \rho' F'_j - \frac{\partial P'_{jk}}{\partial x'_k}. \tag{2.15}$$

2.2.4 Ideal fluids

For a fluid in static equilibrium, it is an experimentally proved fact that the force acting across an element of area inside the fluid or on its boundary is always perpendicular to that element of area. In fact, this is often taken as the definition of a fluid. A fluid is defined as a substance in which motions are induced whenever there is a part of the surface not perpendicular to the surface (i.e. a shear force). This is in contrast to elastic solids within which shear forces can be in static equilibrium. Mathematically, for a static fluid, we write

$$P'_{jk} = p'\delta_{jk} \tag{2.16}$$

which subsituted in (2.11) gives

$$d\boldsymbol{R}'_{surface} = -p' d\boldsymbol{\Sigma}'. \tag{2.17}$$

Pressure is introduced here as p which is defined as the force acting per unit area. The negative sign (2.17) implies that the pressure force acting across the bounding surface of a fluid volume is always inward directed, whereas the vector area $d\boldsymbol{\Sigma}'$ is taken by convention as outward directed.

Although (2.16) holds for a fluid at rest, it is generally no longer valid when there are no motions inside the fluid. If the surface force of two layers of a fluid having

different velocities on the two sides of a surface was given by (2.17), then the force across the surface of separation can only be in the vertical direction. In reality, it is expected that a horizontal tangential shear force will act across the surface of separation and will transport momentum from faster-moving layer to the slower layer such that the faster layer slows down and the slower layer speeds up. These tangential stresses are handled by introducing the coefficient of viscosity which will be discussed in the next subsection. Fluids for which the condition (2.16) holds are known as ideal fluids. Subsituting (2.16) into (2.15) and using (2.3) we have the following equation for an incompressible fluid which is named after Euler.

$$\frac{\partial v'_j}{\partial t'} + (v'_j v'_k)_{,k'} = -\frac{1}{\rho'} p'_{,j'} + F'_{j'}, \tag{2.18}$$

$$v'_{j,j'} = 0. \tag{2.19}$$

Ideal fluids are defined by Euler equation which is the simplified version of Navier-Stokes equation where the coefficient of viscosity is set to zero. An ideal incompressible irrotational fluid is often called potential flow which is a simplified version of ideal fluid.

2.2.5 Viscous flows

From everyday experience it is known that the internal friction (which we call viscosity) in a fluid opposes relative motions amongst different layers of a fluid. Fluids obeying the proportonality relation between shear stress and velocity gradient are known as Newtonian fluids. It is found experimentally by many researchers (see Batchelor (1967)) that a great many fluids display Newtonian characteristics. The formulation of this kind of flow is given by the Navier-Stokes equation which is the equation investigated in this thesis.

The surface forces inside a fluid was handled by the term P'_{jk} appearing in (2.11). Herein we introduce π_{jk} which is assumed to be zero in ideal fluids so that the surface forces on an element of a fluid is always normal. It is pointed out that the ideal fluid equations do not reproduce some of the properties of real fluids. That is, the shear force is expected to be larger for a larger velocity gradient and an improved description of surface forces is given by

$$P'_{jk} = p'\delta_{jk} + \pi'_{jk} \tag{2.20}$$

For a Newtonian fluid, the shear stress depends linearly on the velocity gradient. For an incompressible isothermal viscous flow π'_{jk} is defined as

$$\pi'_{jk} = \mu'(\frac{\partial v'_j}{\partial x'_k} + \frac{\partial v'_k}{\partial x'_j}) \tag{2.21}$$

which together with (2.10), (2.14) and (2.20) provides the basis of the Navier-Stokes equation written in the following form for incompressible flow

$$\frac{\partial v'_j}{\partial t'} + (v'_j v'_k)_{,k'} + \frac{1}{\rho'} p'_{,j'} - \frac{1}{\rho'}[\mu'(v'_{j,k'} + v'_{k,j'})]_{,k'} + F'_{j'} = 0 \tag{2.22}$$

$$v'_{j,j'} = 0. \tag{2.23}$$

Chapter 3

BOUNDARY ELEMENT DISCRETISATION OF EQUATIONS

In this chapter flow fields from transversely oscillating circular cylinders in water at rest are studied by numerical solutions of the two-dimensional unsteady incompressible Navier–Stokes equations adopting a primitive-variable formulation. These findings are successfully compared with experimental observations. A control action of oscillation of the cylinder is further investigated in the following chapters for a cylinder in uniform flow. Herein we only concentrate on the oscillations of the cylinder in fluid at rest.

The cell viscous boundary element scheme developed is first validated to examine convergence of solution and the influence of discretisation within the numerical scheme of study before comparisons are undertaken. A hybrid approach utilising boundary element and finite element methods is adopted in the cell viscous boundary element method. That is, cell equations are generated using the principles of a boundary element method with global equations derived following the procedures of finite element methods.

The influence of key parameters, i.e. Reynolds number Re, Keulegan–Carpenter number KC and Stokes number β, on overall flow characteristics and vortex shedding mechanisms are investigated through comparisons with experimental findings and theoretical predictions. The latter extends the study into assessment of the values of the drag coefficient, added mass or inertia coefficient with key parameters and the variation of lift and in-line force results with time derived from the Morison's equation.

The cell viscous boundary element method as described herein is shown to produce solutions which agree very favourably with experimental observations, measurements and other theoretical findings.

3.1 INTRODUCTION

Bodies oscillating in a stationary or unsteady fluid flow and stationary bodies in an oscillating unsteady flow are fluid–structure interaction problems of immense practical and theoretical interest in the fields of naval architecture, aerospace, civil and offshore engineering. For example a ship or aircraft manoeuvring, a submersible oscillating under prescribed experimental conditions to measure fluid actions, cylindrical tubular structures (i.e. offshore platforms, risers, etc.) subject to current and wave loads, bodies (i.e. bridges, chimneys, etc.) experiencing steady or wind gust loads, etc. are practical illustrations of fluid-structure interactions, facets of which are discussed by Duncan (1959) , Burcher (1972), Etkin (1972), Sarpkaya & Isaacson (1981) and Faltinsen (1990).

In offshore engineering, in particular, bluff bodies in the form of cylinders are extensively used in construction and, in many ways, they form the cornerstone of developments in oil extraction from beneath the sea. For such reasons, the interaction between viscous fluid flows and circular cylinders is of significant importance stimulating extensive experimental and theoretical investigations. These aim to understand the underlying complex physical interaction mechanisms, to simulate the behaviour and characteristics of the fluid flow within the interaction process and to model mathematically the fluid actions experienced by circular cylinders. Sarpkaya & Isaacson (1981), Faltinsen (1990) and Baltrop & Adams (1991) provide extensive overviews of such studies.

The flow past a circular cylinder fixed in a steady stream, the flow experienced by a circular cylinder in an oscillating flow or the flow generated by an oscillating cylinder in a stationary or unsteady flow are fluid-structure interaction problems investigated both experimentally and theoretically. They provide information through observation, measurement and predictions of the strengths, trajectories and frequencies of generated vortices, the magnitudes of the fluid actions through lift forces, drag forces, moments and their associated added mass, added inertia and drag coefficients, etc. Such related

information is presented experimentally by Hassan (1962), Bishop & Hassan (1964) , Maull & Milliner (1978) , Bearman (1985) , Williamson (1985,1991), Obasaju, Bearman & Graham (1988) and Tatsuno & Bearman (1990) . As an example, the latter investigators examined the viscous fluid flow characteristics around a circular cylinder of diameter D oscillating transversely with amplitude A, frequency ω and with a translational motion

$$\begin{aligned} x(t) &= -A\sin(2\pi ft) = -A\sin(\omega t), \\ \dot{x}(t) &= -A\omega\cos(\omega t) = -U_m\cos(\omega t). \end{aligned} \tag{3.1}$$

Their experimental findings clearly illustrate the complexity of the vortex patterns generated which were classified on the basis of the parameters:

$$\begin{aligned} \text{Keulegan–Carpenter number} \quad & KC = \tfrac{U_m T}{D} = \tfrac{(\omega A)(2\pi/\omega)}{D} = \tfrac{2\pi A}{D}\ , \\ \text{Stokes parameter} \quad & \beta = \tfrac{\rho D^2}{\mu T}\ , \\ \text{Reynolds number} \quad & Re = KC\beta = \tfrac{\rho\omega AD}{\mu} = \tfrac{\rho U_m D}{\mu}\ , \end{aligned} \tag{3.2}$$

where μ represents the coefficient of viscosity and ρ denotes the fluid density. Figure 3.1 illustrates the dependence of the various flow regimes on Keulegan–Carpenter number and Reynolds number or Stokes parameter as observed by Tatsuno & Bearman (1990)

.

To complement such experimental investigations, several numerical studies of the unsteady flow around a circular cylinder at low KC values have been presented by, for example, Borthwick (1986) , Smith & Stansby (1991) , Justesen (1991) , Wang & Dalton (1991) , Lin, Bearman & Graham (1996) , Zhang & Zhang (1997) and Dütsch *et al* (1998). To model mathematically the unsteady oscillatory force acting on a cylinder, Morison *et al* (1950) developed a semi-empirical formulation which has since been extensively used in offshore engineering. This approach is discussed by Sarpkaya & Isaacson who for an oscillating cylinder in a stationary fluid expressed the force per unit length in the form,

$$F_1(t) = -\frac{1}{2}\rho DC_D\dot{x}|\dot{x}| - \frac{1}{4}\rho\pi D^2C_I\ddot{x} \tag{3.3}$$

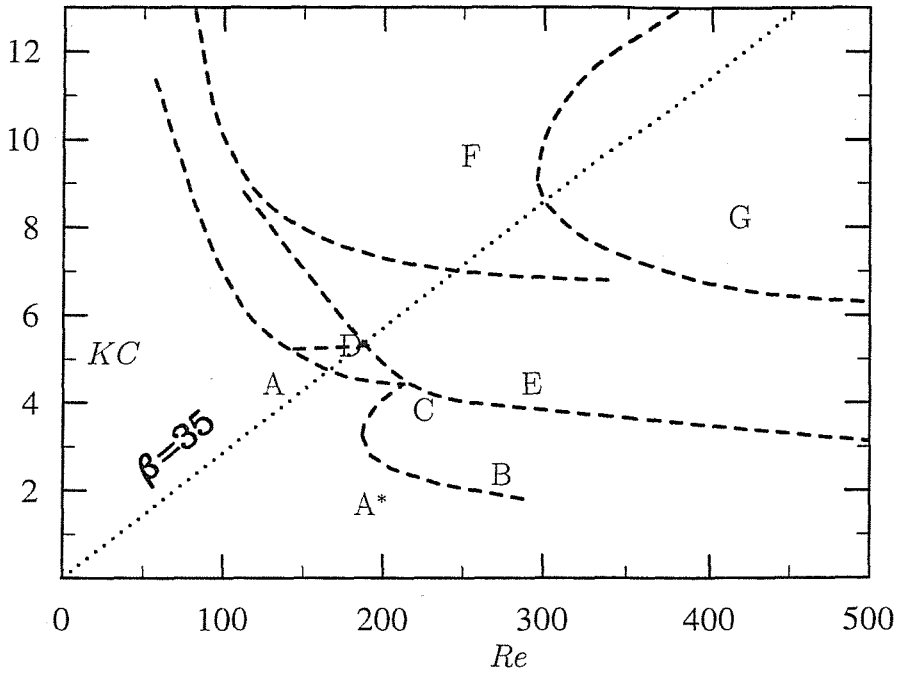

Figure 3.1: Flow regimes defined by Tatsuno & Bearman (1990) and also Dütsch *et al* (1998). The principal features of the regions are: A*-No flow separation, secondary streaming, two-dimensional; A-Two vortices shed symmetrically per half cycle, two-dimensional; B-Three-dimensional instability, longitudinal vortices; C-Rearrangement of large vortices, three dimensional; D-Flow convected obliquely to one side of the axis of oscillation, three-dimensional; E-Irregular switching of flow convection direction, three dimensional; F-Flow convected diagonally, three-dimensional; G-Transverse vortex street, three dimensional.

whereas, for a stationary cylinder in an oscillating fluid the equation is given by

$$F_1(t) = -\frac{1}{2}\rho D C_D \dot{x}|\dot{x}| - \frac{1}{4}\rho\pi D^2 C_M \ddot{x} \tag{3.4}$$

where $C_M = C_I + 1$. Here C_I, C_M and C_D denote the added mass, added inertia and drag coefficients respectively and the difference between C_M and C_I arises because of the change in the defining coordinate system used to describe the fluid–structure dynamics. These coefficients are determined from experiments or from numerical solutions of the Navier–Stokes equations. Estimates of their values can be determined using a variety of analysis techniques and methods (i.e. Fourier, least-squares, etc.) as discussed by Sarpkaya (1976) and Sarpkaya & Isaacson (1981) .

Stokes (1851) first determined analytical expressions for the C_D and C_M coefficients provided that the cylinder flow remains attached, laminar and two-dimensional. It was shown that the forces acting on a sinusoidally oscillating cylinder depend on both KC, Re or β and in an extension of Stokes' theoretical approach, Wang (1968) derived the following expressions:

$$C_D = \frac{3\pi^3}{2KC}[(\pi\beta)^{-1/2} + (\pi\beta)^{-1} - \frac{1}{4}(\pi\beta)^{-3/2}] \,, \tag{3.5}$$

$$C_M = 2 + 4(\pi\beta)^{-1/2} + (\pi\beta)^{-3/2} \,, \tag{3.6}$$

for $Re\,KC \ll 1$ and $\beta \gg 1$. The first two terms in these formulae replicate Stokes' findings.

The values of these theoretical coefficients agree favourably with experimental findings for two-dimensional flows as discussed by Lin *et al* (1996) . However, as illustrated in figure 3.1, such flow regimes are limited and as the KC value increases complex three-dimensional vortex patterns are generated. Honji (1981) observed experimentally, and confirmed theoretically by Hall (1984) , a three dimensional instability on the attached boundary of the cylinder generating counter rotating vortex structures along the cylinder's span. This effect causes an increase in the predicted coefficient values of Wang as confirmed by Sarpkaya (1986) in a comparative analysis of theoretical findings (based on the Stokes and Wang models) and experimental investigations into the influence of

KC value on the occurrence of the Honji instability. Hall (1984) deduced that this occurs at the critical Keulegan–Carpenter number defined by

$$K_{cr} = \frac{Re_{cr}}{\beta} = 5.778\beta^{-\frac{1}{4}}(1 + 0.205\beta^{-\frac{1}{4}} + \cdots). \tag{3.7}$$

In this present study, the flow characteristics and C_D and C_M coefficient values associated with a stationary circular cylinder in an oscillating viscous flow and an oscillating cylinder in a stationary fluid are investigated using the cell boundary element method developed by Tan, Farrant & Price (1999) . This hybrid approach incorporates both boundary element and finite element methods since, in the proposed scheme of study, cell equations based on Navier–Stokes equations are generated using the principles of the boundary element method with global equations applicable over the whole fluid domain derived following the procedures of the finite element method. A primitive-variable formulation with an unstructured fluid domain mesh requirement forms the basis of the hybrid approach. This can be applied to both two-and three-dimensional problems associated with a single cylinder or arbitrary arrangements of circular cylinders or other shaped bodies as discussed by Farrant, Tan & Price (2000), Uzunoglu (2000) . The application of the proposed method focuses on two-dimensional fluid-structure interactions incorporating a validation with experimental vortex shedding flows observed and measured by Tatsuno & Bearman (1990) , Kühtz (1996) and a comparison of predictions derived by Dütsch *et al* (1998) by a finite volume method.

3.2 MATHEMATICAL THEORY

3.2.1 Governing equations

Figure 3.2 illustrates a cell idealisation of the viscous fluid domain. In each typical cell or element Ω, bounded by surface Σ, the fluid is assumed incompressible and of constant viscosity. The Navier–Stokes equations describing the flow velocity $\boldsymbol{v}'(\boldsymbol{x}', t')$ and the mean pressure $p'(\boldsymbol{x}', t')$ of the viscous fluid are given by

$$\frac{\partial v'_j}{\partial t'} + (v'_j v'_k)_{,k'} + \tfrac{1}{\rho'} p'_{,j'} - \tfrac{1}{\rho'}[\mu'(v'_{j,k'} + v'_{k,j'})]_{,k'} = 0 \tag{3.8}$$

$$v'_{j,j'} = 0 \tag{3.9}$$

Here ρ' and μ' represent the fluid density and viscosity. A prime ($'$) indicates the variable is a dimensional quantity.

In order to simplify the mathematical expressions in these equations, a tensor index notation with summation convention is adopted. In the convective term, for example,

$$(v'_j v'_k)_{,k'} \;=\; \sum_{k=1} \frac{\partial (v'_j v'_k)}{\partial x'_k}$$

where the upper limit of the summation takes the value 2 or 3 for two-dimensional or three-dimensional problems respectively.

For viscous fluid-structure interaction problems categorised by a characteristic length L' (e.g. diameter of cylinder, say) and a characteristic velocity U' (e.g. mean fluid velocity), the non-dimensional variables of space $\boldsymbol{x}$, time t, velocity $\boldsymbol{v}$ and pressure p are defined by

$$\boldsymbol{x} \;=\; \frac{\boldsymbol{x}'}{L'} \;,\quad t \;=\; \frac{U'}{L'} t' \;,\quad \boldsymbol{v} \;=\; \frac{\boldsymbol{v}'}{U'} \;,\quad p \;=\; \frac{p'}{\rho' U'^2} \;,$$

such that (3.8) and (3.9) can be expressed in the dimensionless forms,

$$\dot{v}_j \;+\; (v_j v_k)_{,k} \;+\; p_{,j} \;-\; [\nu_e (v_{j,k} + v_{k,j})]_{,k} \;=\; 0 \;, \tag{3.10}$$

$$v_{j,j} \;=\; 0 \;. \tag{3.11}$$

Here ν_e=$1/Re$ where Re denotes the Reynolds number ($= \frac{\rho' U' L'}{\mu'}$).

These equations represent the flow velocity in an inertial or space fixed frame of reference and are appropriate to the analysis of the fluid-structure interaction between a fixed body and an oscillating flow. For a body manoeuvring in an incompressible fluid, Price & Tan (1992) showed that the Navier–Stokes equations formulated in a moving frame of reference attached to the body are given by,

$$\dot{v}_j \;+\; (v_j U_k)_{,k} \;+\; p_{,j} \;-\; [\nu_e (v_{j,k} + v_{k,j})]_{,k} \;=\; 0 \;, \tag{3.12}$$

$$v_{j,j} \;=\; 0 \;. \tag{3.13}$$

Here U_k denotes the relative velocity between the body and the fluid motion i.e. $U_k = v_k - \hat{v}_k$ where $\hat{v}_k$ represents the velocity of the body and/or the fluid mesh attached to the body. This set of equations is suitable to describe the fluid-structure interaction between a cylinder oscillating horizontally and a fluid at rest at infinity or

pulsating and translating in a stationary fluid. As can be seen, these two sets of equations are very similar with (3.10) derived by setting $\hat{v}_k = 0$ in (3.12). Therefore, for generality, (3.12) and (3.13) are used in the following development of the mathematical model and numerical scheme.

3.2.2 Integral equation

To improve the efficiency and effectiveness of the numerical scheme of study for time dependent unsteady flow problems, the nonlinear convective term in the momentum equation is first resolved by a time marching process before the Navier–Stokes equations are transformed into an integral equation (see Tan *et al* (1999)). The procedure is described as follows:

- *First-order scheme*

  In this scheme, the nonlinear convective term can be resolved by a time stepping process. To maintain an accuracy of the order of Δt in the solution, the equation at the $(n+1)th$ time step takes the form

  $$f_j \; + \; (v_j \tilde{U}_k)_{,k} \; + \; p_{,j} \; - \; [\nu_e (v_{j,k} + v_{k,j})]_{,k} \;\; = \;\; 0,$$

  where $f_j = \frac{1}{\Delta t}[v_j - v_j^{(n)}]$, $\tilde{U}_k = v_k^{(n)} - \hat{v}_k$ denotes the relative velocity at the nth time step and the $\hat{v}_k$ represents the corresponding body velocity. Little additional computational time is needed to transform the velocity vector field into a space fixed coordinate system by adding the system velocities.

- *Second-order scheme*

  To achieve a second-order level of numerical accuracy with respect to Δt, the equation for the $(n+1)th$ time step is similar to the first order scheme except in this case,

  $f_j = \frac{1}{2\Delta t}[3v_j - 4v_j^{(n)} + v_j^{(n-1)}]$ and $\tilde{U}_k = 2v_k^{(n)} - v_k^{(n-1)} - \hat{v}_k$.

The mathematical theory for the derivation of above formulations can be found in Stiefel (1963) . The accuracy of the second order scheme is expected to perform better though no systematic analysis was undertaken except for $Re = 100$ and $KC = 5$ regime which no significant deviation was observed. Stability was not investigated for

two different schemes. Stability might decrease with increasing time order.

Thus, with the appropriate definitions of f_j and $\tilde{U}_k$, these previous schemes can be represented by the modified Navier–Stokes equation,

$$f_j \; + \; (v_j\tilde{U}_k)_{,k} \; + \; p_{,j} \; - \; [\nu_e(v_{j,k}+v_{k,j})]_{,k} \;\; = \;\; 0 \; . \tag{3.14}$$

By means of Gauss's theorem, an integral equality involving functions $\boldsymbol{v}$, p and two additional functions $\boldsymbol{v}_s^*$ and p_s^* can be established on a typical cell Ω bounded by its surface Σ with outward normal $\boldsymbol{n}$ (see Tan (1994)). This is written as

$$\begin{aligned}
&\int_\Omega \{v_{sj}^*[f_j + (v_j\tilde{U}_k)_{,k} + p_{,j} - (\nu_e(v_{j,k}+v_{k,j}))_{,k}] + p_s^* v_{j,j}\}d\Omega \\
+ \;& \int_\Omega \{v_j[\tilde{U}_k v_{sj,k}^* + p_{s,j}^* + (\nu_e(v_{sj,k}^* + v_{sk,j}^*))_{,k}] + p v_{sj,j}^*\}d\Omega \\
= \;& \int_\Sigma [v_j(\tilde{U}_k n_k v_{sj}^* + R_{sj}^*) - R_j v_{sj}^*]d\Sigma + \int_\Omega f_j v_{sj}^* d\Omega,
\end{aligned} \tag{3.15}$$

where the term $R_j = -pn_j + \nu_e(v_{j,k}+v_{k,j})n_k$ represents the jth component of the dimensionless traction on the surface Σ and the variable R_{sj}^* is defined as

$$R_{sj}^* = p_s^* n_j + \nu_e(v_{sj,k}^* + v_{sk,j}^*)n_k \; .$$

This integral equality holds for any functions $\boldsymbol{v}$, p, $\boldsymbol{v}_s^*$ and p_s^* provided that all the terms involved are integrable. If functions $\boldsymbol{v}$ and p are reserved to represent the flow velocity and the mean pressure in the fluid on the cell respectively and they satisfy (3.11) and (3.14) then the forms of functions $\boldsymbol{v}_s^*$ and p_s^* can be selected by imposing appropriate conditions to simplify (3.15). In fact an examination of the integral equality shows that there would be significant mathematical simplification by letting $\boldsymbol{v}_s^*$ and p_s^* satisfy the following equations:

$$\tilde{U}_k v_{sj,k}^* + p_{s,j}^* + (\nu_e(v_{sj,k}^* + v_{sk,j}^*))_{,k} \;\; = \;\; -\delta_{sj}\Delta(\boldsymbol{x}-\boldsymbol{\xi}), \tag{3.16}$$

$$v_{sj,j}^* \;\; = \;\; 0, \tag{3.17}$$

where δ_{sj} and $\Delta()$ are Kronecker and Dirac delta functions respectively.

With the functions $\boldsymbol{v}_s^*$ and p_s^* defined by these equations, (3.15) reduces to,

$$C(\boldsymbol{\xi})v_s(\boldsymbol{\xi},t) + \int_\Sigma v_j(\tilde{\boldsymbol{U}}\cdot\boldsymbol{n}v_{sj}^* + R_{sj}^*)d\Sigma \;\; = \;\; \int_\Sigma R_j v_{sj}^* d\Sigma - \int_\Omega f_j v_{sj}^* d\Omega \tag{3.18}$$

where

$$C(\boldsymbol{\xi}) = \begin{cases} 1 & \text{if } \boldsymbol{\xi} \in \Omega, \\ \frac{1}{2} & \text{if } \boldsymbol{\xi} \in \Sigma, \\ 0 & \text{otherwise.} \end{cases}$$

In this equation the velocity of the flow in the cell is expressed as a surface integral of velocity and traction on the boundary, and an additional volume integral involving the contribution from f_j which can be calculated from the values of v_j and $\boldsymbol{v}^{(n)}$ on the cell boundary.

When the boundary values of the velocity are specified, (3.18) can be used to determine the traction $\boldsymbol{R}$ on the boundary and then the velocity field $\boldsymbol{v}$ everywhere in the cell. Thus (3.18) defines a relation between the velocity and force on the cell boundary. Since v^*_{sj} also depends on the value of $\tilde{\boldsymbol{U}}$ in the cell as seen from (3.16), modifications to the values of v^*_{sj} are needed during the time stepping procedures as $\boldsymbol{v}$ is continuously updated in the computation.

3.2.3 Fundamental solution

In the context of this study, the solution of (3.16) and (3.17) is referred to as the fundamental solution of the problem as it describes the response of the system to a point excitation. To simplify the process of solution of these two equations for v^*_{sj} and p^*_s, a further approximation is introduced to replace the convective velocity $\tilde{\boldsymbol{U}}$ (with component $\tilde{U}_k$) in (3.16) by its mean value $\boldsymbol{u}$ (with component u_k) on the cell. Findings from numerical experiments reveal that this approximation is superior to the first-order approximation, in which the value of $\tilde{U}_k$ at any arbitrary point in the cell is used for the convective velocity in (3.16).

With this assumption, the equations defining v^*_{sj} and p^*_s take the following form:

$$u_k v^*_{sj,k} + p^*_{s,j} + (\nu_e(v^*_{sj,k} + v^*_{sk,j}))_{,k} = -\delta_{sj}\Delta(\boldsymbol{x} - \boldsymbol{\xi}), \tag{3.19}$$

$$v^*_{sj,j} = 0. \tag{3.20}$$

The solutions of these equations for both two- and three-dimensional cases can be obtained by means of Fourier transformations as discussed by Price & Tan (1990,1992), or Tan (1994).

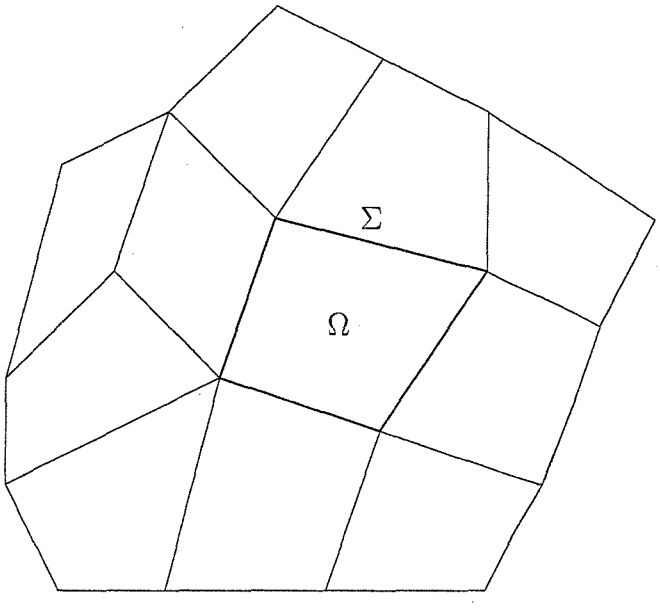

Figure 3.2: Discretisation of the fluid domain by an unstructured mesh.

3.3 NUMERICAL MODELLING

3.3.1 Idealisation

To provide solutions to unsteady fluid-structure interaction problems, the computational fluid domain is discretised into a large number of cells or elements (see figure 3.2) and the integral (3.18) adopted to represent the velocity field on the cell in terms of the values of velocity and traction on the cell boundary.

For simplicity the following discussion is restricted to the two-dimensional time dependent case involving only quadrilateral cells with the control points for the unknown functions taken at the centre of each cell edge. Similar conclusions, however, apply to more general cases, i.e. three-dimensional problems, control points taken at the corners of each quadrilateral, control points at centres and corner points, etc.

3.3.2 Cell equations

On the typical cell shown in figure 3.3, if the first-order time stepping scheme is assumed and the unknown functions $\boldsymbol{v}$ and $\boldsymbol{R}$ on each edge are treated as constants taking their

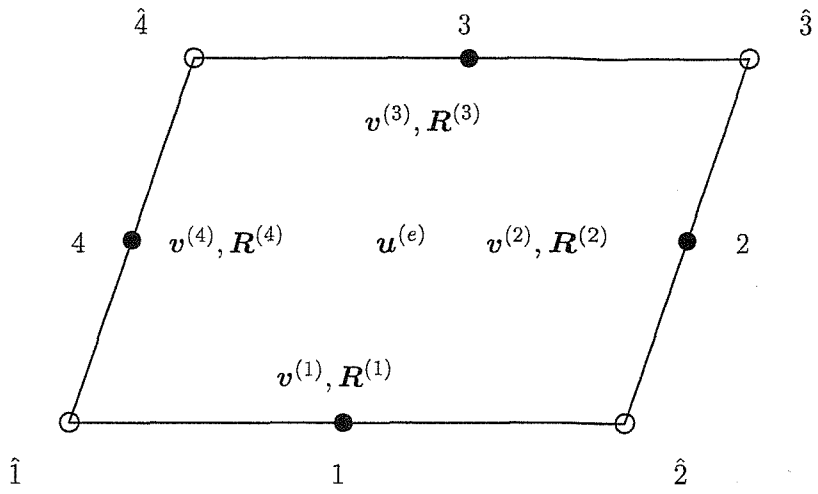

Figure 3.3: A typical cell with ordered notation.

values at the centre of each edge, the cell integral equation can be rewritten as

$$C(\boldsymbol{\xi})v_s(\boldsymbol{\xi},t) + \sum_{l=1}^{4} v_j^{(l)} \int_{(l)} (\boldsymbol{u}\boldsymbol{n}v_{sj}^* + R_{sj}^*)d\Sigma + \tfrac{1}{\Delta t}\int_{\Omega} v_j v_{sj}^* d\Omega$$
$$= \sum_{l=1}^{4} R_j^{(l)} \int_{(l)} v_{sj}^* d\Sigma + \tfrac{1}{\Delta t}\int_{\Omega} v_j^{(n)} v_{sj}^* d\Omega \ . \qquad (3.21)$$

When the coordinates of the control point on each edge are assigned successively to $\boldsymbol{\xi}$, the index s allowed to take values 1 and 2 for the two-dimensional case under examination and the integrations of v_{sj}^* and R_{sj}^* completed, the integral equation is replaced by a discretisation involving a set of 8 simultaneous equations for each cell. Thus if the superscript e denotes the *eth* cell then the relevant algebraic equations can be expressed in the form

$$A_{\mathrm{v}}^{(e)} V^{(e)} \ = \ A_{\mathrm{r}}^{(e)} R^{(e)} \ + \ b^{(e)} \ . \qquad (3.22)$$

Here $V^{(e)}$ and $R^{(e)}$ are single column arrays constructed from the velocity $\boldsymbol{v}^{(l)}$ and traction $\boldsymbol{R}^{(l)}$ values at the centre of each edge ($l = 1, 2, 3, 4$) on the cell boundary, i.e.

$$V^{(e)} = \begin{Bmatrix} \boldsymbol{v}^{(1)} \\ \boldsymbol{v}^{(2)} \\ \boldsymbol{v}^{(3)} \\ \boldsymbol{v}^{(4)} \end{Bmatrix} , \qquad R^{(e)} = \begin{Bmatrix} \boldsymbol{R}^{(1)} \\ \boldsymbol{R}^{(2)} \\ \boldsymbol{R}^{(3)} \\ \boldsymbol{R}^{(4)} \end{Bmatrix}$$

where $A_{\rm v}^{(e)}$ and $A_{\rm r}^{(e)}$ are 8×8 matrices and $b^{(e)}$ a vector with 8 elements. These terms are the results of the integration of v_{sj}^* and R_{sj}^* on the cell and can be expressed formally as

$$A_{\rm v}^{(e)} = [\tfrac{1}{2}\delta_{sj} + \int_{(l)} (\boldsymbol{u}\boldsymbol{n}v_{sj}^* + R_{sj}^*)d\Sigma + \tfrac{1}{4\Delta t}\int_{\Omega} v_{sj}^* d\Omega], \tag{3.23}$$

$$A_{\rm r}^{(e)} = [\int_{(l)} v_{sj}^* d\Sigma] \ , \qquad b^{(e)} = \{\tfrac{\bar{v}_j^{(n)}}{\Delta t}\int_{\Omega} v_{sj}^* d\Omega\}, \tag{3.24}$$

where $\bar{v}_j^{(n)}$ is the averaged velocity of the *nth* time step on the cell and only the contribution from the mean acceleration on the cell is included in the equations.

From (3.22), an expression for $R^{(e)}$ can be obtained in the form

$$R^{(e)} = C^{(e)}V^{(e)} - d^{(e)} \ , \tag{3.25}$$

where $C^{(e)}$ and $d^{(e)}$ are solutions of the equations

$$A_{\rm r}^{(e)}C^{(e)} = A_{\rm v}^{(e)} \quad , \qquad A_{\rm r}^{(e)}d^{(e)} = b^{(e)} \ .$$

In this formulation, the matrix $A_{\rm r}^{(e)}$ is nearly singular because the flow is incompressible. This term is the integration over the surface of the fundamental solution which is derived with this condition. When integration of fundamental solution over the surface is made, the integration which generates this matrix coefficients will be nearly singular. The details of this integration can be found in Tan *et al* (1999) where the accuracy of the integration is also addressed.

The singular value decomposition method (see §2.9, Press *et al* (1986)) can be adopted to solve these equations to find $C^{(e)}$ and $d^{(e)}$.

3.3.3 Global equations

The action-reaction relation of the traction $\boldsymbol{R}$ and the continuity of the velocity field $\boldsymbol{V}$ across the control point on the cell boundary require $\boldsymbol{R}$ and $\boldsymbol{V}$ to satisfy the expressions

$$\boldsymbol{R}^{(l)} + \boldsymbol{R}'^{(l')} = \boldsymbol{0} \ , \ \boldsymbol{V}^{(l)} = \boldsymbol{V}'^{(l')} \ . \tag{3.26}$$

Here $\boldsymbol{R}^{(l)}$, $\boldsymbol{R}'^{(l')}$, $\boldsymbol{V}^{(l)}$ and $\boldsymbol{V}'^{(l')}$ are the values of the traction and velocity on the same control point belonging to different cells.

To construct the global equations for the whole fluid domain from the cell equations, the assembly process used in a finite element method to obtain the stiffness matrix is adopted (§1.3–§1.7, Zienkiewicz (1977)). The control points are organised into a consecutive global order after each point is given an unique control point identifying number. When conditions (3.26) are applied to each control point and the contributions from all cell equations to each and every control point collected, a set of algebraic equations in terms of velocity can be obtained for the whole computational domain, i.e.

$$D\,V \;=\; F \tag{3.27}$$

where V is the array of velocity values on all the control points in the global order, F contains the contributions of $b^{(e)}$ from all cells and D is formed by assembling the cell matrix $C^{(e)}$ according to the global order of each control point.

Before this set of equations can be solved, global boundary conditions need to be implemented. The two most commonly encountered conditions are prescribed traction and prescribed velocity on the boundary.

3.4 NUMERICAL RESULTS

3.4.1 Discretisation parameters and convergence

In this study, a selection of viscous flow characteristics, predicted by the cell boundary mathematical model, is compared with observations, measurements and other relevant theoretical findings. Such an exercise provides a measure of verification and validation of the proposed approach and the developed numerical scheme of study as well as providing a degree of confidence to extend the theoretical model to tackle more complex unsteady fluid–structure interaction problems as considered by Farrant *et al* (2000) .

Figure 3.4 illustrates the flow domain surrounding a circular cylinder of non-dimensional unit diameter. The overall size of the discretised fluid domain adopted in the calculations is defined by the magnitude of the quantity denoted by h (i.e. h=3, 6, 9, etc.). Figure 3.5 shows a typical unstructured mesh of the fluid domain with each rectangular cell of grid size (Δx, Δy), where Δx, Δy denote horizontal and vertical dimensions respectively. In a study to assess the influence of the domain size, grid dimension and

idealisation two different sets of boundary conditions were assumed, each associated with a particular fluid problem. Namely, in figure 3.4, the boundary conditions (1,2) refer to a transversely oscillating cylinder with the far field fluid at rest. At the top and the bottom of the domain the same velocity boundary conditions are assumed. By slight modification of these conditions a numerical towing tank experiment can be devised in which the cylinder translates with a forward speed $v = V(t)$ and transversely oscillates with prescribed motion $u = U(t)$ as given in (3.1).

For the fluid flow at $Re = 100$, $KC = 5$, designated two-dimensional by Tatsuno & Bearman (1990) in figure 3.1, tables 3.3–3.5 show the variations of the values of the drag coefficient C_D and added mass coefficient C_I with time step Δt, domain size h, grid size (Δx, Δy) and boundary conditions. Overall the computed C_D, C_I results show small variations between themselves even for significant changes to the stated parameter values. To examine the sensitivity of inlet–outlet boundary condition at $x = \pm h$, table 3.4 includes predictions for velocity boundary conditions i.e. $u = 0 = v$ and a mixed boundary condition involving velocity and traction components i.e. $u = 0 = R_2$. From the evidence presented in table 3.4 it is observed that provided h is sufficiently large the boundary conditions imposed at $x = \pm h$ influence C_D and C_I values insignificantly. In all these findings a larger variation of value is exhibited in the drag coefficient rather than the added mass coefficient which remains relatively constant.

In a wide ranging computational investigation, additional results were further substantiated. Namely, boundary conditions (1,2) produce similar predictions for each set of chosen parameter values and, secondly, the observed flow characteristics associated with a cylinder oscillating in a stationary fluid and those for a stationary cylinder subject to an oscillating flow showed very close agreement confirming the study of Garrison (1990) . Such studies provide assurance that the numerical schemes of study produce convergent results and this is further confirmed by the finite volume investigation of Dütsch *et al* (1998) who determined drag and added mass coefficient values of $C_D = 2.09$ and $C_I = 1.45$, for $Re = 100$ and $KC = 5$, respectively. These latter values were obtained using the finest mesh in their analysis and they lie within the range of data shown in tables 3.3–3.5. It is interesting to note that although favourable comparisons of predicted results are demonstrated between the cell boundary element approach and the finite volume method, the computational domain used herein is smaller and

incorporates a coarser mesh than used by Dütsch *et al* (1998) .

Thus, from the presented evidence on accuracy of computation and convergence of solution, in subsequent calculations for transversely oscillating cylinders, it was decided to take grid dimensions $\Delta x = 0.15 = \Delta y$; to discretize the fluid domain h=9 for symmetric flow regimes (i.e. see figures 3.7, 3.8) and h=15 for asymmetrical flows (i.e. C, E, F in figure 3.1) to capture details of the more complex flow behaviours (see figure 3.9); to utilize a uniform unstructured mesh (see figure 3.5); to adopt approximately 80 time steps per cycle and velocity boundary condition (1). That is, the mathematical modelling of the experiments performed by Tatsuno & Bearman (1990) , Knörnschild (1994) and Dütsch *et al* (1998) . The results for the convergence tests of the present method in the oscillating cylinder flow problems are consistent with similar tests carried out for other flow problems including driven cavity flow, backfacing step channel flow and vortex shedding flows etc. The details of these investigations and more comparison with other methods can be found in Tan *et al* (1999) and Farrant *et al* (2000a,2000b) .

3.4.2 Observations and numerical simulations

As illustrated in figure 3.1, Tatsuno & Bearman (1990) through an experimental visualization study provide an extensive categorization of the flow regimes around an oscillating circular cylinder over a range of Re and KC numbers. Three such examples are shown in figures 3.7(a)–3.9(a) consisting of streakline patterns at Re=81.4, KC=11.0 in regime A, Re=165.79, KC= 3.14 in regime A* and Re=210.0 and KC=6.0 in regime E. They confirmed the first two flow fields as two-dimensional and these cases are on either side of the $\beta = 35$ line shown in figure 3.1. Knörnschild (1994) independently substantiated these findings. Case E is on the $\beta = 35$ line and is deemed a physical three-dimensional flow (see figure 3.1).

Figures 3.7(b)–3.9(b) illustrate the equivalent computed streakline patterns to figures 3.7(a)–3.9(a). These streaklines were simulated by releasing 40 massless particles at each time step into the computational domain. The overall impression gained by comparison of the respective figures indicates close similarities. The particles used to compute the streakline patterns are passive markers. This method is equivalent to the experimental electrolytic precipitation method used by Tatsuno & Bearman (1990) .

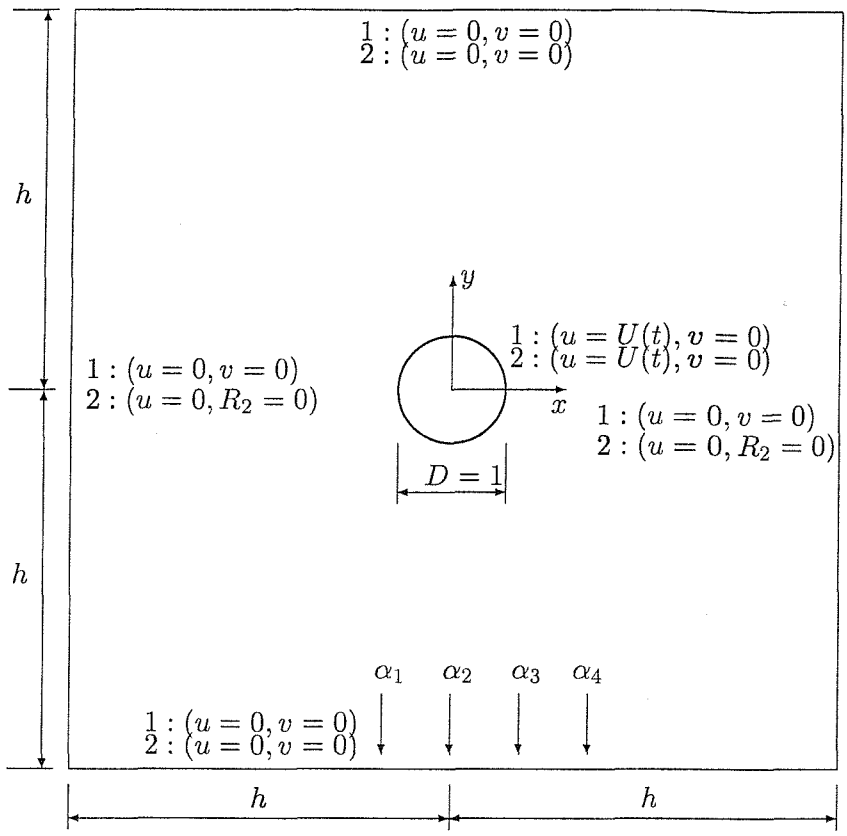

Figure 3.4: Computational domain definition and boundary conditions for an oscillating cylinder. All the variables and quantities are nondimensional. (The indicated positions $\alpha_1, \alpha_2, \alpha_3, \alpha_4$ relate to the transverse measurements of Dütsch *et al* (1998) illustrated in (figure 3.11.))

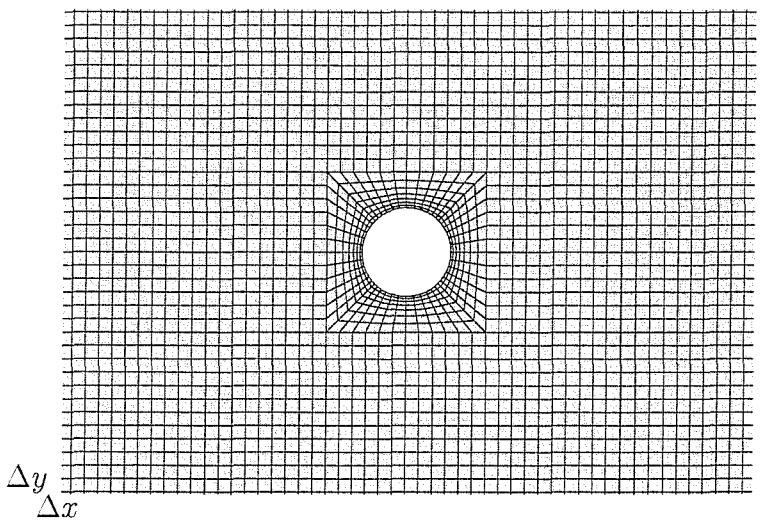

Figure 3.5: Typical mesh idealising the fluid around the cylinder.

Figures 3.7(c)–3.9(c) and 3.10(a-c) illustrate the vortex shedding mechanisms in the numerical simulations during various stages of the cycle for cases A, A* and E.

Figures 3.7(b,c) and 3.10(a) show symmetric and periodic vortex shedding. In this regime two contra-rotating vortices are formed symmetrically behind the cylinder during each half cycle. These vortices stay behind the cylinder at the end of each cycle and as the cylinder reverses direction, the vortices are convected towards the cylinder. The vortices do not survive into the next half cycle agreeing with the observations of Tatsuno & Bearman (1990) .

Figure 3.8(b,c) illustrates computed streakline patterns during a cycle for case A* i.e. Re=165.79, KC=3.14. The computed velocity field for this regime at a specific instant in the cycle is illustrated in figure 3.10(b). No vortex shedding occurs in this symmetric regime confirming the experimental findings. Large regions of contra-rotating crescent like flow are observed on both sides of the cylinder.

According to the classification of Tatsuno & Bearman (1990) , figure 3.9(a) belongs to regime E and is three-dimensional in form. The two-dimensional flow calculation at Re=210.0, KC=6.0 is illustrated in figure 3.9(b,c) suggesting that the three-dimensional flow feature is not too strong although a slightly sharper V fluid shedding formation appears in the simulation. This is a regime where the flow sheds with temporarily stable V-type vortex streets as illustrated in figures 3.9(b,c) and 3.10(c). In this regime intermittent changes of direction of convection and switching of the flow field triggered by small disturbances were observed by Tatsuno & Bearman (1990). However, no artificial disturbances (e.g. see the discussion of Zhang & Zhang (1997)) were added in the present computations to simulate this mechanism and vorticity convection occurred only on one side of the cylinder with no switching of the flow field.

To further validate the proposed theoretical and numerical approach, computations were compared with measurements taken by Dütsch *et al* (1998) at Re=100 and KC=5.0 for the velocity components (u, v) at prescribed phase angles and at different cross-sections in the flow measured from the centre of the cylinder. Figure 3.4 indicates the four transverse positions of measurement $\alpha_1, \alpha_2, \alpha_3, \alpha_4$. Figure 3.12 illustrates such a comparison at these cross-sections behind and ahead of the cylinder. The excellent comparison between these findings and the experimental and numerical results of Dütsch *et al* (1998) further confirms with confidence the applicability of the mathematical model to fluid–structure interaction problems defined by low-Reynolds-number

and Keulegan–Carpenter number.

3.4.3 Predicted forces and coefficients

To illustrate the influence of Reynolds number and Keulegan–Carpenter number on force and coefficient values a series of computations were undertaken along the $\beta = 35$ line shown in figure 3.1 for $0 \leq KC \leq 8$. This range covers two- and three-dimensional flow regimes and therefore, for KC values greater than approximately 5 along $\beta = 35$ the predicted values can only be approximations to the physical flow reality. As indicated in the introduction, the KC parameter, in effect, compares the distance the cylinder moves relative to the cylinder's diameter. β parameter can be seen as the ratio of the time that the vorticity takes to diffuse a distance equal to the cylinder diameter to the flow oscillation period. As β increases, boundary layer gets thinner Kühtz (1996) .

For illustration purposes, figures 3.12 and 3.13 show the variation of the drag (F_1) and lift (F_2) force components over a cycle at Re=100, KC=5 and Re=210, KC=6 respectively. The information is computed directly by the cell boundary element method and through analysis using the Morison equation (3.3) after determining C_D and C_I values by Fourier analysis. As to be expected, a reasonable agreement exists between the drag force component from the two analyses. The individually calculated time force histories of the components illustrated in figure 3.13 are shown in figure 3.14(a,b). The initially zero valued lift force component indicates a symmetric flow field before the presence of the lift force is experienced which significantly lags the drag force. For the two dimensional flow regime at Re=100, KC=5 the lift force component F_2 remains zero or very near to zero over the cycle confirming a symmetric flow field and the drag force is the only significant component. In both cases a reasonable correlation exists between the Morison type approach and results derived from the cell boundary element approach.

Table 3.6 presents information on the drag C_D and added mass C_I coefficients from the series of computations over KC number. These coefficients for $KC \geq 5$ were obtained by Fourier analysis of the cycles after periodic states are established. This table also includes a comparison with the findings of Dütsch *et al* (1998) for $0 \leq KC \leq 8$, $\beta = 35$ using a finite volume method. In flow region F(KC=8.0) a time

averaging process is applied to the cyclical data after the occurrence of flow instability. All these data are included in figure 3.15(a,b) together with the experimental results of Kühtz (1996) , who presented the data in this inertia–drag coefficient format, and analytical solutions of Wang (1968) derived from (3.5) and (3.6). From this limited evidence, the agreement between experimental drag data and cell boundary element method or finite volume method predictions are favourable although for the added inertia coefficient the predicted values lie below the experimental data. Furthermore the information illustrates the restricted accuracy of the series expansion as performed by Wang and confirms the limited applicability of such an approach as discussed by Chester (1990) .

3.4.4 Predicted force coefficients at low Keulegan–Carpenter number.

In a previous study to validate the cell viscous boundary element method, Uzunoğlu *et al* (2000) compared numerical predictions of viscous flow field characteristics at low-Reynolds-number with selected experimental data presented by Tatsuno & Bearman (1990), measurements of force coefficients by Kühtz (1996) and finite volume calculations performed by Dütsch *et al* (1998). This exercise proved very successful. In the limited extension herein, we focus on the effects of Stokes number β on force coefficients associated with symmetric flow regimes at low Keulegan–Carpenter number KC through comparisons with experimental data (i.e. Kühtz (1998)) and other theoretical findings (i.e. Wang (1968) and Lin *et al* (1968)). In a series of extensive numerical experiments undertaken it was shown that for the case $Re = 100$, $KC = 5$ and $\beta = 20$, convergent solutions for drag C_D and added mass C_I coefficients were derived independent of time step Δt, outer domain size, grid size and boundary conditions imposed at the outer domain boundary. In this present study, the previous numerical scheme of study reflects into a square mesh of 6592 cells within a domain defined by an outer boundary at 12 times the radius of the circular cylinder, zero velocity components imposed on the outer boundary of the fluid domain, oscillating velocity boundary conditions on the surface of the cylinder and 80 time steps taken per cycle.

Table 3.1 for $\beta = 76$ and Table 3.2 for $\beta = 53$ show comparisons of the added mass

C_I and drag coefficients C_D determined by the cell viscous boundary element method described herein, the theoretical findings of Wang (1968) who extended the analytical results of Stokes and the numerical results of Lin *et al* (1996) derived by a hybrid Lagrangian/Eulerian discrete vortex method.

KC	0.1	0.2	0.4	0.8	1.0	1.5	2.0	2.5	3.0
Viscous cell boundary element method									
C_D	32.973	16.473	8.265	4.235	3.447	2.452	2.005	1.784	1.720
C_I	1.251	1.250	1.249	1.242	1.239	1.227	1.212	1.193	1.148
Hybrid Lagrangian/Eulerian Discrete Vortex Method Lin *et al* (1996)									
C_D	31.729	15.980	8.128	4.169	3.407	2.427	1.980	–	–
C_I	1.263	1.261	1.257	1.254	1.152	1.242	1.229	–	–
Wang (1968)									
C_D	32.016	16.018	8.004	4.002	3.202	2.134	1.601	1.281	1.067
C_I	1.259	1.259	1.259	1.259	1.259	1.259	1.259	1.259	1.259

Table 3.1: Drag C_D and added mass C_I coefficients for $\beta = 76$

These results, with slight modifications i.e. $C_M = C_I + 1$, are also shown in figure 3(a, b) with the experimental measurements of Kühtz (1996). These data bases illustrate the small theoretical dependence of C_I or C_M on β value with changing KC value though this is not clearly evident in the limited range of experimental findings; the theoretical dependence of C_D on β value with changing KC value which is confirmed by the experimental data; the limited applicability of the analytical result of Wang (1968), and the increasing effects of flow separation on C_D and C_M values with increasing value of KC number.

3.4.5 Two oscillating cylinders

The cell boundary element method has also been used in multi-body problems and the application is straightforward since this method works with unstructured meshes.

KC	0.5	1.0	1.5	2.0	2.5	3.0
Viscous cell boundary element method						
C_D	8.003	4.127	2.911	2.334	2.055	1.913
C_I	1.300	1.292	1.280	1.266	1.247	1.222
Wang (1968)						
C_D	7.757	3.878	2.586	1.939	1.551	1.292
C_I	1.310	1.310	1.310	1.310	1.310	1.310

Table 3.2: Drag C_D and added mass C_I coefficients for $\beta = 53$

Examples presented here involve two identical cylinders oscillating in synchronization with parameters $Re = 100$ and $KC = 5$ based on the diameter D of the cylinders. Two arrangements with the cylinders in tandem and side-by-side are considered and in both cases the gap between the two cylinders is the same as the diameter of the cylinders. That is, the distance from centre to centre of the cylinders is $2D$. The simulated streakline patterns predicted using the cell boundary element method are presented in figure 3.16 with (a) for the tandem arrangement and (b) for the side-by-side arrangement. As can be seen in figure 3.16, the streakline pattern of the tandem arrangement appears to be similar to the single cylinder case in the same regime whereas the side-by-side arrangement produces a very different streakline pattern.

The drag C_D and added mass C_I coefficients and time averaged values of in-line force $\bar{F}_1$ and lift $\bar{F}_2$ are shown in table 3.7 for each cylinder in different arrangements. The C_I values in both the two cylinder cases are lower for each arrangement when compared with the C_I value of a single cylinder, whereas the C_D values show a different trend. The values of $\bar{F}_1$ and $\bar{F}_2$ in table 3.7 suggest that the two cylinders are subject to a net repulsive force in the tandem arrangement and a net attractive force in the side-by-side arrangement. The results also show that the interactions between the two cylinders are significant in both arrangements under the given conditions.

This approach is used for the bodies in fixed relative positions. If the bodies are moving relative to each other, a suitable approach will be to formulate the problem in

Table 3.3: Drag C_D and added mass C_I coefficients at $Re = 100$ and $KC = 5$ for different time steps.

Δt	Boundary Condition (figure. 3.4)	Domain Size h	Grid Size $(\Delta x, \Delta y)$	C_D	C_I
0.25000	1	6.0	(0.15, 0.15)	1.98	1.48
0.12500	1	6.0	(0.15, 0.15)	2.09	1.44
0.06250	1	6.0	(0.15, 0.15)	2.10	1.43
0.03125	1	6.0	(0.15, 0.15)	2.10	1.43

Arbitrary Lagrangian Eulerian formulation.

3.5 CONCLUSION

The cell boundary element method developed by Tan *et al* (1999) and modified herein to study oscillating cylinders or manoeuvring bodies has proven successful, reproducing the detailed characteristics of experimental observations, correlations with theoretical predictions presented by others and experimental measurements of drag and lift coefficients over a range of Re, KC numbers for fixed Stokes parameter $\beta = 35$. This has been achieved by adopting an unstructured mesh to idealise the fluid domain and a primitive-variable formulation to construct a hybrid approach involving boundary element and finite element methods. Through developments of suitable numerical schemes of study associated with the cell boundary element method integrated with the relevant boundary conditions for transversely oscillating cylinders or a cylinder fixed in oscillating flows, the presented computed unsteady flows provide a measure of verification, validation and confidence in the proposed overall approach when compared with other experimental and theoretical findings.

Table 3.4: Drag C_D and added mass C_I coefficients at $Re = 100$ and $KC = 5$ for different boundary conditions and domain size.

Δt	Boundary Condition (figure 3.4)	Domain Size h	Grid Size (Δx, Δy)	C_D	C_I
0.06250	1	3.0	(0.15, 0.15)	2.27	1.47
0.06250	2	3.0	(0.15, 0.15)	2.24	1.49
0.06250	1	6.0	(0.15, 0.15)	2.10	1.43
0.06250	2	6.0	(0.15, 0.15)	2.13	1.44
0.06250	1	9.0	(0.15, 0.15)	2.10	1.43
0.06250	2	9.0	(0.15, 0.15)	2.10	1.43

Table 3.5: Drag C_D and added mass C_I coefficients at $Re = 100$ and $KC = 5$ for meshes of different refinement.

Δt	Boundary Condition (figure 3.4)	Domain Size h	Grid Size (Δx, Δy)	C_D	C_I
0.06250	1	6.0	(0.20, 0.20)	2.12	1.41
0.06250	1	6.0	(0.15, 0.15)	2.10	1.43
0.06250	1	6.0	(0.10, 0.10)	2.10	1.45
Finite volume method, Dütsch *et al* (1998) [a]				2.09	1.45

[a] Numerical results derived using the finest mesh in their analysis.

Table 3.6: Drag C_D and added mass C_I coefficients for $\beta = 35$ at different regimes.

KC	0.5	1.0	1.5	2.0	2.5	3.0	4.0	5.0	6.0	8.0
regime	A*	A*	A*	A*	A*	A*	A	C	E	F [a]
Viscous cell boundary element method										
C_D	10.0	5.13	3.56	2.83	2.43	2.18	1.94	1.84	1.75	1.74
C_I	1.37	1.36	1.35	1.33	1.32	1.30	1.29	1.23	1.14	1.05
Finite volume method, Dütsch *et al* (1998)										
C_D	10.4	5.39	3.72	2.98	–	2.28	1.97	1.82	1.73	1.72 – 1.73
C_I	1.37	1.36	1.35	1.34	–	1.31	1.30	1.30	1.17	1.14 – 1.15

[a] Cycle averaged after flow instability.

Table 3.7: Key parameters for two oscillating cylinders at $Re = 100$ and $KC = 5$.

Parameters	Single cylinder	Two cylinders in tandem		Two cylinders side-by-side	
		Left	Right	Bottom	Top
C_D	2.10	1.77	1.77	2.63	2.63
C_I	1.43	1.25	1.25	1.30	1.30
$\bar{F}_1$	0.0	-0.10	0.10	0.0	0.0
$\bar{F}_2$	0.0	0.0	0.0	0.30	-0.30

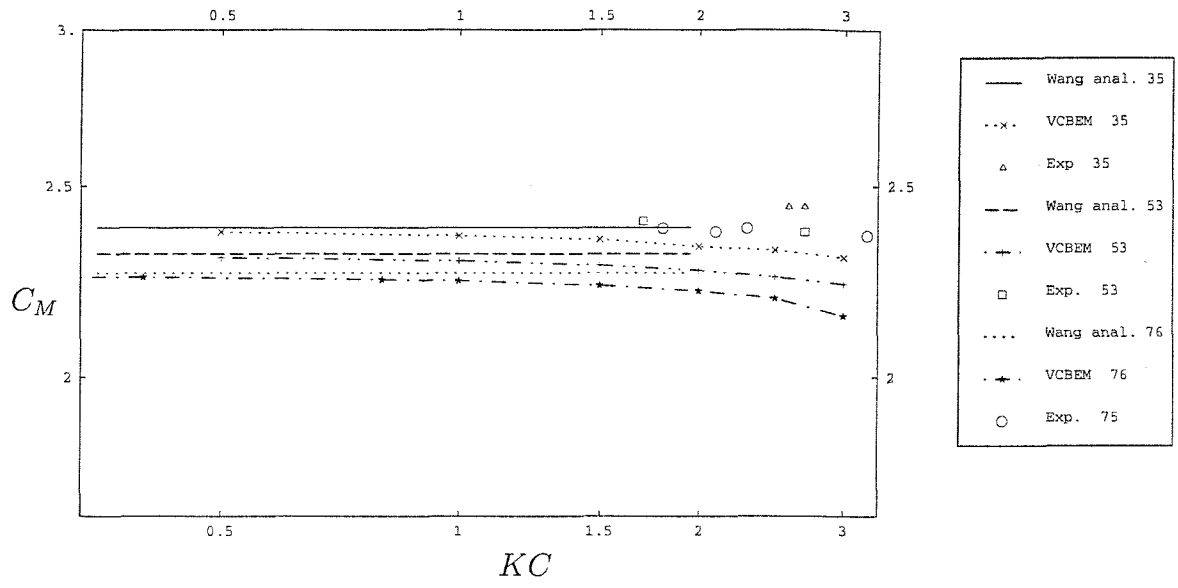

(a)

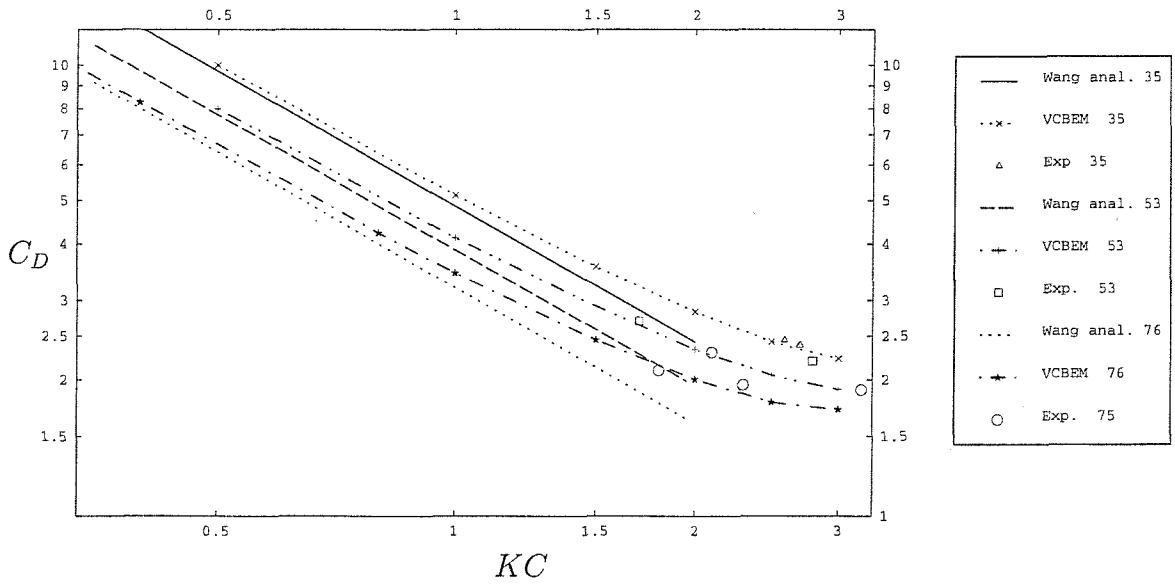

(b)

Figure 3.6: Variation of inertia figure (a) drag coefficient figure (b) with Keulegan–Carpenter number for $\beta = 35, 53, 75$ and 76.

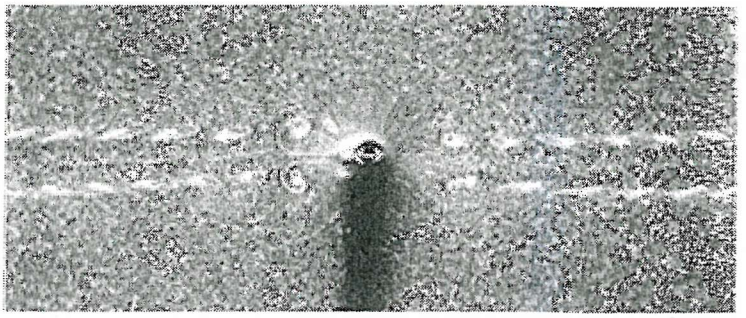

(a)

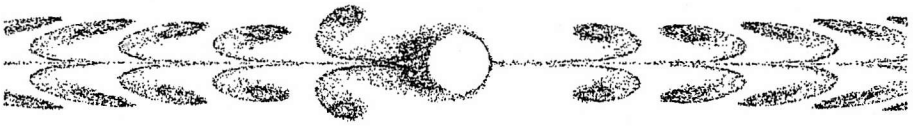

Ut/D=247.54

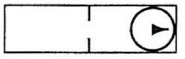

(b)

Ut/D=245.73

Ut/D=246.90

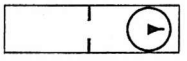

Ut/D=247.54

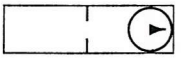

Ut/D=250.21

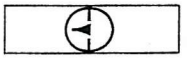

(c)

Figure 3.7: (a) Flow visualization of the streakline pattern generated by a transversely oscillating circular cylinder at $Re = 81.4$, $KC = 11.0$ in two-dimensional flow regime A as observed by Tatsuno & Bearman (1990) ; (b) overall numerical simulation comparable with the visualization in (a); (c) numerical simulation at different stages over a half cycle illustrating the vortex shedding mechanism.

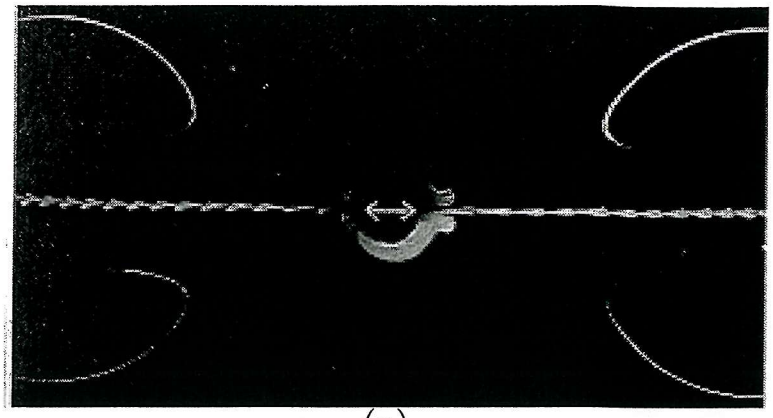

(a)

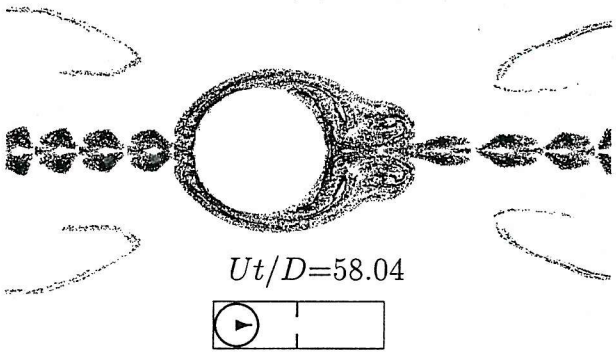

(b)

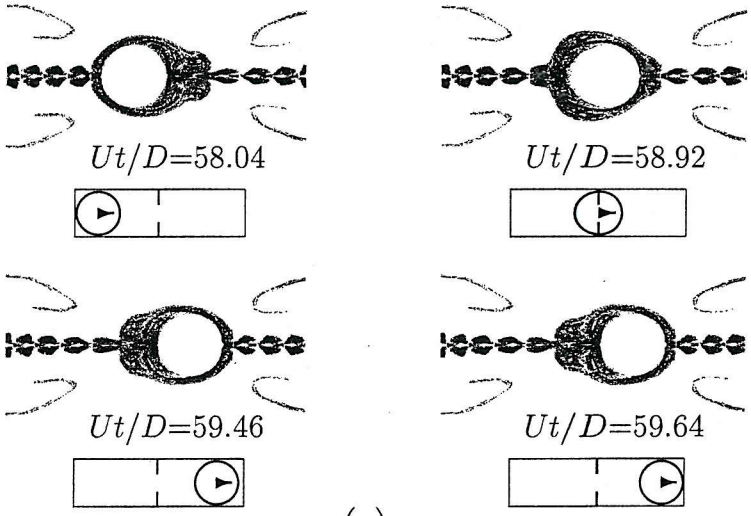

(c)

Figure 3.8: (a) Flow visualization of the streakline pattern generated by a transversely oscillating circular cylinder at $Re = 165.79$, $KC = 3.14$ in two-dimensional flow regime A* as observed by Tatsuno & Bearman (1990); (b) overall numerical simulation comparable with the visualization in (a); (c) numerical simulation at different stages over a half cycle illustrating the contra-rotating crescent like flow observed.

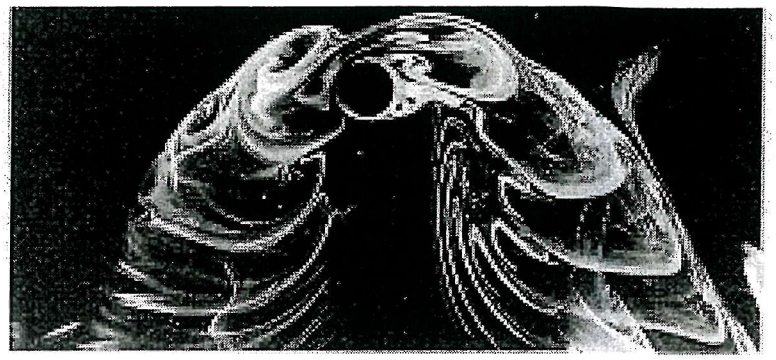

(a)

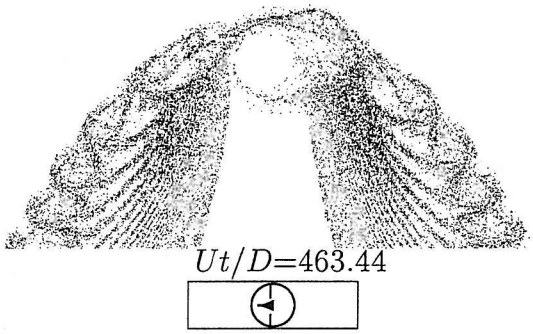

(b)

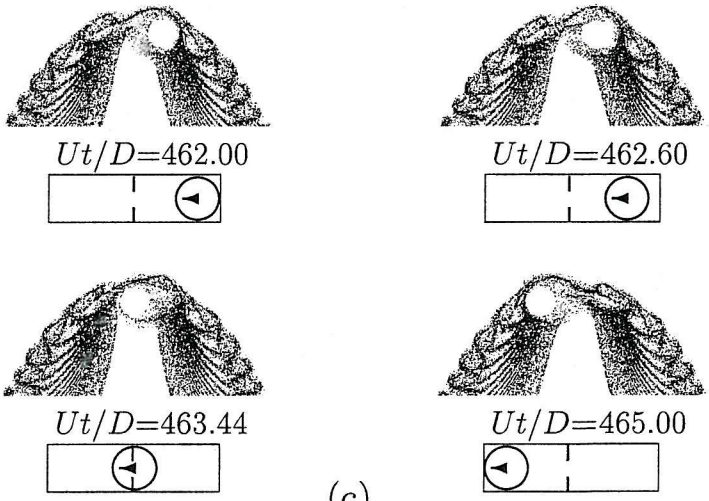

(c)

Figure 3.9: (a) Flow visualization of the streakline pattern generated by a transversely oscillating circular cylinder at Re=210.0, KC=6.0 in three-dimensional flow regime E as observed by Tatsuno & Bearman (1990); (b) overall two-dimensional numerical simulation comparable with the visualization of three-dimensional flow in (a); (c) numerical simulation at different stages over a half cycle of a stable V-type vortex street which is sharper than observed in (a) due to the confinement of the two-dimensional flow.

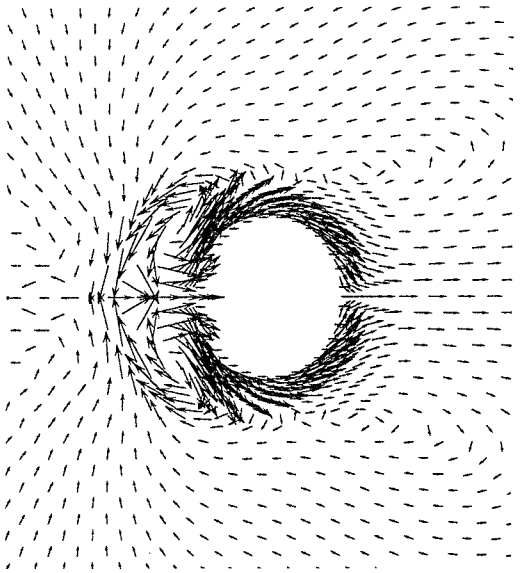

(a) Re=81.4, KC=11.0, Ut/D = 250.21

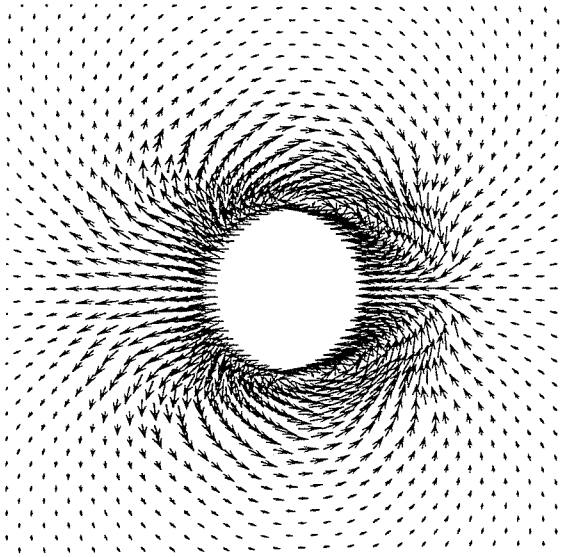

(b) Re=165.79, KC=3.14, Ut/D = 59.64

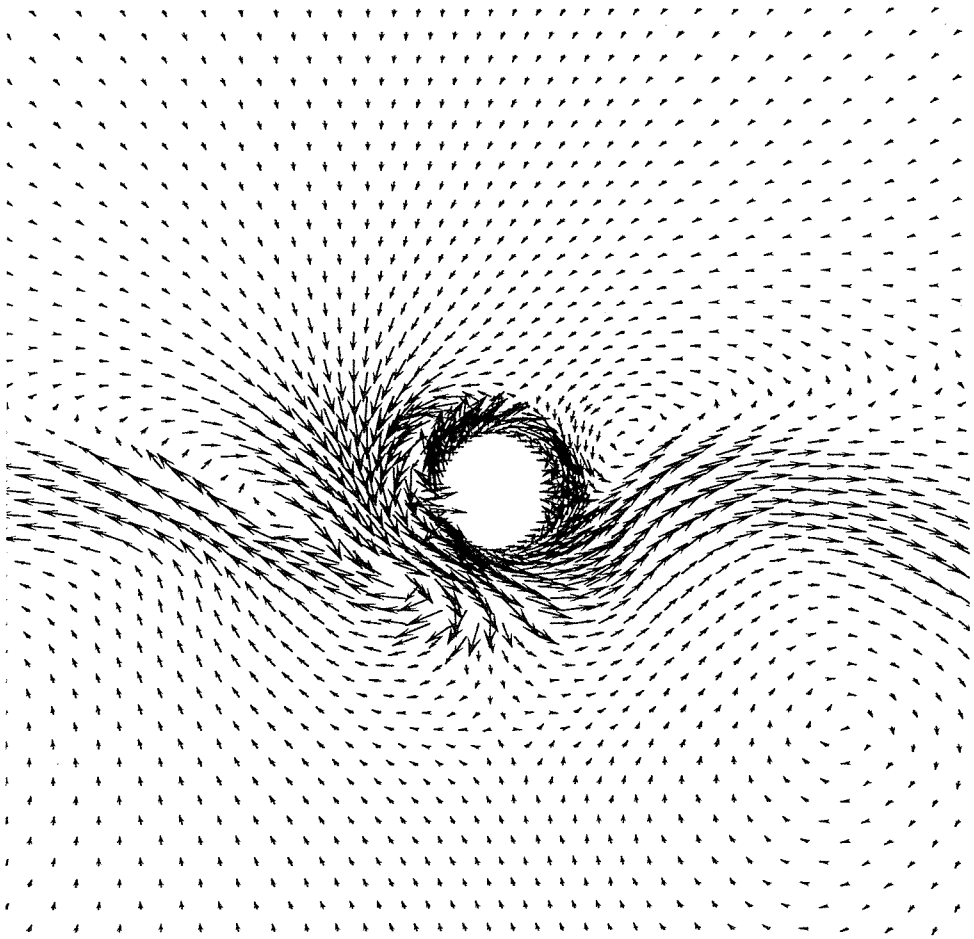

(c) Re=210.0, KC=6.0, Ut/D = 465.00

Figure 3.10: An enlargement of the velocity field at a presented instant in the vicinity of the transversely oscillating cylinder for the flow regimes illustrated in figures 3.7(c)–3.9(c).

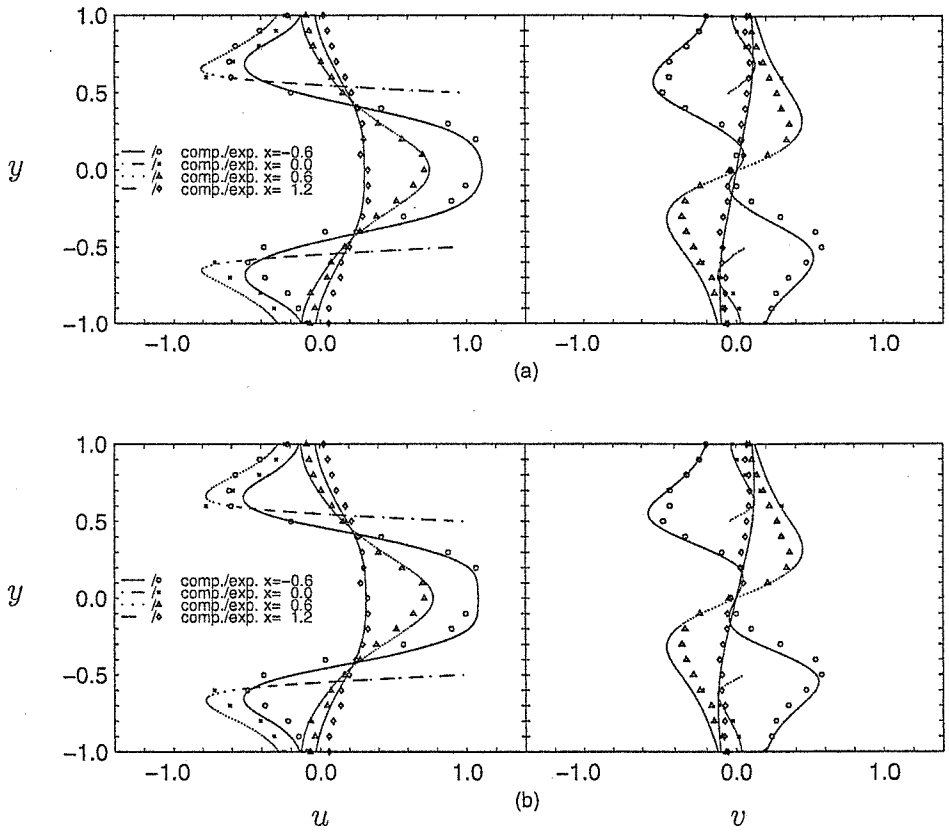

Figure 3.11: Comparison of the velocity components at four cross-sections at constant x values of $\alpha_1, \alpha_2, \alpha_3, \alpha_4$ as illustrated in figure 3.4. These results relate to a phase position 180^o computed by discretisation utilizing (a) a coarse mesh (see table 3.5, row 1); (b) a medium mesh (see table 3.5, row 2).

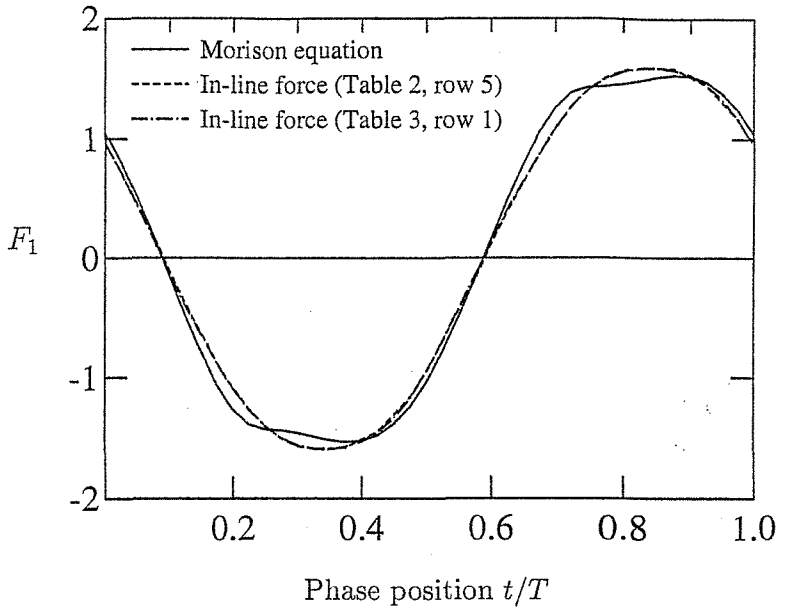

Figure 3.12: In-line force computed over a cycle at Re=100 and KC=5. (Note that the computed results associated with – – – and ·–· coincide.)

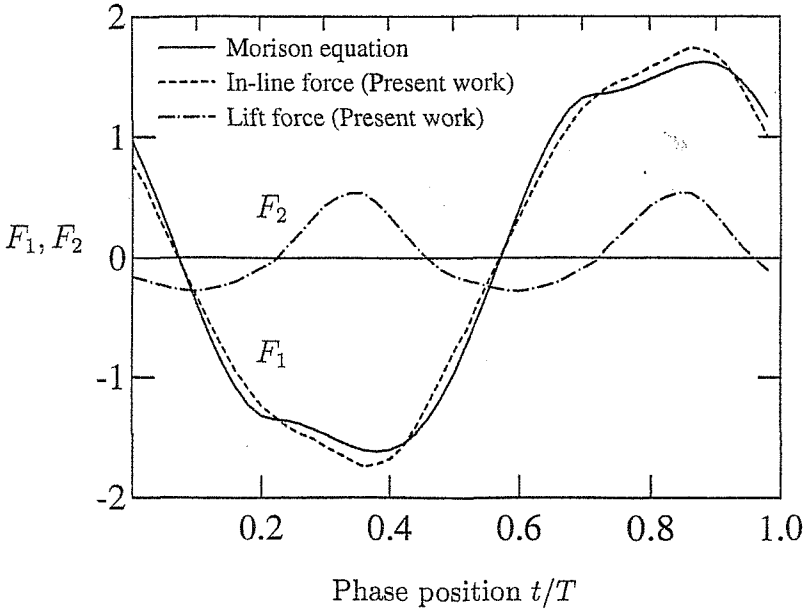

Figure 3.13: In-line and lift forces computed over a cycle at $Re = 210$ and $KC = 6$.

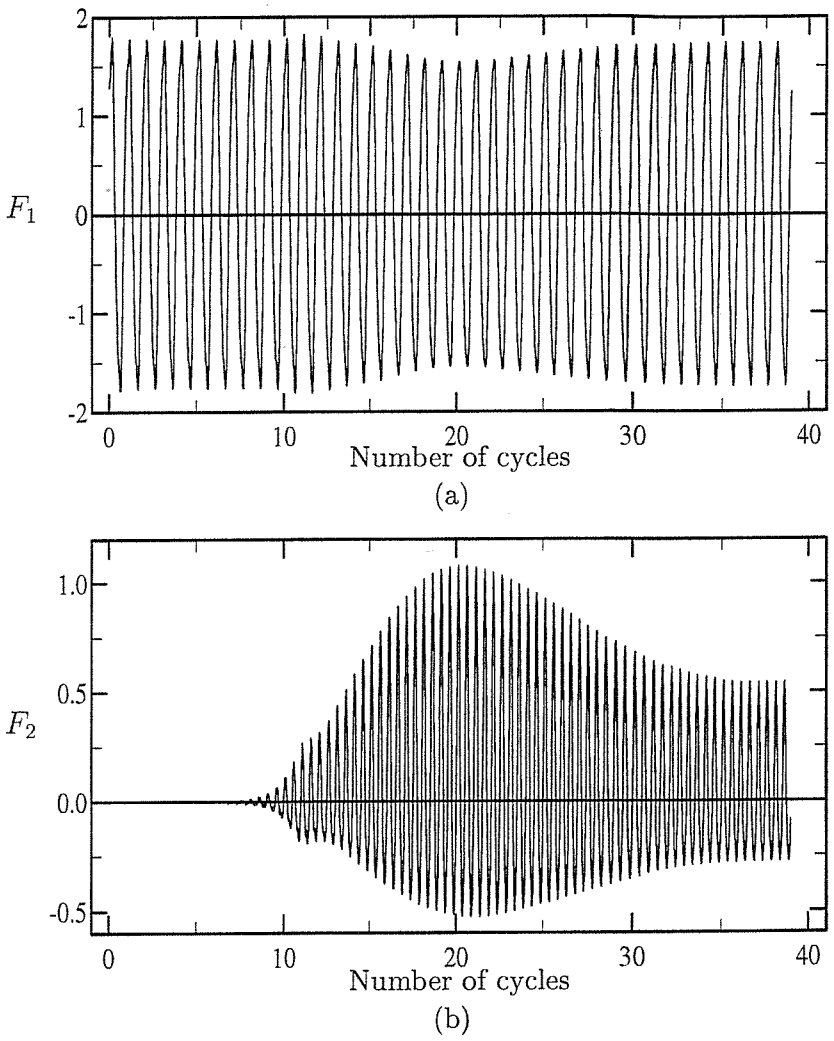

Figure 3.14: Time history of (a) in-line force and (b) lift force computed at $Re = 210$ and $KC = 6$.

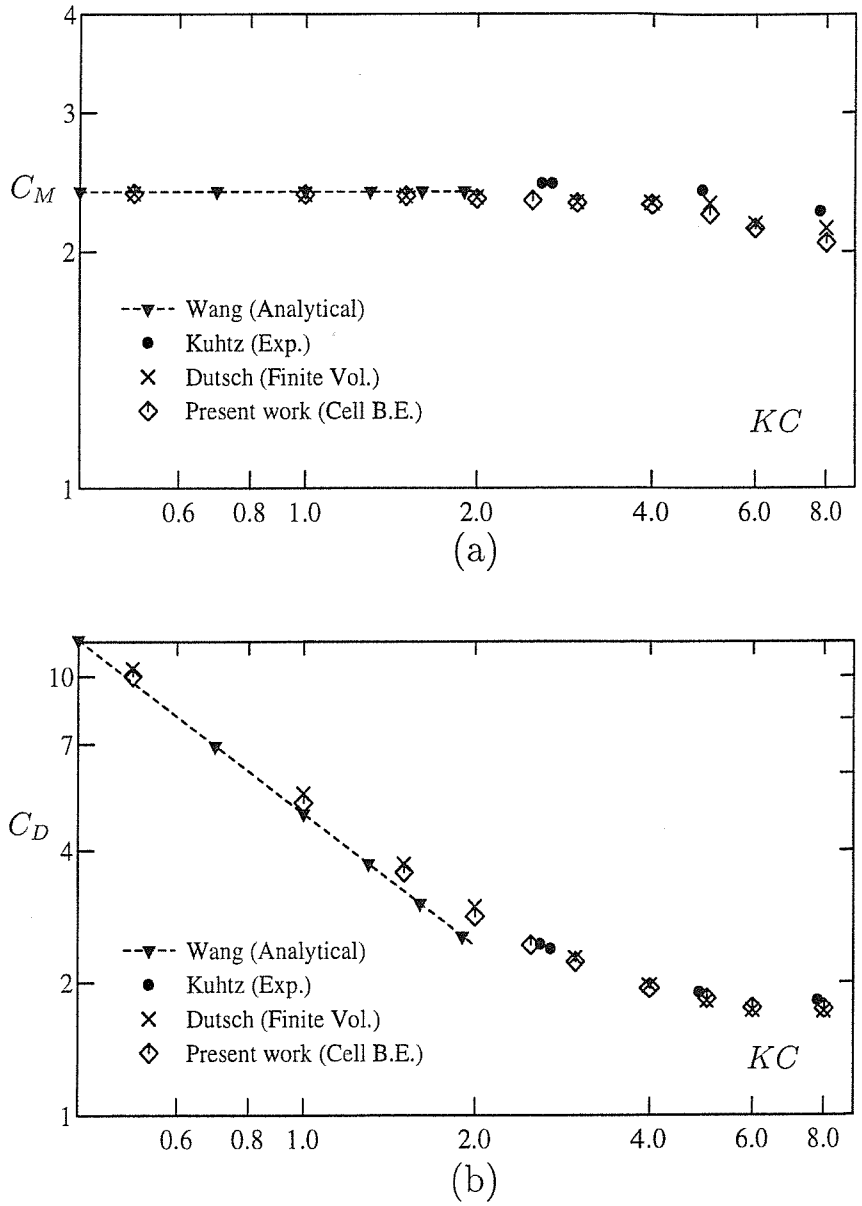

Figure 3.15: Variation of (a) inertia coeffient C_M and (b) drag coefficient C_D with Keulegan–Carpenter number KC for $\beta = 35$.

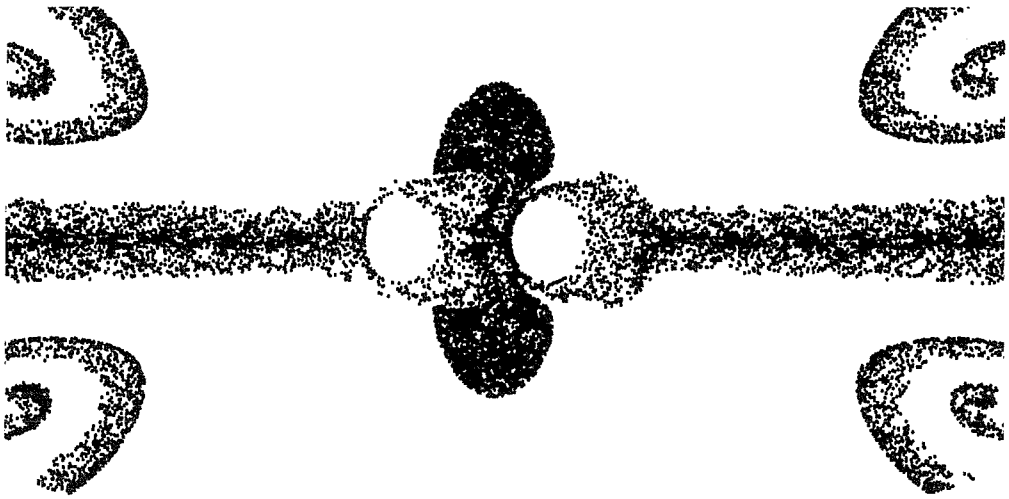

(a)

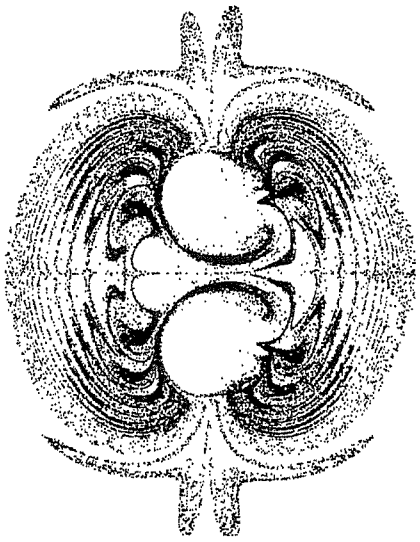

(b)

Figure 3.16: The simulated streakline patterns generated by two oscillating circular cylinders at $Re = 100$, $KC = 5$ in (a) tandem arrangement and (b) side-by-side arrangement. The gap clearance between the two cylinders is D in both cases where D is the diameter of the cylinders.

Chapter 4

REDUCED ORDER MODELLING OF FLOW

The basic idea of reduction methods is the compression of a large system (of algebraic and/or differential equations) to a similar (in some sense) much smaller substitute. Many of the reduction methods reported in the literature can be thought of as two-step hybrid analysis techniques combining a discretization method with a direct variational technique. In the first step, a number of global approximation vectors (modes or basis vectors), to approximate/estimate the response of the system, are generated using a discretization method and in the second step the amplitudes of the global approximation vectors are determined via a direct variational technique. The mentioned hybrid analysis techniques combine the modelling variety of contemporary discretization methods (eg. finite elements, boundary elements, finite differences and their combinations) with the reduction in total number of degrees-of-freedom provided by the direct variational technique.

In this chapter reduced modelling techniques, based on a Proper Orthogonal Decomposition (POD) method, are applied to an investigation of the incompressible Navier-Stokes equations with inputs. A circular cylinder in uniform flow with and without inputs is studied. Reduced dynamical models are created by POD and by extended POD (EPOD) approaches for the forced flow which is statistically non-stationary. A direct control action is applied to the flow at particular points and this investigation provides insights to the applications of this approach coupled with a full solver.

4.1 INTRODUCTION

A problem of considerable interest is presented by the construction of explicit low-order models to design controllers for distributed parameter systems which, in this context, are fluid flows. Once a control design has been constructed using such a low order model, it can be tested by comparing its performance against a full high-order simulation.

The difference between modelling for control, and modelling for analysis of dynamical behaviour is that in the latter case the system behaviour is statistically stationary with no external inputs driving the system. However for controlled systems, we are concerned with preserving the relationship between the system behaviour and the system inputs and outputs, or actuators and sensors.

One model reduction method which has been successfully used for dynamical systems analysis is a Proper Orthogonal Decomposition (POD) method developed and discussed by Sirovich (1987) . This method has become popular as a means of extracting dominant energy-containing structures from flow field data and by using these structures as basis functions, generating low order dynamical models for the associated systems. The method has been applied to fluid problems by Sirovich (1987) and many other researchers, e.g Berkooz *et al* (1993) and Deane *et al* (1994) and to understand the important dynamical features or coherent structures seen in fluid flows.

A full model of the dynamics of such a system is normally represented by a set of high dimensional nonlinear differential equations which can be only solved by numerical methods. In this study a cell viscous boundary element method developed by Tan *et al* (1999) is used to generate the required data for the reduced model. The POD method describes the system behaviour as an attractor which is a point of evolution for the state space in a subspace of higher dimensions. A reduced solution can be obtained as a linear combination of an optimal set of empirical basis functions using an integral equation method such as the Galerkin projection method.

These bases are created by applying a POD method for statistically stationary data. When a fluid flow is subject to a time-dependent control, the statistical properties of the flow are usually non-stationary. In this case, an extended POD method (EPOD) developed by Glezer *et al* (1999) can be adopted. Herein applications of the POD and EPOD methods are investigated in order to derive a reasonable approximation to

time-dependent flows associated with vortex shedding.

Several model reduction methods have been proposed and applied for statistically non-stationary systems with control inputs. A control function method has been applied by Ravindran *et al* (1998) to channel flows. Graham *et al* (1996) applied a control function method and penalty method for rotating cylinders in uniform flow. Balanced truncation Lall *et al*(1999), and Ott-Grebogi-Yorke (OGY) (1990) methods have been proposed to incorporate the control input into the model. Neural networks and reduced basis methods can also be adopted to construct reduced flow models with control inputs. The advantages and disadvantages of the applications of some of these approaches in real-time applications in flow control are discussed by Gillies(1998) .

This chapter describes an investigation of POD and EPOD methods to the flow generated by a circular cylinder in uniform flow and reduced dynamical models are established for the non-stationary forced flow.

4.2 FULL MODEL

4.2.1 Mathematical model

A cell viscous boundary element method Tan *et al*(1999) , developed to solve Navier-Stokes equations, is employed to generate the required data for POD and EPOD analyses by conducting numerical flow simulations for vortex shedding flows behind a circular cylinder. This numerical scheme of study is a hybrid approach combining boundary element and finite element methods. The boundary element method is applied to fluid cells idealising the fluid domain and global equations are obtained by means of finite element procedures. A brief description of the method is included herein whereas, a detailed account, is described in the third chapter.

The governing equations of the flow defined in a body fixed coordinate system translating with a given velocity $\hat{v}_j(t)$, in terms of a non-dimensional velocity field v_j and pressure p relative to a space fixed coordinate system, can be written as

$$\dot{v}_j + (v_j v'_k)_{,k} + p_{,j} - [\nu_e(v_{j,k} + v_{k,j})]_{,k} = 0 \tag{4.1}$$

$$v_{j,j} = 0 \tag{4.2}$$

where $\nu_e = 1/\mathrm{Re}$, $v'_k = v_k - \hat{v}_j(t)$ and Re is the Reynolds number.

An integral equation can be formulated from equations (3.10) and (3.11) following the methodology of the boundary element method. That is,

$$C(\boldsymbol{\xi})v_s(\boldsymbol{\xi},t) + \int_\Sigma v_j(v'_k n_k v^*_{sj} + R^*_{sj})d\Sigma$$
$$= \int_\Sigma R_j v^*_{sj} d\Sigma - \int_\Omega f_j v^*_{sj} d\Omega \tag{4.3}$$

where $C(\boldsymbol{\xi})$ is a constant the value of which depends on the location of the field point $\boldsymbol{\xi}$. v^*_{sj} and R^*_{sj} denote the fundamental solution and related function Price *et al* (1992) respectively. R_j is the traction force on the cell boundary and f_j is the resultant term derived from the acceleration $\dot{v}_j$ after a finite difference scheme is introduced.

An extensive validation of this numerical method has been carried out using a number of well documented flow solutions. Good agreement was achieved against data produced from other sources, including theoretical solutions, other numerical predictions, and experimental observations as discussed by Uzunoğlu (2001) .

4.2.2 Vortex shedding problem

Numerical calculations were performed to quantify and describe the vortex shedding behaviour behind a circular cylinder in a uniform current with or without control actions. Forcing of the wake at particular points in the flow is taken as an example of the control actions to be considered. The boundary conditions and geometry description of this cylinder–fluid interaction problem are defined in fig.4.1. Mixed boundary conditions associated with both traction and velocity are used.

4.3 MODEL REDUCTION FOR STATIONARY FLOWS

Model reduction methods are applied to the non-linear stationary flow system which can be expressed formally as,

$$\dot{\boldsymbol{v}}(\boldsymbol{x},t) = NS(\boldsymbol{v}(\boldsymbol{x},t)) \tag{4.4}$$

where NS denotes the nonlinear operator of steady Navier-Stokes equations.

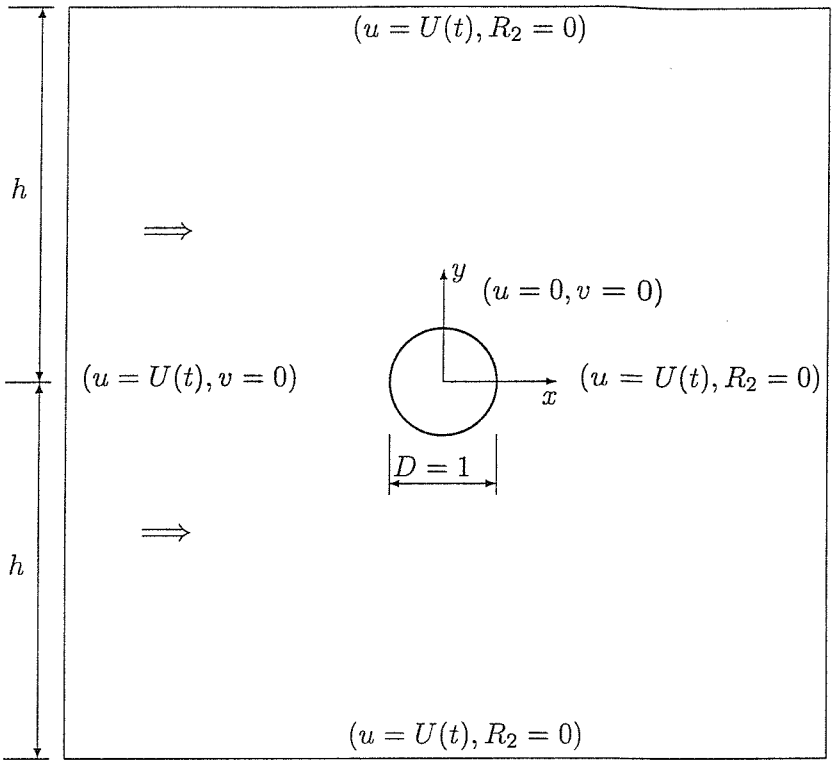

Figure 4.1: Computational domain definition and boundary conditions for a cylinder in a uniform flow. All the variables and quantities are nondimensional.

The approach adopted is essentially data based and the type of data we wish to analyze are generated by a nonlinear flow system.

4.3.1 Proper orthogonal decomposition method for stationary flows

It is assumed that a velocity field $\tilde{\boldsymbol{v}}(\boldsymbol{x}, t)$, described by a set of spatio-temporal data $\tilde{\boldsymbol{v}}(\boldsymbol{x}, t_i)_{i=1}^{i=m}$ obtained at discrete time values t_i and at fixed points in space, is expressible in the form

$$\tilde{\boldsymbol{v}}(\boldsymbol{x}, t) \;=\; \bar{\boldsymbol{v}}(\boldsymbol{x}) + \boldsymbol{v}(\boldsymbol{x}, t), \tag{4.5}$$

where $\bar{\boldsymbol{v}}(\boldsymbol{x})$ is the temporal mean of the velocity field.

The components of $\tilde{\boldsymbol{v}}(\boldsymbol{x}, t_i)$ correspond to scalar values taken at given points in space. Such spatio-temporal data can be usually obtained from either experimental measurements or numerical simulations of the physical process under study.

There are a number of ways to determine quantitatively the underlying spatial structure of a spatio-temporal data set. For example, a simple approach to analyze

such data is to perform a Fourier decomposition Lumley (1993) . This is successful if only a few dominant peaks appear in the power spectrum of the spatial modes, suggesting relatively simple spatial structures. However, this would not be the best approach if there exists a coherent spatial structure composed of many Fourier modes.

A proper orthogonal decomposition method computes these coherent spatial structures directly. The structures computed are optimal for a given data set Sirovich (1987) and once the major spatial structures are known, their temporal behaviour can be analyzed using dynamical system theory as discussed by . Sirovich (1987) , Berkooz *et al* (1993) and Deane *et al* (1991) . The proper orthogonal decomposition method is a well known analysis technique with the original concept traced to Pearson (1901) . Several different names including principal component analysis, Karhunen-Loève decomposition and total-least-squares estimation have been given to the procedure.

To review briefly the approach, let us consider a data set $\tilde{\boldsymbol{v}}(\boldsymbol{x},t)$ defined over a finite spatial domain Ω and a finite interval $0 \leq t \leq T$. To investigate the structures of fluctuations in the data, the temporal mean is removed from the velocity field. Thus, the time average of $\boldsymbol{v}(\boldsymbol{x},t)$, written as $\langle \boldsymbol{v}(\boldsymbol{x},t) \rangle$, is then zero as can be seen from equation (4.5).

A function $\boldsymbol{\phi}_k(\boldsymbol{x})$ can be chosen such that the projection of the data set onto all possible functions of $\boldsymbol{\phi}_k(\boldsymbol{x})$ is maximal with respect to normalized $\boldsymbol{\phi}_k(\boldsymbol{x})$ (*i.e.* $(\boldsymbol{\phi}_k, \boldsymbol{\phi}_k) \equiv \int \boldsymbol{\phi}_k(\boldsymbol{x}) \cdot \boldsymbol{\phi}_k(\boldsymbol{x}) \mathrm{d}\boldsymbol{x} = 1$). In some average sense, we are therefore trying to maximize

$$\frac{1}{m} \sum_{i=1}^{m} \frac{|(\boldsymbol{v}(\boldsymbol{x},t_i), \boldsymbol{\phi})|^2}{(\boldsymbol{\phi}, \boldsymbol{\phi})} = \frac{(\boldsymbol{K}\boldsymbol{\phi}, \boldsymbol{\phi})}{(\boldsymbol{\phi}, \boldsymbol{\phi})} = \lambda \tag{4.6}$$

where m stands for the number of solutions at different time steps.

In this way, a set of functions $\boldsymbol{\phi}_k(\boldsymbol{x})$ can be found which are the eigenfunctions of the Fredholm type integral equation,

$$\int_{\Omega} \boldsymbol{K}(\boldsymbol{x},\boldsymbol{x}') \cdot \boldsymbol{\phi}(\boldsymbol{x}') \, \mathrm{d}\boldsymbol{x}' \; = \; \lambda \boldsymbol{\phi}(\boldsymbol{x}) \tag{4.7}$$

where the kernel $\boldsymbol{K}(\boldsymbol{x},\boldsymbol{x}')$ is the time averaged correlation function

$$\boldsymbol{K}(\boldsymbol{x},\boldsymbol{x}') \; = \; \langle \boldsymbol{v}(\boldsymbol{x},t) \, \boldsymbol{v}(\boldsymbol{x}',t) \rangle. \tag{4.8}$$

These functions $(\boldsymbol{\phi}_k(\boldsymbol{x}), \; k = 1, \cdots)$ are called the *empirical eigenfunctions* or the

coherent structures. It was shown by Sirovich (1987) that any projection of the data onto a finite set of $\boldsymbol{\phi}_k(\boldsymbol{x})$ is given by

$$\boldsymbol{v}_n(\boldsymbol{x},t) = \sum_{k=1}^{n} a_k(t)\boldsymbol{\phi}_k(\boldsymbol{x}). \tag{4.9}$$

A particular eigenvalue λ_k is used to denote the variance of the data in the direction of the kth eigenfunction. The error is given by $\epsilon_n = \|\boldsymbol{v} - \boldsymbol{v}_n\|^2$ and it is a minimum over all possible sets of orthonormal functions for any given n. Any sample vector using the eigenfunctions can be reconstructed such that

$$\tilde{\boldsymbol{v}}(\boldsymbol{x},t) = \bar{\boldsymbol{v}}(\boldsymbol{x}) + \sum_{k=1}^{n} a_k(t)\boldsymbol{\phi}_k(\boldsymbol{x}) \tag{4.10}$$

where coefficients $a(t)$ are to be determined from the reduced dynamical equations.

Since the building blocks of low dimensional attractors need to be identified from spatio-temporally complex data, a high resolution in space is usually required and, to do so, the size of the spatial data $D \gg m$. In this case, the practical approach to calculate the correlation function is not to determine the $D \times D$ correlation matrix but to use the dual approach on the m snapshots as discussed by Sirovich (1987). This method is also known as *sample space setting*, see for example Preisendofer (1988). Here we consider the snapshot vectors $\boldsymbol{v}(\boldsymbol{x},t_i)$, $i = 1,\ldots,m$ and determine the empirical eigenfunctions $\boldsymbol{\phi}_k(\boldsymbol{x})$ as a linear combination of the snapshots given by

$$\boldsymbol{\phi}_k(\boldsymbol{x}) = \sum_{i=1}^{m} \alpha_i^{(k)} \boldsymbol{v}(\boldsymbol{x},t_i) \tag{4.11}$$

such that equation (4.7) holds. The corresponding eigenvalue problem is to find the eigenvalues and eigenfunctions of a symmetric $m \times m$ matrix defined by,

$$\boldsymbol{A}\,\boldsymbol{\alpha}^{(k)} = \lambda_k \boldsymbol{\alpha}^{(k)} \tag{4.12}$$

where

$$A_{ij} = \frac{1}{m}\int_{\Omega} \boldsymbol{v}(\boldsymbol{x},t_i)\cdot\boldsymbol{v}(\boldsymbol{x},t_j)\,\mathrm{d}\boldsymbol{x} \tag{4.13}$$

and $\boldsymbol{\alpha}^{(k)}$ is a single column array with $\alpha_i^{(k)}$ introduced in equation (4.11) as elements.

Since the trace of the matrix $\boldsymbol{A}$ represents the averaged energy retained in the snapshots, the energy corresponding to the velocity data is the sum of the eigenvalues of the correlation function, in the sense that

$$E = \sum_{i=1} \lambda_i. \tag{4.14}$$

An energy percentage can be assigned to each eigenfunction based on the eigenvalue associated with the eigenfunction, such that

$$E_k = \frac{\lambda_k}{E} \tag{4.15}$$

Under the assumption that the eigenvalues are arranged in descending order from the largest to the smallest, then we have an ordering of the eigenfunctions from most energetic to least energetic.

When the eigenvector $\boldsymbol{\alpha}^{(k)}$ of equation (4.12) is scaled such that $\|\boldsymbol{\alpha}^{(k)}\|^2 = (m\lambda_k)^{-1}$, the eigenfunctions $\boldsymbol{\phi}_k(\boldsymbol{x}), k = 1, \cdots, m$ form a set of orthonormal functions. Namely

$$\int_\Omega \boldsymbol{\phi}_k(\boldsymbol{x}) \cdot \boldsymbol{\phi}_l(\boldsymbol{x}) \, \mathrm{d}\boldsymbol{x} = \delta_{kl}. \tag{4.16}$$

The coefficients $a(t)$ at given discrete times t_i can be computed from a projection of the sample vector onto an eigenfunction given by

$$\begin{aligned} a_k(t_i) &= \int_\Omega \boldsymbol{v}(\boldsymbol{x}, t_i) \cdot \boldsymbol{\phi}_k(\boldsymbol{x}) \, \mathrm{d}\boldsymbol{x} \\ &= m\lambda_k \alpha_i^{(k)}. \end{aligned} \tag{4.17}$$

This expression can be used to determine the initial conditions and projection data required in the time integration of $a(t)$.

The sampling of snapshots can be based on a signal which is related to some physical aspect of the system. In the vortex shedding problem, lift coefficient might be a suitable signal. The chosen signal must be bandlimited that is the frequency spectrum must be limited to contain frequencies up to some maximum frequency and no frequencies beyond that. The sampling must be chosen at least twice the maximum frequency. The minimum sampling rate allowed is called Nyquist rate which is the maximum frequency.

4.3.2 Reduced modelling based on POD method

The Galerkin projection will be used to construct lower order mathematical models. The objective of this approach is to replace the given dynamics by the dynamics of the subspace in the form

$$\dot{a}(t) = f(a(t)) \tag{4.18}$$

where $a(t)$ is the time-dependent amplitude of the basis functions.

For reduced modelling of the flow field, it is assumed that

$$\tilde{\boldsymbol{v}}(\boldsymbol{x},t) = \bar{\boldsymbol{v}}(\boldsymbol{x}) + \sum_{k=1}^{n} a_k(t)\boldsymbol{\phi}_k(\boldsymbol{x}) \tag{4.19}$$

with $a_k(t)$ determined from the Navier-Stokes equations given in equation (3.10).

If the operator $\int_\Omega \phi_{ji}\ ()\ d\Omega$, defined in a Hilbert space, is applied to the Navier-Stokes equation, the following reduced model can be obtained, i.e.

$$\frac{da_i}{dt} + b_i + \sum_{j=1}^{N} c_{ij}\ a_j + \sum_{j=1}^{N}\sum_{k=1}^{N} d_{ijk}\ a_j\ a_k = 0 \tag{4.20}$$

$$\begin{aligned} b_i \ &= \ \int_\Omega \nu_e \phi_{ji,k}\ (\bar{v}_{j,k}\ +\ \bar{v}_{k,j})\,\mathrm{d}\boldsymbol{x} \\ +\ \int_\Omega \phi_{ji}\ \bar{v}_k\ \bar{v}_{j,k}\,\mathrm{d}\boldsymbol{x} \ &+\ \int_\Sigma \phi_{ji} R_j\,\mathrm{d}\boldsymbol{x}, \end{aligned} \tag{4.21}$$

$$\begin{aligned} c_{ij} \ &= \ \int_\Omega \phi_{li}\ \bar{v}_{l,k}\ \phi_{kj}\,\mathrm{d}\boldsymbol{x} \\ &+\ \int_\Omega \phi_{li}\ \bar{v}_k\ \phi_{lj,k}\,\mathrm{d}\boldsymbol{x} \\ +\ \int_\Omega \nu_e \phi_{li,k}\ (\phi_{lj,k}\ &+\ \phi_{kj,l})\,\mathrm{d}\boldsymbol{x}, \end{aligned} \tag{4.22}$$

$$d_{ijk} \ = \ \int_\Omega \phi_{li}\ \phi_{mk}\phi_{lj,m}\,\mathrm{d}\boldsymbol{x} \tag{4.23}$$

where a tensor index notation with summation convention is adopted in equations (4.21–4.23) to simplify the expressions. Here the first subscript of $\boldsymbol{\phi}$ refers to the component of $\boldsymbol{\phi}$ as a vector whereas the second subscript denotes the order of $\boldsymbol{\phi}$ as an eigenfunction. In the problems under examination the boundary integral term in equation (4.21) is usually zero since $\boldsymbol{\phi}_i \cdot \boldsymbol{R} = 0$ on the boundary Σ for most cases. Note also that equation (3.11) is satisfied automatically since the basis functions created by the POD method are divergence free because of their definition see, for example, Sirovich (1987) .

4.4 MODEL REDUCTION FOR NON-STATIONARY FLOWS

For problems associated with non-stationary flows with forcing, the system under examination is of the form

$$\begin{aligned} \dot{\boldsymbol{v}}(\boldsymbol{x},t) &= NS(\boldsymbol{v}(\boldsymbol{x},t), c(\boldsymbol{x},t)) \\ z(t) &= h(\boldsymbol{v}(\boldsymbol{x},t)) \end{aligned} \tag{4.24}$$

where c denotes the control input and z represents an output signal.

4.4.1 Proper orthogonal decomposition method for non-stationary flows

If the fluid flow is time-periodically forced, phase relationships may not be captured by statistically stationary two-point correlations and therefore simultaneous measurements are required as discussed by Glezer (1989) . The classical POD method is based on two-point correlations of time series and is therefore not the best approach to non-stationary flows. For flows subject to time-dependent excitations, phase-independent correlations may not exist. As a result of the lack of stationarity, correlations therefore depend on the initial and final points in the time series.

Because of the statistical non-stationarity of the data, the computed eigensets derived from snapshots of the velocity field depend on the initial and final times of the portions of the time series under examination. For this purpose the POD method requires extension as described by Glezer *et al* (1989) in developing the EPOD method. This is an ensemble average of two-point correlations of velocity. For statistically stationary data, the EPOD is equivalent to the classical POD.

However, in an EPOD suboptimal control approach, the basis of the reduced model can be reset using the velocity field generated from the full flow solver from previous iterations.

For a flow simulation subject to an external forcing term $\boldsymbol{F}(\boldsymbol{x},t)$, the reduced model to determine the time-dependent amplitude of the basis functions $a_k(t)$ has a form similar to the one given in equation (4.20) with the right-hand-side 0 term replaced by

the generalized forcing term of $f_i(t)$ given by

$$f_i(\boldsymbol{x},t) = \int_\Omega \boldsymbol{F}(\boldsymbol{x},t)\cdot\boldsymbol{\phi}_i \,\mathrm{d}\boldsymbol{x}. \tag{4.25}$$

If the continuous forcing is specified as combinations of point forces acting at given locations in the fluid such that $\boldsymbol{F}(\boldsymbol{x},t) = \sum_l \tilde{\boldsymbol{F}}^{(l)}(t)\Delta(\boldsymbol{x}-\boldsymbol{\xi}^{(l)})$ then $f_i(t)$ can be expressed as

$$f_i(\boldsymbol{x},t) = \sum_l \tilde{\boldsymbol{F}}^{(l)}(t)\cdot\boldsymbol{\phi}_i(\boldsymbol{\xi}^{(l)}). \tag{4.26}$$

This type of forcing may be typified by a model of a distributed forcing in a flow field. This control strategy is physically very hard to implement however consistent with the control strategy argument in this thesis. A different control such as oscillating wires can be adopted for the same system with most probably similar behaviour.

4.5 NUMERICAL RESULTS

4.5.1 Performance of POD and EPOD basis

The POD, EPOD and ensemble-averaged POD methods are applied to data which are generated for different frequencies in $0.76<F<0.86$ associated with an oscillating circular cylinder for $Re = 500$. F is nondimensional frequency obtained by the dividing the frequency by vortex shedding frequency for $Re = 500$. The velocity profiles and eigenvectors from all the methods are comparable for the flow field examined in figures .4.4 to .4.11. Since the data sets are collected from the transient part of wake flow behind the oscillating cylinder, the EPOD method shows a better convergence behaviour than the POD and ensemble-averaged POD methods.

The data set from a fixed frequency F=0.76 is used in the POD method whereas data sets from different frequencies in $0.76<F<0.86$ are used in EPOD and ensemble-averaged POD methods. The size of the correlation matrix is the same for POD and ensemble-averaged POD methods but different for EPOD method depending on the number of realizations.

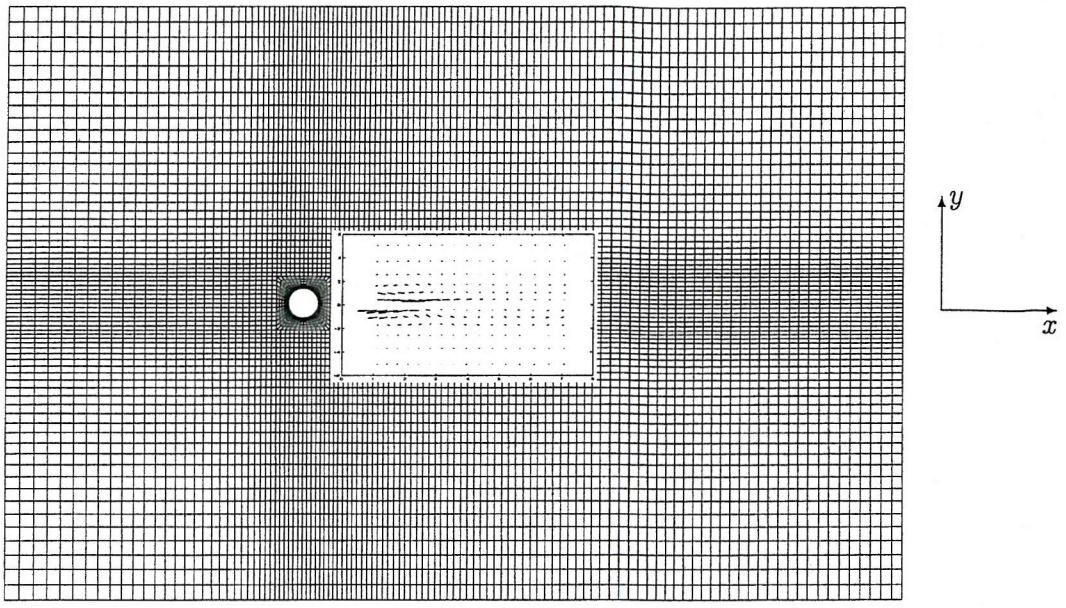

Figure 4.2: Typical uniform structured mesh idealising the fluid around the transversely oscillating cylinder. Within the domain shown the recorded velocity field where data are collected at each instant.

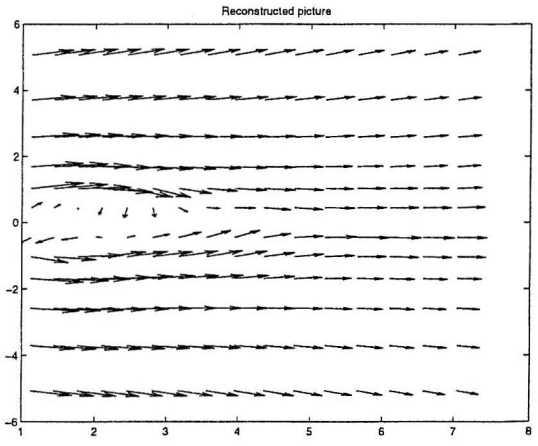

Figure 4.3: Simulated flow field and POD vector field using 20 modes superimposed. No visual difference can be observed from the flow.

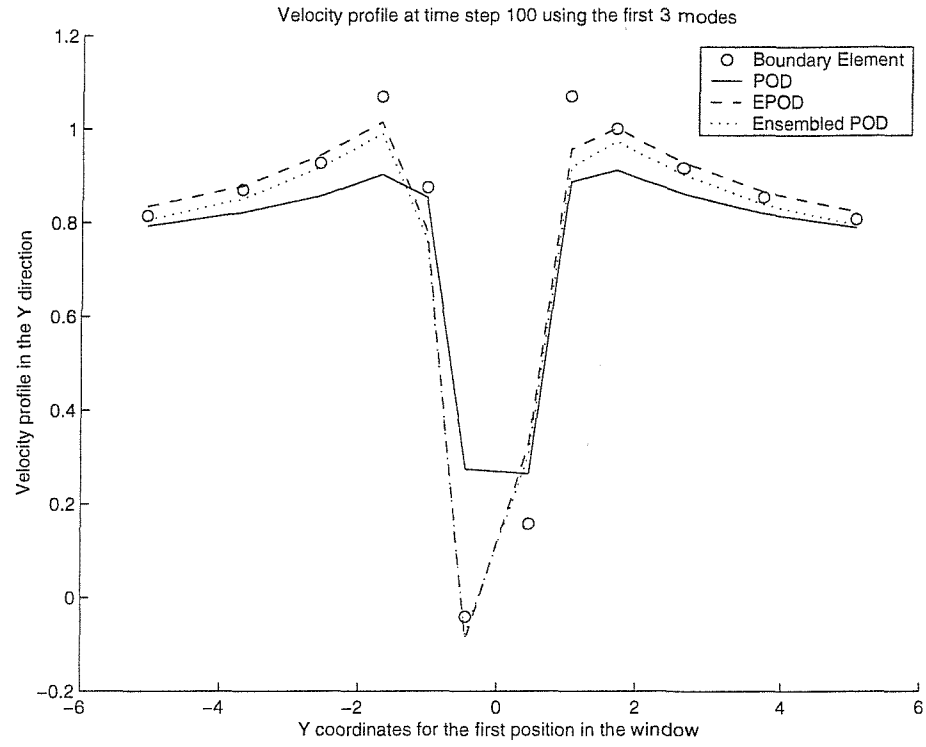

Figure 4.4: Velocity profiles for step 100 using different POD and 3 modes.

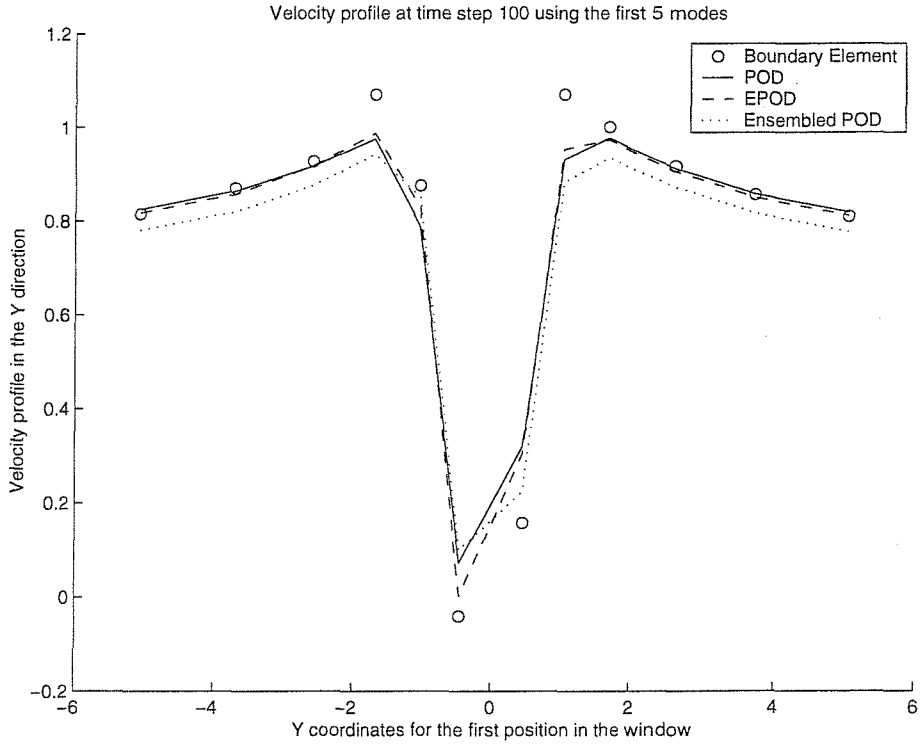

Figure 4.5: Velocity profiles for step 100 using different POD and 5 modes.

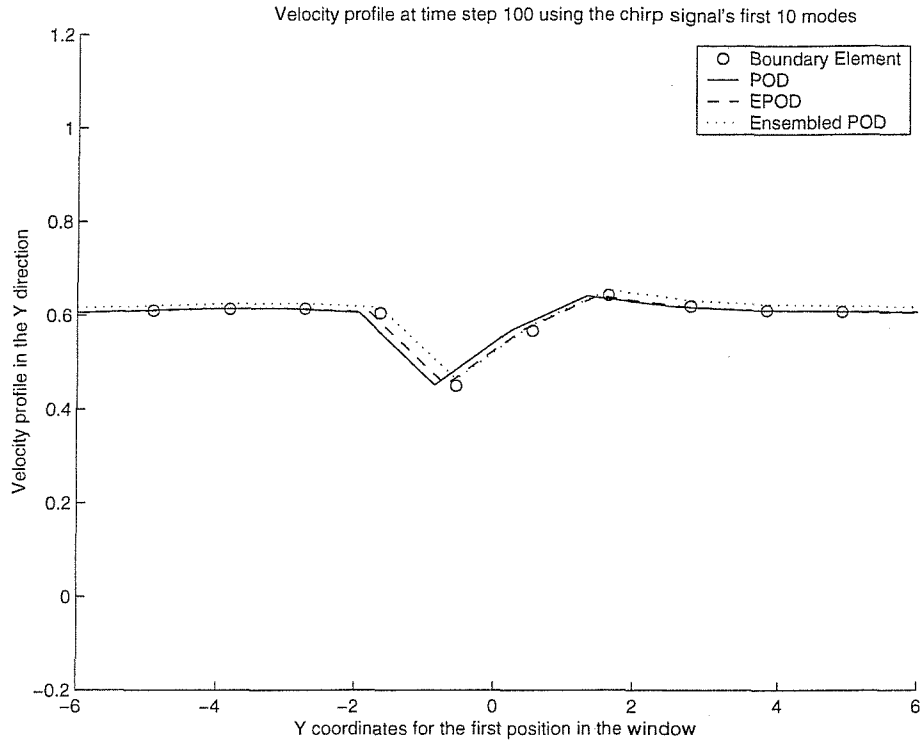

Figure 4.6: Velocity profiles for step 100 using different POD and 7 modes.

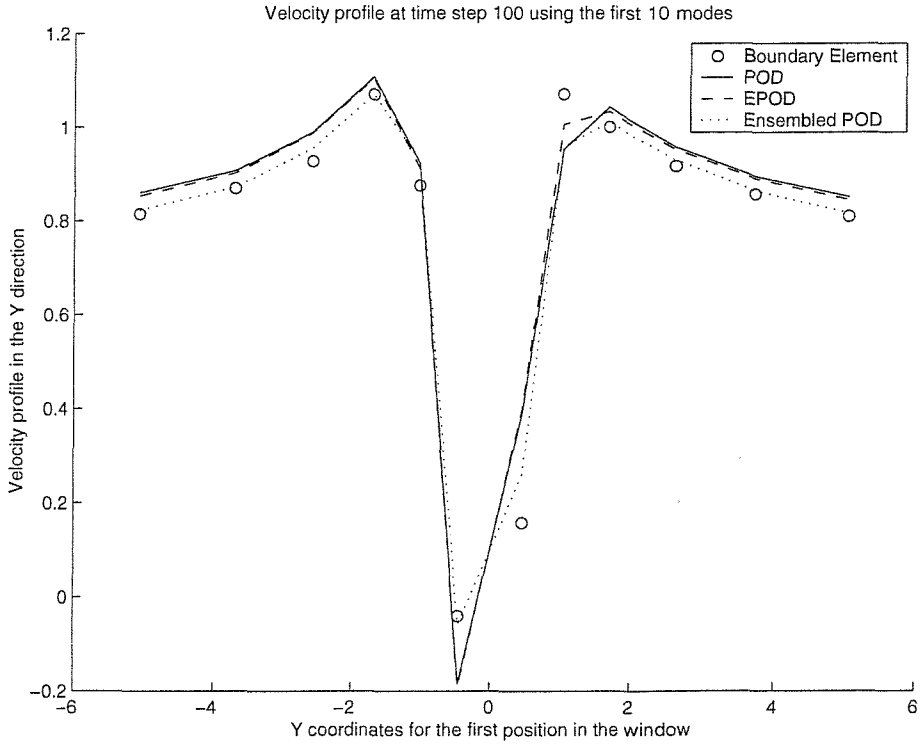

Figure 4.7: Velocity profiles for step 100 using different POD and 10 modes.

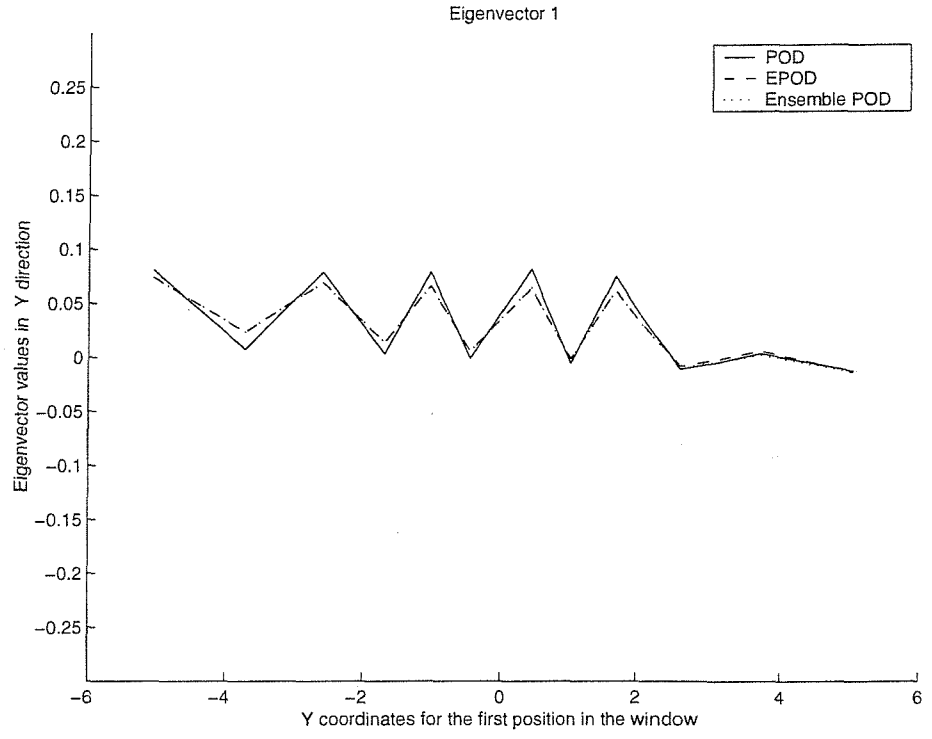

Figure 4.8: Eigenvectors 1 for POD, EPOD and ensemble POD.

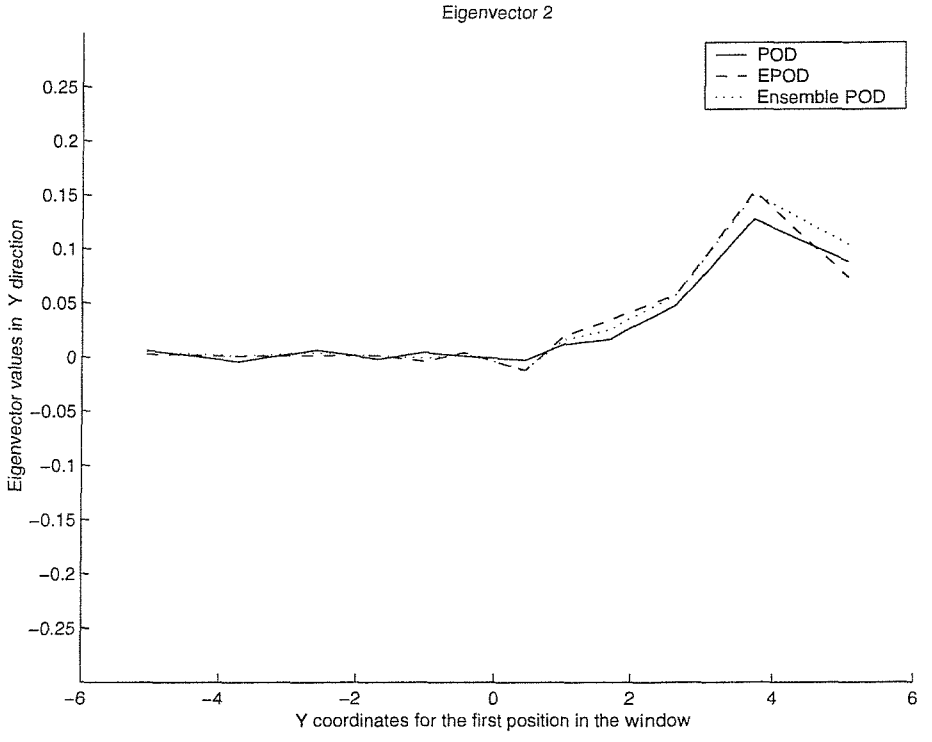

Figure 4.9: Eigenvectors 2 for POD, EPOD and ensemble POD.

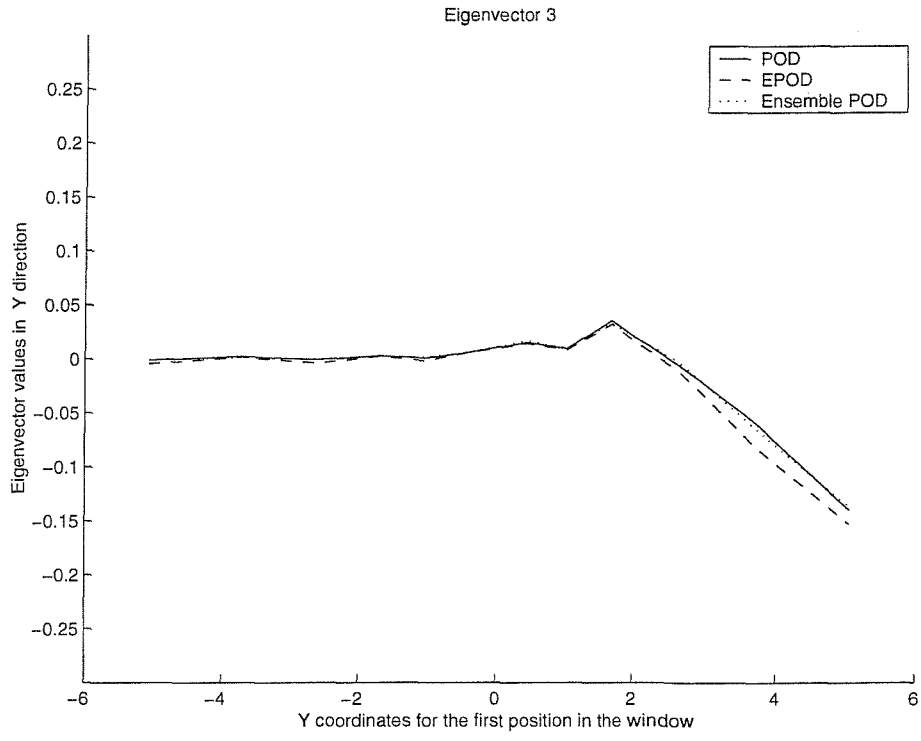

Figure 4.10: Eigenvectors 3 for POD, EPOD and ensemble POD.

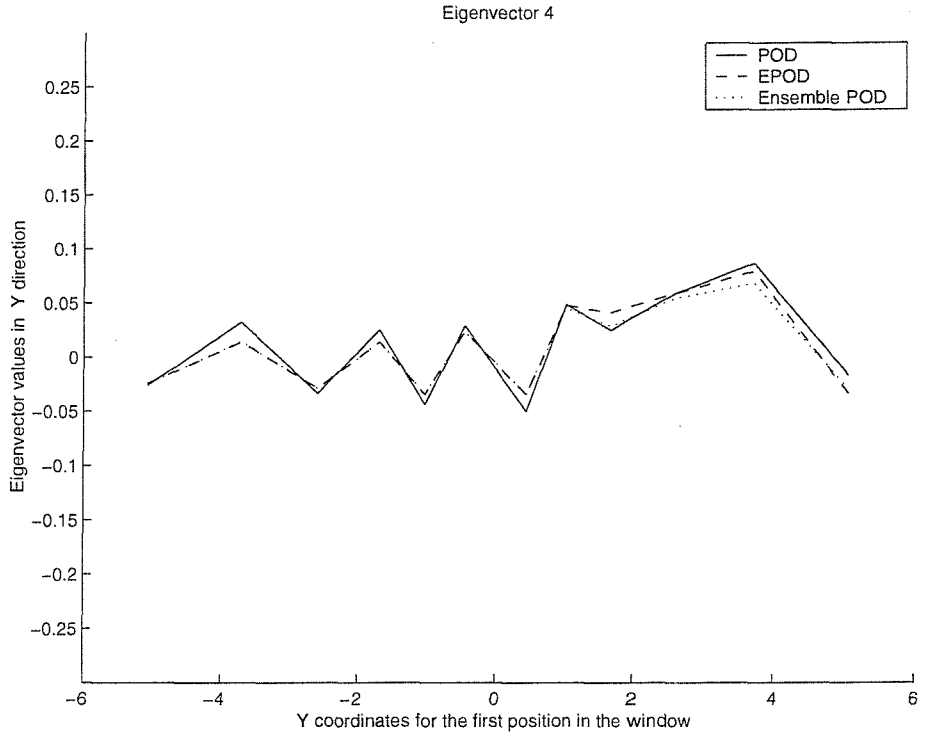

Figure 4.11: Eigenvectors 4 for POD, EPOD and ensemble POD.

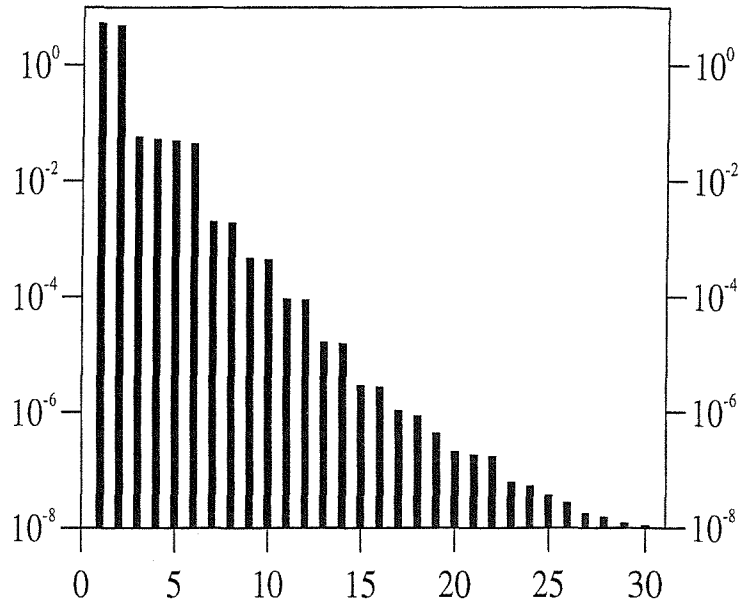

Figure 4.12: Magnitudes of the eigenvalues associated with different modes characterising the wake flow behind a cylinder in uniform flow at Re=200.

4.5.2 Reduced modelling for stationary flows

Using a cell viscous boundary element method, numerical data were derived describing the characteristics of vortex shedding in the wake of a circular cylinder in uniform flow at Re=200. Forty snapshots per cycle were collected. Fig.4.12 shows the magnitudes of the eigenvalues produced from this set of data. It confirms the rapid decrease of the magnitudes of the eigenvalues of higher modes and since they indicate the energy level in each mode, the results show that the first few modes contain most of the energy associated with this steady vortex shedding flow. Thus it is possible to capture the main features of the flow with a much reduced model as long as the dominant modes capturing this energy are included in the model.

Fig.4.13(a) shows the vector plots of a flow field represented by the time averaged flow in one cycle and fig.4.13(b,c) show the first two most energy dominant dynamic modes. The main features of the vortex shedding process can be constructed from these modes involving a phase shift in time.

When these eigenfunctions are used as basis functions in the POD method, their

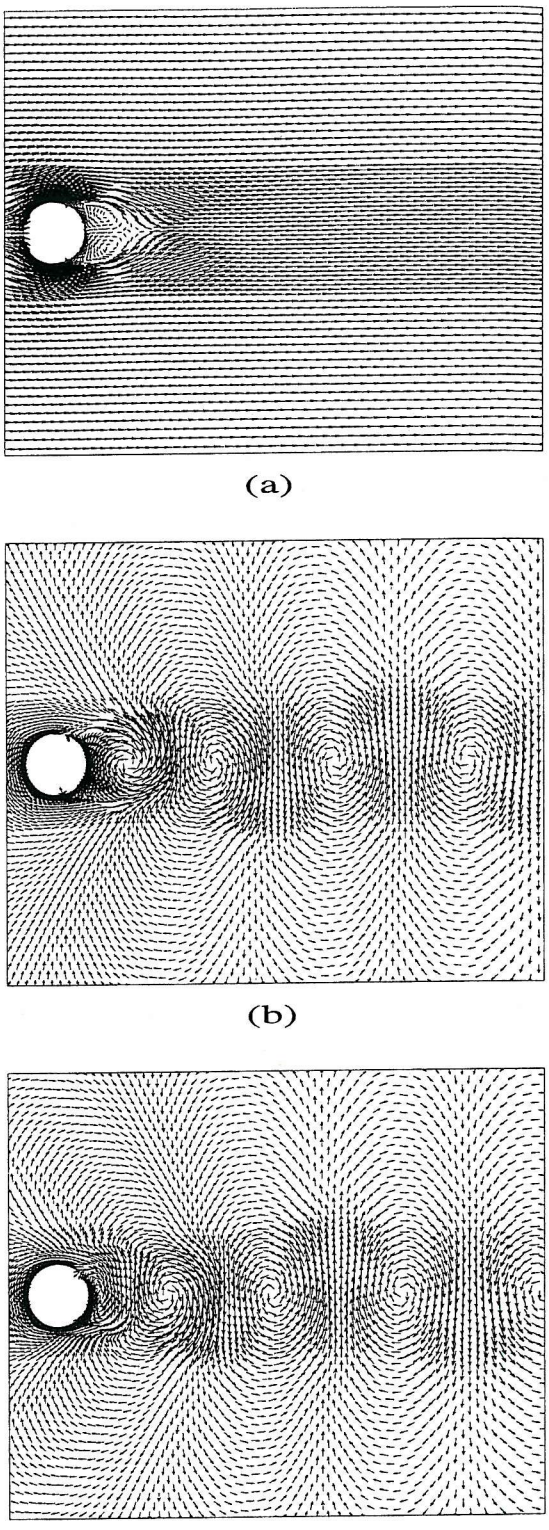

Figure 4.13: The vector plots of velocity of (a) mean flow, (b) mode 1, (c) mode 2.

No. of	Energy retained (%)		
modes	Re=100	Re=150	Re=200
2	97.195	97.754	97.996
4	99.161	98.955	99.058
6	99.970	99.955	99.952
8	99.997	99.992	99.989

Table 4.1: Percentage of energy retained in the reduced models vs. number of modes included.

amplitudes can be found by integrating equation (4.20). Here a 4th order Runge-Kutta method is used for the time integration and the results are plotted in fig.4.14 for the first 6 functions. The good agreement between the predicted and projected amplitudes of these basis functions confirms the validity and benefit of the POD method to model the type of flows under examination using low order models.

Table 4.1 illustrates the energy retained in the reduced model against the number of modes admitted in the analysis as a percentage of the total energy of all the dynamic modes. For the three cases examined, i.e. Reynolds number Re=100, 150 and 200, more than 99.9% of energy is retained if only the first 6 modes are adopted in the reduced models. It should be mentioned that before reaching Re=200, 3-D vortex shedding is onset (see Williamson (1988)).

Although Reynolds number (i.e. $\nu_e = 1/\mathrm{Re}$) is one of the parameters in the reduced model described by equations (4.20–4.23), equation (4.20) cannot be used to model flows at different Reynolds number without modifying the modes involved as well. In some cases, however, the snapshots of flows at different Reynolds numbers may be combined to approximate the snapshots at another Reynolds number which then can be used to produce basis functions in the POD method. As an example, 40 snapshots were collected from each flow simulation at Re=100 and Re=200. New snapshots at other Reynolds numbers (i.e. 100 <Re< 200) were generated by linear interpolation of these snapshots and this information incorporated in the reduced models to predict shedding frequencies. The results of the calculated Strouhal number are presented in

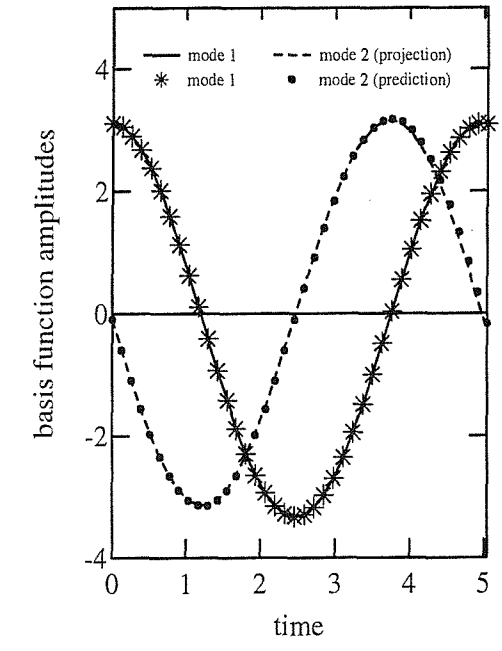

(a)

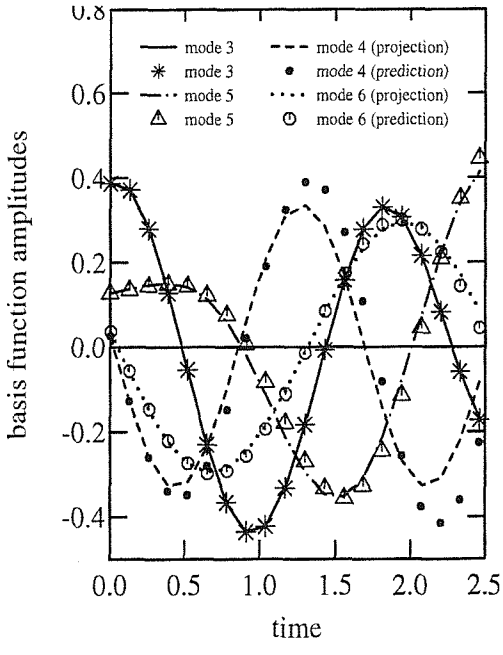

(b)

Figure 4.14: Comparisons of predicted and projected amplitudes of (a): first two modes; (b): modes 3-6.

Reynolds number	Strouhal number		Relative error (%)
	Predicted	Williamson (1988)	
100	0.1650	0.1643	0.4
110	0.1680	0.1690	0.6
120	0.1720	0.1731	0.6
130	0.1760	0.1768	0.5
140	0.1805	0.1802	0.2
150	0.1845	0.1834	0.6
160	0.1875	0.1864	0.6
170	0.1905	0.1892	0.7
180	0.1935	0.1919	0.8
190	0.1955	0.1945	0.5
200	0.1980	0.1970	0.5

Table 4.2: Predicted shedding frequencies vs. Reynolds number.

table 4.2 for a series of Reynolds numbers. Also included are data generated by the 'universal' empirical relationship given by Williamson (1988) . The experimentally determined Strouhal values of Williamson have an accuracy claimed 'to the 1% level' and the 'universal' empirical relationship was obtained through interpolation of the observed data. As can be seen from table 4.2, the agreement between the predicted Strouhal numbers and Williamson's data is very good.

4.5.3 Reduced modelling with control actions

Oscillatory body forces applied to the fluid are treated as an example of control actions. In the case considered, four oscillatory point forces are applied at the four points $(0.34, \pm 0.43)$ and $(1.05, \pm 0.68)$ behind the cylinder and their frequency of oscillation

is close to that observed in the vortex shedding process.

Three flow simulations were carried out using the reduced model with (a) no forcing included and (b) forcing applied in the x-direction only and (c) forcing applied in the y-direction only. The streakline patterns of these simulations are shown in fig.4.15 which illustrates clearly the effect of forcing on the vortex shedding process.

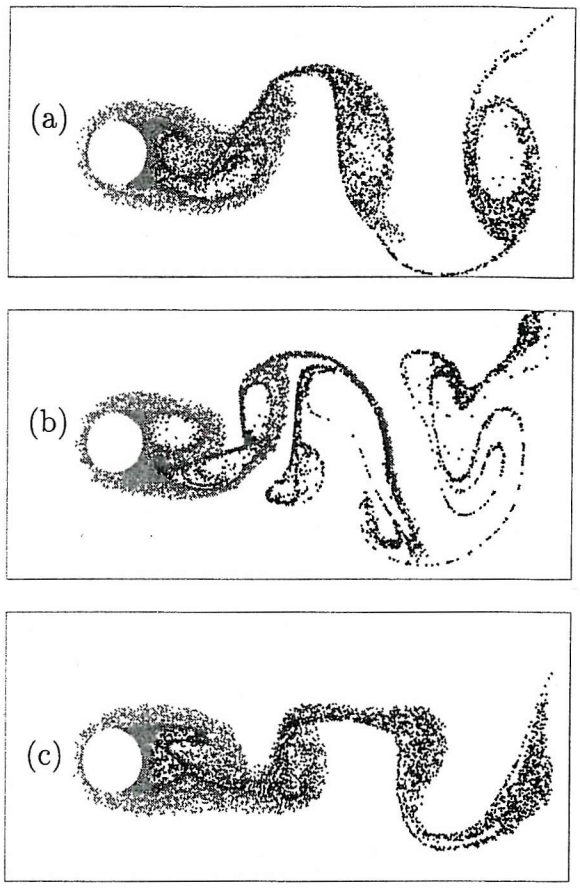

Figure 4.15: The streakline patterns of flows with (a): no forcing; (b): forcing in x direction; (c): forcing in y direction.

In order to investigate further the effect of the control actions in the reduced model, calculations were performed using forcing functions with different frequencies and amplitudes. The power spectrum of the velocity field generated by the reduced model was studied under different forcing conditions and data were obtained for the entrainment region defined by Gillies (1998) . The data are illustrated in fig.4.16 and the best fit curve shows a familiar V shape similar to Gillies' results.

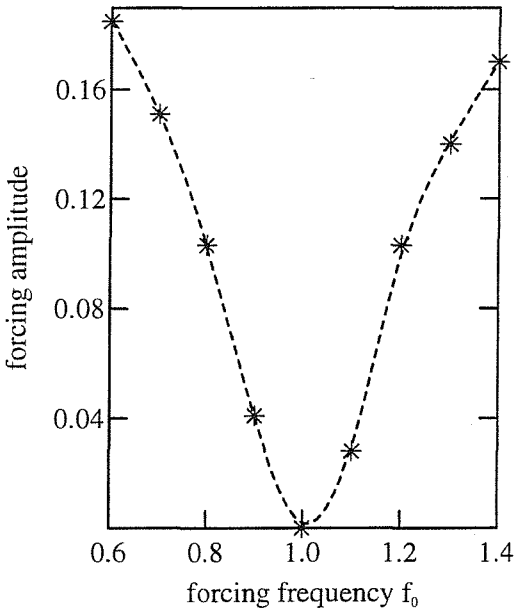

Figure 4.16: Forcing entrainment region .

4.6 CONCLUSION

A Proper Orthogonal Decomposition method is used to investigate reduced flow modelling of the vortex shedding wake exhibited behind a circular cylinder. The method is found very effective in creating reduced models to describe vortex shedding processes. The method can also be applied for different Reynolds number cases with modified snapshots or data sets.

A reduced model has also been constructed where forcing terms are treated as control actions in the fluid domain and flow simulations with different forcing descriptions have been conducted.

The method discussed herein can also be adopted to the situation when the control action is the forced oscillation of the cylinder. In this case the oscillation of the cylinder is treated as an inertial force term in the Navier-Stokes equations, if the problem is formulated in a body fixed reference system.

Chapter 5

FLOW CONTROL

The ability to manipulate actively or passively a flow field to effect a desired change has technological importance. Methods of control to achieve transition delay, separation postponement, lift enhancement, drag reduction, turbulence augmentation, or noise suppression are reviewed in this chapter. This chapter mainly concentrates on external flows. Internal flows are also mentioned. The physical aspects of the flow control along with the basics of the flow regime and flow stability classification are reviewed rather than aspects which are related to mathematical modelling methods of controller design. A limited review of some of these methods are found in the next chapter.

5.1 INTRODUCTION

Flow control involves passive or active devices to effect a beneficial change in wall-bounded or free-shear flows. The task might be to delay/advance transition, to suppress/enhance turbulence or to prevent/provoke separation. Drag reduction, lift enhancement and flow-induced noise suppression are some of the possible outputs. Complex reactive control devices have been used to control the flow as discussed by Hak (1989) . Theoretical advances such as chaos theory, neural networks, etc also help the development in this field parallel to technological developments.

The first developments in flow control were empirical and can be traced back to prehistoric times when streamlined spears, sickle-shaped boomerangs, and fin-stabilized arrows were used (see Hak (1989)) . Manipulating an external boundary-layer flow

such as that developing on the exterior surface of an aircraft or a submarine, to achieve transition delay, separation postponement, lift enhancement, drag reduction, turbulence augmentation, or noise suppression is a particular field of flow control which is of interest to naval and aeronautical engineer.

5.2 WALL-BOUNDED AND FREE-SHEAR FLOWS

The control strategy is chosen based on the kind of flow and the control goal on what the designer plans to achieve. Presence or lack of walls, Reynolds number, Mach number, and the character of flow instabilities are all important considerations for the type of flow to be controlled. Herein, these concepts are reviewed.

5.2.1 Inviscid and viscous instabilities

Free-shear flows which are jets, wakes or mixing-layers, have inflectional velocity profiles. In an inflectional velocity profile, the second derivative of the velocity profile is equal to zero at certain inflectional points. These flows are easily influenced by inviscid instabilities (see Hak(1989)) . Viscosity is only a damping influence in this case, and the prime instability mechanism is vortical induction (see Hak(1989)). Control aims for these kind of flows consist of transition delay/advancement, mixing enhancement and noise suppression. External and internal wall-bounded flows, such as boundary layers and channel flows, can have inflectional velocity profiles, but in the absence of opposing pressure-gradient and similar effects. These are characterized by non-inflectional profiles, and viscous instabilities must then to be considered. Free-shear flows and separated boundary layers are as of nature unstable and they can be much easily manipulated.

Free-shear are the flows that originate from some kind of surface upstream be it a nozzle, a moving body or a splitter plate, and flow control devices can therefore be placed on the corresponding walls far from the fully developed flows (see Williams (1989) .

5.2.2 Reynolds and Mach numbers

The Reynolds number determines if the regime is turbulent or laminar. For low-to-moderate Reynolds number such as (0¡Re¡200) for the cylinder in an uniform flow, the flow is laminar. As a result of existing instabilities free-shear flows undergo transition at extremely low Reynolds number as compared to wall-bounded flows. A set of technologies are available to delay laminar to turbulence for both kind of flows (see Hak (1996)), but it is not aimed to do similarly to indefinitely high Reynolds number flows. For Reynolds numbers beyond a reasonable limit, one should not attempt to prevent transition but rather deal with the ensuing turbulence for instance to achieve separation delay, enhanced mixing or augmented heat transfer. Advancing transition is observed to be simpler than trying to delay it as discussed by Hak (1989) .

Mach number determines whether the flow is incompressible ($Ma < 0.3$) or compressible ($Ma > 0.3$). The latter regime is further divided into subsonic ($Ma < 1$), transonic ($0.8 < Ma < 1.2$), supersonic ($Ma > 1$), and hypersonic ($Ma > 5$). For each of these flow regimes, different methods of flow control schemes are employed. For example during laminar-to-turbulence transition initial disturbances and disturbances are subsequently amplified by various linear and non-linear mechanisms. Under the assumption of avoiding by-pass mechanisms (surface roughness, high levels of freestream turbulence) as discussed by Hak (1989) delaying transition can be reduced to controlling a variety of possible linear modes: e.g. Tollmien-Schlichting modes, crossflow instabilities and Gortler instabilities. Tollmien-Schlichting instabilities dominate the transition process for two-dimensional boundary layers defined by $Ma < 4$, and are damped by increasing the Mach number, by wall cooling(in gases), and by the presence of favourable pressure-gradient. Mach instabilities are also damped by increasing the Mach number and by presence of favourable pressure gradient, but are destabilized by wall cooling. Crossflow and Gortler instabilities are caused by, respectively, the development of inflectional crossflow velocity profile.

5.2.3 Convective and absolute instabilities

In addition to grouping different kinds of hydrodynamic instabilities as inviscid or viscous, one could classify them as convective or absolute based on the linear response of the system to an initial localized impulse as discussed by Huerre (1990) . A flow

is convectively unstable if all the growing disturbances convect downstream from their source. Suppression of convective instabilities is particularly effective when applied near the point where the perturbations originate. The flow is absolutely unstable if the local system response to an initial impulse grows in time. In this case, some of the growing disturbances can travel back upstream and continually disrupt the flow even after the initial disturbance is neutralized. Absolute instabilities are generally more dangerous and more difficult to control; nothing short of complete suppression will work. In some flows, for example two-dimensional blunt-body wakes, certain regions are absolutely unstable while others are convectively unstable.

5.2.4 Classical control tools used to supress these regimes and instabilites

Natural laminar flow (NLF) is related to control of flow by changing the shape of the body to achieve lower-skin friction drag and favourable pressure-gradient. Laminar flow control (LFC), in contrast, uses suction, wall heating/cooling, and other active ways of control to supress the proper instability modes. LFC is developing with removal of technological problems related to cost, maintenance and reliability (see Hak (1996).

LFC is an active boundary-layer flow control usually employing a suction technique employed to maintain the laminar state at Reynolds number beyond that which is normally characterized as being transitional or turbulent in the absence of control. LFC does not imply the relaminarization of a turbulent flow state but the suppression of the state. The energy requirements for relaminarization are observed typically to be an order of magnitude greater than that required for LFC. Finally, LFC is a capability that is designed to benefit an aircraft or a ship during cruise by reducing the drag. A significant advancement made in the development of LFC technology is the concept of Hybrid Laminar Flow Control (HLFC). HLFC integrates the concepts of NLF with LFC to reduce suction requirements and reduce system complexity. LFC is complex, involving suction and ducts, flutes, and pump source over the whole-wing chord.

The reason laminar flow is usually more desirable than turbulent flow for external aerodynamic and hydrodynamic vehicles lies with the reduction of the viscous drag. We have some understanding of the fundamental flow physics for the problem to de-

sign an optimal, reliable cost-effective system to control the flow. The first theoretical contributions to the study of boundary-layer transition were made by Kelvin (1880), Reynolds (1883), Rayleigh(1879,1880,1887) . These early investigations neglected the effects of viscosity, the second derivative of the mean velocity proved to be of key importance in explaining boundary-layer instabilities. These fundamental studies proved to be the basis for future breakthroughs in theoretical development, including inviscid jet-flow instabilities and shear-layer instabilities. Adding viscous effects, Orr (1907) and Sommerfeld (1908) developed an ordinary differential equation (Orr-Sommerfeld equation) that governs the linear instability of two-dimensional disturbances in incompressible boundary-layer flow on flat plates. Later, Squire (1933) accounted for three-dimensional waves by introducing a transformation from three to two dimensions. This analysis showed that two-dimensional waves were dominant in flat plate boundary layers. Tollmien (1929) and Schlichting (1932) discovered convective travelling-wave instabilities now termed Tollmien-Schlichting (TS) instabilities, and Liepmann (1943) and Schubauer and Skramstad (1947) experimentally confirmed the existence and amplification of these TS instabilities in the boundary layer. This disturbance can be imagined by the picture of water waves created by dropping a pebble into a still lake or puddle. The waves which are generated decay as they travel from the source. It is the same case for boundary-layer flow, except that the waves grow in strength when certain critical flow parameters, such as Reynolds number, are reached and lead to turbulent flow. Taylor-Gortler vortex disturbances arise when the surface geometry becomes concave and they are created by counter-rotating vortices. The design engineer would have to be sensitive to this disturbance only if there is concave curvature such as on the lower surface of a wing; otherwise, this disturbance is not too significant for LFC applications. See Smith (1955) , Wortmann (1969) and Hall (1983) for more detailed discussions of Taylor-Gortler vortices. In addition to transition dominated by TS distur bance, a dynamic instability, termed the crossflow (CF) disturbance, is an important factor in the extent of laminar flow realized.

Compliant coatings offer a simple method to deal with laminar-to-turbulence transition. It is a passive technique relatively easy to apply to an existing vehicle or device. To reduce skin-friction drag in turbulent wall-bounded flows include riblets, polymers. Polymers, for example, have been used in the Trans-Alaskan pipeline (see Hak (1989)).

5.3 DIFFERENT CLASSIFICATION SCHEMES FOR FLOW CONTROL METHODS

Different classification schemes for flow control methods exist. This section gives a summary of the major flow classification methods that are found in literature.

5.3.1 Classification by distance to a wall

One can consider whether the technique is applied at the wall or away from it. The surface parameters influencing the flow include roughness, shape, curvature, rigid-wall motion, compliance, temperature, and porosity. Heating and cooling of the surface influence the flow via the resulting viscosity and density gradients. Mass transfer takes place through a porous wall or a wall with slots. Suction and injection of primary fluid have significant effects on the flow field, influencing particularly the shape of the velocity profile near the wall and thus the boundary layer susceptibility to transition and separation. Different additives, such as polymers, surfactants, micro-bubbles, droplets, particles, dust or fibers, can also be injected through the surface in water or air wall-bounded flows. Control devices located away from the surface can also be beneficial. Large-eddy breakup devices, acoustic waves bombarding the shear layer from outside, additives introduced in the middle of a shear layer, manipulation of freestream turbulence levels and spectra, gust, and magneto- and electro- hyrodynamic body forces are examples of flow control strategies applied away from the wall.

5.3.2 Classification by energy expenditure and the control loop involved

Energy expenditure and the control loop involved is one criterion used for classification. A control device can be a passive device, requiring no auxiliary power, or active, requiring energy expenditure (see Hak (1996)). Active control is further divided into predetermined and active control. Predetermined control includes the application of steady or unsteady energy input without regard to the particular state of the flow. The control loop in this case is open. Reactive control is a special case of flow control where

the control input is continuously adjusted based on measurements of some kind. The control loop in this case can either be an open, feedforward one or a closed, feedback loop (see Hak (1996)). Classical control theory deals, for the most part, with reactive control. In feedforward control, the measured variable and the controlled variable differ. For example, the pressure or the velocity can be sensed at an upstream location, the resulting signal is used together with an appropriate control law to trigger an actuator which in turn influences the velocity at a downstream position. Feedback control, on the other hand, necessitates that the controlled variable be measured, fed back and compared with a reference point. Reactive feedback control includes adaptive, physical model-based, dynamical systems-based, and optimal control.

Another way of classification is considering if the control technique directly modifies the shape of the instantaneous/mean velocity profile or selectively influence the small dissipative eddies.

5.4 IMPLEMENTATION ISSUES

Any feedback control system consists of three components: actuators, sensors, and the control law. The most development in the past few years in the area of implementing turbulence control ideas has been the emergence of Micro Electro Mechanical Systems (MEMS) technology, which benefit from the methods developed for the fabrication of silicon chips to construct very small mechanical devices as discussed by Wise (1991) and Moin (1994). Miniaturization of this scale for both sensors and actuators is necessary for feedback control of turbulence due to the very small scales of the coherent structures in high Reynolds number flows of engineering interest. Researchers are attempting to miniaturize several of the devices reviewed herein using MEMS technology.

5.4.1 Methods of sensing

Two desirable attributes of flow sensors are that they be robust and they create minimum disturbance in the flow. For these reasons, most practical sensors for active flow control are mounted on a wall. At a wall, we may measure both skin friction and wall pressure. For situations in which the wall pressure is important ,for instance, in control schemes designed to reduce flow-induced noise, there are a set of devices, essentially

small microphones, which have been developed for measuring pressure fluctuations. One example by Cho (1989) is a capacitive pressure sensor built with a small flexible membrane. Note, however, that it has been found by Choi (1994) that pressure is not a good indicator for detecting and controlling the sweep and ejection events which accompany near-wall coherent structures in wall-bounded flows. Using a Taylor series extrapolation, the near wall flow may be estimated directly from shear stress measurements on the wall, though these estimates are only valid fairly near the wall as discussed Choi (1994) . In order to measure shear stress at a wall, several types of sensors have been investigated recently (see Bewley (1994)). We will review the most popular ones: floating element sensors, piezo-electric foils, hot films, and surface acoustic wave (SAW) sensors. A floating element sensor consists of a small rectangular patch of silicon supported by thin beams. The flow over the device exerts shear forces on the patch and the resulting stresses in the supporting beams may be measured by various methods, including the differential measure of capacitance and an active electrostatic re-balancing technique with a comb actuator as discussed by Jaecklin (1992) . This device is attractive because it directly measures shear stress in a way that does not interfere with the flow. Further improvements of design and manufacturing techniques may make this device quite promising. Nitsche *et al* (1989) describe piezoelectric foils consisting of thin films of polyvinylidene fluoride (PVDF) coated with a very thin layer of aluminum. Portions of the PVDF films are crystallized, and the resulting artificial polarization exhibits a piezoelectric effect when subjected to normal and shear stresses. Detectors placed below the films then sense the field created by the piezo effect of the sheared crystal. The production of these devices is simple and robust, but their sensitivity to both normal and shear stresses create difficulties. To measure shear stress, Nische (1989) proposed placing two detectors side by side in opposite configurations so that, by combining the signals from the two sensors, the effects of the normal stress cancel and the resulting signal is proportional to the shear stress. However, it has been observed that the small magnitude of the measured signals result in the familiar problem of losing the signal in the noise created by imperfect cancellation of the contributions due to the normal stress fluctuations. As an indirect measure of skin friction, a hot film sensor may be used by calibrating the heat transfer of the film as a function of the applied shear; although care must be taken in this calibration, as the static and dynamic responses differ and the response is nonlinear. This kind of a sensor is easy

to manufacture but difficult to use as it is unable to measure skin friction directly; if used underwater, a hot film sensor must be thermally coupled but electrically isolated from the flow, and the thermal cross talk from other sensors and/or actuators must be minimized. Instruments can also be built to measure the propagation speed of surface acoustic waves. The surface wave propagation speed is a function of the stresses caused by the flow. By building devices which measure the wave speed in alternate directions, it is possible to estimate the instantaneous shear stress. These devices are quite sensitive and respond linearly to shear stress. However, they are also sensitive to the normal stress, temperature fluctuations, electric noise, and drift of the resonant frequency of the oscillator circuit and any system using SAW devices must be able to account for these dependencies in a way that encapsulates the signal in the noise created by imperfect cancellation in the differencing process (see Moin *et al* (1994) for SAW sensors and hot film sensors).

5.4.2 Methods of actuation

A series of ideas for the active manipulation of small scale turbulent structures near a wall are investigated (see Moin *et al* (1994)). A beam situated over a cavity which is allowed to passively fill with fluid from all sides is one manipulation method. By vibrating the beam at its resonant frequency, it can be made to force the fluid out of the cavity. The vibration can be created by a piezoelectric effect or by periodic optical heating of one side of the beam. The output through the narrow gap is concentrated and directed primarily in the vertical direction. By taking advantage of the different flow patterns caused by upward and downward motions of the beam, a strong flow pattern may be established. It has been observed that the flow field created by such a device is a set of counter-rotating vortices centred over the narrow gap with common flow up. By modulating the vibration amplitude, the magnitude of this disturbance may be controlled. An advantage of this method is the strong flow field it can create; disadvantages are that this flow field is necessarily quite complicated and the beam itself is difficult to manufacture and rather fragile.

Electrostatic forces or conventional speakers may be used to pump the fluid inside a cavity, the cavity has to a small hole through which the excess volume of fluid must travel. This results in very precise blowing and suction applied through the

actuation hole. Difficulties include the fragility of the membrane and the tendency of the membrane to short out by touching the lower wall of the cavity. A bump on a surface which may be regulated by a piezoelectric material underneath a membrane is another manipulation method as proposed by Lumley (1989). In Lumley's configuration, the bump is approximately Gaussian in shape. The flow field caused by the bump may be visualized as a horseshoe vortex with a common flow towards the wall immediately downstream of the device. One problem with this device is that getting sufficient displacement with piezo material is difficult. Another different mechanism which brings out this problem but has a significant activation time is a solenoid-activated valve leading to a high pressure source below the membrane. A modification of this idea is to create the pressure below the membrane by a controlled phase transition boiling. Bumps may also be activated by attaching magnets to the membrane and situating electromagnets below or electrostatically forcing the membrane itself. Variable bump devices have the potential of being more robust than cantilevered beams and pumped cavities; however, the perturbation to the flow field caused by the bump has been observed to be complex (see Moin *et al* (1994)). Differential wall heating is another possible method of control. Using wall heating to create the velocity fluctuations has several simultaneous effects, including the alteration of the specific volume of the heated fluid, associated buoyancy effects, and changes in viscosity, all of which should be accounted for by the control scheme. The idea has been attractive from the robustness standpoint because it has no moving parts. However, for control of turbulence in practical applications, very high power heaters and very low thermal capacitance of the wall is required to achieve the necessary frequency response. This might be possible using a laser with optical fibre access to small metal patches on the surface (see Bewley *et al* (2000)). Finally, if the fluid is electrolytic or can easily be made that way by addition of salts, hydrodynamic Lorenz forcing is another control option as discussed by Nosenchuck *et al* (1993). The upper loop work of Nosenchuck, though open loop, is an example of the effectiveness of this forcing technique. In their configuration, electric and magnetic fields are applied in the streamwise and spanwise directions with the use of well-positioned magnets and electrodes. By varying the electric field with an active control circuit, this configuration could be used in a feedback configuration. However, manufacturing such units on a scale small enough to interact actively with turbulent coherent structures might prove to be difficult.

5.5 CONCLUSION

Current investigations of several different methods of possible feedback control schemes provide the theoretical groundwork for future applications. Current investigations of the feedback control of turbulence are enhancing our fundamental understanding of the mechanisms responsible for the maintenance and regeneration of turbulence itself. The advent of Micro Electro Mechanical Systems technology for both sensors and actuators allows us to begin to consider practical implementations. The areas which are currently most promising for the implementation of feedback control schemes have critical areas where the flow is quite sensitive to modification, such as areas of separation or transition.

Chapter 6

CONTROLLER DESIGN

As traditional scientific disciplines grow towards maturity, many new opportunities for significant advances lie at their interaction. For example, significant developments in control theory in the last few decades have expanded the selection of available tools which may be applied to regulate physical and electrical systems (see Bewley *et al* (2001)). These techniques hold great promise for several applications in fluid mechanics, including the delay of transition and the regulation of turbulence. Such applications of control theory require a view, in which one considers the relevant flow physics when designing the control algorithms and conversely takes into account the requirements and limitations of control algorithms when designing both reduced-order flow models and the fluid-mechanical systems to be controlled themselves.

6.1 INTRODUCTION

The development of the technology necessary to produce micro-scale mechanical devices, referred to as Micro-Electro-Mechanical Systems (MEMS), has initiated researchers to investigate the possibility of using micro-scale actuation for the control of unstable phenomena in order to achieve macro-scale effects that such control effort is possible in chaotic systems,such as turbulence, is due to the extreme sensitivity of such systems to small levels of control forcing. Fundamental interest in such problems, of course, is the determination of when and where control should be applied to maximize the desired effect. The original idea for the development of MEMS was given

by Richard Feynman (1959) in his classic lecture at the American Physical Society entitled "There's Plenty of Room at the Bottom" which Feynman foresaw many of the techniques and challenges investigated by the MEMS community today. The technology developed for the fabrication of silicon chips has been a development in research focussing on MEMS. For reviews of recent developments of MEMS technology which relate to micro-scale measurement and control in fluid mechanics, the reader is referred to Ho and Tai (1996), McMichael (1996), Gad El Hak (1996) and Moin and Bewley (1994) . These reviews discuss a variety of sensors and actuators currently under development suitable for application in feedback control. The problems in MEMS development today are how to design such devices to be durable in hostile environments and how to produce such devices at high yield and low cost. In the future it might be possible to use MEMS technology to measure small-scale turbulent fluctuations of a flow and to apply coordinated small-scale forcing to the flow in order to achieve a desired large scale effect. Examples of problems of particular interest include reducing drag, reducing heat transfer, delaying transition, delaying separation, increasing mixing, and reducing levels of wall-pressure fluctuations and/or radiated sound.

We now summarize a few of the recent approaches used to determine implementable feedback control algorithms for flows, categorizing these approaches to the feedback control problem by examining their mathematical dependence on the equation governing the system. This brief survey of this active field of research puts the present approach in context with a sampling of the other techniques currently under investigation. For a more thorough discussion in this area, see Moin and Bewley (1994) .

6.1.1 Adaptive networks

The first class of schemes which are proposed to achieve small scale flow control actually makes no explicit reference to the dynamics known to take place in the flow or the Navier-Stokes equation which governs these dynamics. Instead, a reasonable network is generated which takes as input those measurable flow quantities assumed to be most relevant to the control problem and produces as output the requisited control velocity. The coefficients of this network are then trained by applying the control network to the flow and gradually adjusting the coefficients in a heuristic manner based on the resulting

evolution of the flow. Note that there are many different approaches to adaptive control. Hertz *et al* (1991) and Ioannou *et al* (1996) discuss several possible techniques. The main advantage of the adaptive approach is that the feedback coefficients can be adjusted to compensate for changing characteristics of the system being controlled, such as modification of the mean flow speed and direction, the sensitivity of the sensors, and the responsiveness of the actuators. As an example of one adaptive approach, an adaptive inverse technique has been applied by Lee *et al* (1996). This approach first develops an approximate inverse model between measurable quantities as input and the control forcing as output with an adaptive technique. This is done by forcing the system with small, sufficiently rich control signals which force the system, with a variety of different directions while monitoring the response of the measurements. From these data, a network is constructed, which attempts to reproduce and model the control used, based on the measurements taken. In an inherently nonlinear system such as turbulence, this is a challenging proposition, as any simple linear expression of this relationship would probably be highly nonstationary. Each iteration of the adaptation for this inverse model consists of three steps: (i) computing the error of the model output with respect to the desired model output the actual control forcing used, (ii) determining the influence of the various weights in the model on this error and (iii) updating all the weights in the model a small amount to reduce the error. When applied to the nonlinear adaptive networks commonly used for this purpose, known as neural networks, this is referred to as back-propagation of the error. Once the approximate inverse model between the flow measurements and the control converges for the open-loop system, the inverse model is used to determine a control which drives the flow measurements towards some desired state. This control is applied to the flow, and the inverse model is further trained to adapt it to the new characteristics of the closed-loop system.

6.1.2 Schemes based on understanding of dominant physics

In situations in which the dominant physics is well understood, judgment can guide an engineer to design effective control schemes. Success is limited, however, by the engineer's understanding of the physical processes involved; in the case of turbulence, our understanding is still limited despite several decades of intense research.

6.1.3 Extrapolation of linear control theory

The application of linear control theory to the linearized Navier-Stokes equation can be found in literature see, e.g., Joshi *et al* (1997) and Baramov *et al* (2000) and Bewley *et al* (1998) for the application of modern control theory. There are some critical points that there are concerning the practicality of the algorithms.

One issue is the most appropriate method for linear model reduction. Cortelezzi *et al* (1999) obtains a linear model reduction by truncating those linear eigenmodes with low observability or controllability from a model of a 2D unsteady channel flow. Researchers are beginning to consider the extrapolation of the linear control feedback determined by linear control theory directly to the fully nonlinear problem of a turbulent flow. The first reason to try such an approach is simply because the tools for determining and implementing linear control feedback are already available and we can therefore attempt to exploit everything we can from our ability to compute linear controls. Though the significance of this result has been debated by Farrell *et al* (1993) whatever information the linearized equation actually contains about the real mechanisms for formation of streamwise vortices and streamwise streaks, the linear controllers can exploit. Important possible pitfalls of applying linear control feedback to stabilize large flow perturbations, such as those on a chaotic attractor where the effects of the nonlinear terms are essential to describe the system's behaviour are illustrated for a simple model problem by Bewley (1999). It is shown by Bewley (1999) that such an approach can lead to closed-loop systems which can either converge to the wrong state or even blow up unless the appropriate nonlinear phenomena are introduced.

6.1.4 Reduced order nonlinear models

When considering the control of the multi-scale phenomena of turbulence, it is clear that an accurate reduced-order nonlinear model as an alternative to direct numerical simulation would simplify the control problem greatly. An efficent reduced-order representation is a necessity if we are ever to attempt to implement an estimator-based control algorithm, even if the dynamics of such a reduced-order model does not follow closely the dynamics of the full Navier-Stokes system without substantial measurement feedback. Such reduced-order models for turbulent flows have been sought for years, though the suitability of current approaches to provide such models for a controlled

turbulent flow for which the dynamics is substantially altered from that of the uncontrolled turbulent flow is still an open question. The techniques of dynamical systems theory have encountered some success to analyze and interpret turbulence dynamics as discussed by Aubry *et al* (1988); Holmes *et al* (1996). An example of one approach to determine reduced-order models is the ongoing work of anatomizing the coherent structures of turbulence using the proper orthogonal decomposition (POD) by Berkooz *et al* (1993). This decomposition provides a numerically determined set of modes which is particularly efficient, at least when no control is applied to the flow. However, the equation expressing the evolution of and interaction between these modes might be complex. It remains to be determined the best way to extract POD modes for a controlled turbulent flow. Some sort of iterative technique, in which the control algorithm and the POD modes are sought simultaneously, might be required in order to extract a set of modes which efficiently captures the energetic structures actually present in the controlled flow. As the controlled flow is not statistically stationary one might ultimately need a sequence of different POD models/control algorithms to completely relaminarize an initially turbulent flow, with the controller scheduling required based on an evolving bulk flow statistic such as total drag or total kinetic energy. As a preliminary example of control using such a reduced-order model, Coller *et al* (1994) considers the control of a simple model problem developed by Aubry *et al* (1988) governed by a two-component equation with dynamics similar to that of a POD model of near-wall longitudinal vortices. This model equation is subjected to random excitation to account roughly for unmodelled system dynamics and disturbances. A strategy is developed and demonstrated which delays heteroclinic transitions in this simple model as long as possible by sensing when the state is near an unstable fixed point and maintaining it there with feedback control for as long as possible. Once the state diverges from this fixed point, presumably due to the significant unmodelled dynamics of the flow e.g., the passage of the head of a coherent structure, control is turned on until the state approaches the neighbourhood of another unstable fixed point.

6.2 CONTROL OF THE CIRCULAR CYLINDER WAKE

Above a critical Reynolds number, the wake of a circular cylinder exhibits vortex shedding oscillations that persists purely a result of flow instability and which are not caused by the external forcing, noise, or internal pressure feedback. The flow exhibits self-excited oscillations and this has important consequences for flow control.The response of the cylinder wake to open loop forcing can be characterized by two qualitatively different regimes "lock-in" and "beat" as discussed in chapter 4 for the reduced model for different oscillation frequencies. Several different forcing techniques affect the behaviour of the cylinder flow. The wake response to forcing is similar for each whether acoustic excitation of the wake, longitudinal or lateral vibration of the cylinder, rotation of the cylinder, alternative blowing and suction at the seperation points or vibrating wires are used. A review of these concepts is given by Gillies (1998) .

6.2.1 Low-dimensional control of self-excited cylinder wakes

Convectively unstable flows can be controlled by single point forcing. However control of global flow oscillations are usually the result of an absolute instability as observed in the cylinder wake and are therefore possibly more difficult to characterize by a single sensor Gillies (1998). The existence of multiple global modes in the absolutely unstable cylinder wake necessitates the use of multiple control sensors at various streamwise locations for the supression of all possible modes. The spatio-temporal response of the wake is nonlinear. A control strategy must be based on the nonlinear model of the flow dynamics.

The absolutely unstable region can be properly represented by multiple control sensors. Many flow variables at many points are needed to be used within the control algorithm. The control algorithm will be complicated as a result. If however we can create a low-dimensional model of the flow with an external forcing, we can have significant reduction in computations.

6.2.2 External forcing

The governing equations of the flow defined in a body fixed coordinate system translating with a given velocity $\hat{v}_j(t)$, in terms of a non-dimensional velocity field v_j and pressure p relative to a space fixed coordinate system, was written in chapter 3 in the dimensionless forms,

$$\dot{v}_j + (v_j v_k)_{,k} + p_{,j} - [\nu_e(v_{j,k} + v_{k,j})]_{,k} = 0 , \tag{6.1}$$

$$v_{j,j} = 0 . \tag{6.2}$$

Here ν_e=$1/Re$ where Re denotes the Reynolds number ($= \frac{\rho' U' L'}{\mu'}$).

These equations represent the flow velocity in an inertial or space fixed frame of reference and are appropriate to the analysis of the fluid-structure interaction between a fixed body and an oscillating flow. For a body manoeuvring in an incompressible fluid, Batchelor (1967) showed that the Navier–Stokes equations formulated in a moving frame of reference attached to the body are given by,

$$\dot{v}_j + (v_j U_k)_{,k} + p_{,j} - [\nu_e(v_{j,k} + v_{k,j})]_{,k} = 0 , \tag{6.3}$$

$$v_{j,j} = 0 . \tag{6.4}$$

Here U_k denotes the relative velocity between the body and the fluid motion i.e. $U_k = v_k - \hat{v}_k$ where $\hat{v}_k$ represents the velocity of the body and/or the fluid mesh attached to the body. This set of equations is suitable to describe the fluid-structure interaction between a cylinder oscillating horizontally and a fluid at rest at infinity or pulsating and translating in a stationary fluid. This equation is formulated relative to fixed coordinate system. If the same equation is formulated relative to a moving coordinate system the fictitous body force $-\dot{\hat{v}}_k$ will be added to our equation.

$$\dot{U}_j + (U_j U_k)_{,k} + p_{,j} - [\nu_e(U_{j,k} + U_{k,j})]_{,k} = -\dot{\hat{v}}_k , \tag{6.5}$$

$$U_{j,j} = 0 . \tag{6.6}$$

The later equation will be used as an approximation to oscillation of the cylinder in reduced model. The oscillation of the cylinder can be treated as an inertial force term in the Navier-Stokes equations, if the problem is formulated in a body fixed reference

system. This is perceived as distributed control for the reduced model. Herein the body forcing is the external input for the reduced model. The optimized control history is fed to the full model.

6.2.3 Nonlinear reduced optimization

This part of the thesis presents a study on the application of trust-region augmented variable-fidelity modelling approaches to optimal flow control. In the proposed approach, the full-order state equations and a reduced-order model based on proper orthogonal decomposition are interleaved in the optimization procedure. The objective is to achieve significant savings in the computational cost by reducing the number of high-fidelity flow solutions during the optimization iterations. Some preliminary results are presented for optimal control of flow around a circular cylinder at Reynolds number, $Re = 100$ (see Uzunoğlu *et al* (2001)).

Optimal control of complex time-dependent physical processes governed by partial differential equations is a computationally expensive problem, particularly when the governing equations are modelled with high-fidelity. As a result, the construction of reduced-order models to design controllers for distributed parameter systems which, in this context, are fluid flows, is of considerable interest. One model reduction method which has been successfully used for dynamical systems analysis is the Proper Orthogonal Decomposition (POD) method of Sirovich (1987) . This method provides a means of extracting dominant energy-containing structures from flow field data. Further, using these structures as basis functions, a reduced-order model of the governing equations can be constructed.

The POD method has been applied to fluid problems by Sirovich (1987) and many other researchers, e.g. Berkooz *et al* (1993) and Deane *et al* (1991) to understand the important dynamical features or coherent structures seen in fluid flows. A reduced basis solution of the flow is obtained as a linear combination of an optimal set of empirical basis functions using an integral equation method such as the Galerkin projection scheme. Nonstationarity of the flow field as a result of the control action can also be considered in a global reduced model as investigated in Glezer *et al* (1989) and Tan *et al* (2000) . Note that the POD model is constructed using the solution of the full-order governing equations for a particular control input. Hence, the accuracy of the POD

model may deteriorate when the control input is changed during the course of an optimization scheme. As a consequence, there is no theoretical guarantee that an optimal control strategy developed using a reduced order model converges to the optimal control computed using the full-order state equations. In particular, an optimal control strategy based on a reduced-order model alone may lead to controller spillover effects, which can potentially make the higher modes unstable. A number of earlier studies have applied full-order modelling and adjoint sensitivity analysis techniques to optimal flow control; see, for example, Ghattas *et al*(1997). If the numerical optimization algorithm is run until convergence, this approach guarantees that an optimal solution (local optimum) for the control input is obtained. However, from a practical viewpoint, this approach is computationally expensive, particularly when the governing equations are modelled with high-fidelity using a large number of state equations.

In the structural optimization literature, the computational cost issue is typically tackled by combining approximate analysis models and the high-fidelity solver in the optimization procedure as discussed by Chang *et al* (1993) . An important issue in developing such a scheme is to ensure that asymptotic convergence to the high-fidelity optimum can be achieved. Alexandrov (1997) *et al* proposed a trust-region framework for interleaving the exact and approximate objective function models in numerical optimization. The trust-region framework can be interpreted as an adaptive method to monitor the amount of optimization done with the approximation model, before the high-fidelity model is run to check the validity of the current iterate. By comparing the approximation model prediction to the exact prediction periodically, useful information about the accuracy of the reduced-order model is obtained. This information is then employed to decide the move limits to be enforced in the next optimization iteration, as well as to update the approximation model. More recently, Arian *et al* (2000) presented an extension of this approach to optimal flow control. It was shown that, under some mild assumptions on the accuracy of the reduced-order model, convergence to the high-fidelity optimal solution can be guaranteed. An attractive feature of this approach is that, by checking the effects of control input on the flow field using high-fidelity simulation (at various stages of the optimization iterations), the effects of control spillover are minimized.

This chapter presents a study on the application of trust-region augmented variable-fidelity modelling approaches to optimal flow control. The objective is to interleave the

full-order state equations with a reduced-order model to achieve significant reductions in the computational cost of numerical optimization. In contrast to Arian *et al* (2000) , we impose a zero-order consistency condition on the reduced-order model. It is argued that this leads to an improvement in the accuracy of the reduced-order model, which in turn may lead to a reduction in the number of optimization iterations required for convergence. Some preliminary results are presented for optimal control of flow around a circular cylinder for $Re = 100$.

Oscillating distributed body force has been as an example of the control actions to be considered for the reduced model. Mixed boundary conditions associated with both traction and velocity are used. The boundary conditions for an oscillating cylinder in body fitted coordinate system relative to space fixed coordinate system are defined with the velocity of the cylinder in time for a cylinder in a uniform flow. This control action as an oscillation of the cylinder is considered for the full model.

6.2.4 Optimal control strategy

In the present study, we use a nonlinear programming approach to optimal control. The controller design problem involves determining the time history of the control force $c(\boldsymbol{x}, t)$, which minimizes the objective function

$$f(c) = \int_{t_1}^{t_2} \int_{\Omega_{obs}} |\boldsymbol{v}(c; \boldsymbol{x}, t) - \boldsymbol{v}^d(\boldsymbol{x}, t)|^2 d\Omega dt \tag{6.7}$$

where $\boldsymbol{v}(c; \boldsymbol{x}, t)$ is the solution of the two-dimensional Navier-Stokes (NS) equations for prescribed control input $c(\boldsymbol{x}, t)$. $\boldsymbol{v}^d(\boldsymbol{x}, t)$ is a desired state, which can be chosen as Stokes flow in the vortex shedding problem, and Ω_{obs} denotes the domain over which the state of the system is observed. $[t_1, t_2]$ is the time-interval over which the objective function is computed.

If the full-order NS equations are used to compute $\boldsymbol{v}(\boldsymbol{x}, t)$, minimization of $f(c)$ will be a computationally intensive problem. An alternative approach is to use a reduced-order model as a surrogate for the full-order state equations. The approximate objective functions are defined as

$$m(c) = \int_{t_1}^{t_2} \int_{\Omega_{obs}} |\boldsymbol{v}^{pod}(c; \boldsymbol{x}, t) - \boldsymbol{v}^d(\boldsymbol{x}, t)|^2 d\Omega dt \tag{6.8}$$

where $\boldsymbol{v}^{pod}(c;\boldsymbol{x},t)$ is the solution of the POD reduced-order model for control input $c(\boldsymbol{x},t)$.

Note that the reduced-order model is constructed using the flow snapshots obtained by solving the NS equations for given $c(\boldsymbol{x},t)$. In general, the accuracy of $m(c)$ will tend to deteriorate when the control input is changed significantly from the baseline $c(\boldsymbol{x},t)$. Hence, for two arbitrary control inputs c_1 and c_2, $m(c_2) < m(c_1)$ does not imply that $f(c_2) < f(c_1)$. This suggests that a naive strategy based on minimization of $m(c)$ alone leads to minimization of the full-order objective function $f(c)$. In order to ensure that we are minimizing the actual objective $f(c)$, the optimization strategy must interleave both the full-order and reduced-order objective function prediction models.

For example, let $c_0(t)$ denote an initial guess for the optimal control input, at which the full-order NS equations are solved to obtain a set of flow snapshots. We may then use these snapshots to construct a reduced-order model of the flow. The next step involves determining the control input $c_1(t)$ which minimizes the surrogate objective function defined in equation (6.8). In order to improve the reduced-order model, we may now solve the full-order NS equations using $c_1(t)$ as the control input to compute a new set of flow snapshots, which is then used to create an updated reduced model. This iterative process continues till no further reduction in $f(c)$ is achieved. If reasonably tight move limits are placed on the control input amplitudes, this procedure *may* converge close to the optima of the full-order objective function $f(c)$.

This sequential approximation model updating strategy has been used by Chang (1993) to reduce the computational cost of numerical optimization. From a theoretical viewpoint, there is no guarantee that the sequential iterative procedure described earlier converges to the minima of $f(c)$. Recently, Alexandrov *et al* (1997). proposed a trust-region framework for integrating variable-fidelity analysis models in nonlinear programming formulations. This framework is theoretically guaranteed to converge to the minima of $f(c)$ under rather weak assumptions. Since analysis models with varying fidelity are used here to improve computational efficiency, this approach is referred to as *variable-fidelity modeling* Alexandrov *et al* (2000). Arian *et al* (2000) present an extension of the trust-region framework to optimal flow control. The optimal control strategy used in the present discussion is based on this extended framework. For a detailed exposition of trust-region frameworks, the reader is referred to Alexandrov *et al* (1997)). and Arian *et al* (2000). In the present discussion, we present a brief overview

of the approach, emphasizing those aspects which differ from earlier work. The trust-region procedure guarantees the convergence of the variable-fidelity modelling approach by reformulating the optimization problem as

$$\textbf{Minimize}: \quad m_k(c_k + s) \tag{6.9}$$

$$\text{s.t.}: \quad ||s|| \leq \delta_k \tag{6.10}$$

where the minimization is carried out with respect to s, and c_k denotes the control input at which the snapshots are computed to construct the reduced-order model. δ_k denotes the trust-region radius at iteration number k. $m_k(c_k+s)$ is the objective function based on the reduced-order model, which is constructed using flow snapshots computed for control input c_k. The subscript k is used to indicate that the reduced-order model is updated at each iteration.

The basic idea of the trust-region approach is to adaptively increase or decrease the radius δ_k or move limits at each iteration, depending on how well $m(c_k)$ correlates with $f(c_k)$. In general, at the beginning of each iteration k, $m_k(c_k) \neq f(c_k)$ and $\nabla m_k(c_k) \neq \nabla f(c_k)$. Arian *et al* (2000) showed convergence to the minima of $f(c)$ can still be guaranteed under some assumptions. This is because information about the accuracy of m_k does not enter into the convergence theorems based on traditional trust-region theory directly. However, ∇m_k should approximate ∇f sufficiently well Arian *et al* (2000) for the convergence theory to hold true.

In the present research, we impose the zero-order consistency conditions of Alexandrov *et al* (1997) . This involves computing a constant β_k, such that at each iteration k, $\beta_k m_k(c_k) = f(c_k)$. The motivation for this is to improve the accuracy of the objective function predicted using the reduced-order model. It is expected that this may lead to accelerated convergence as compared to the approach used in Arian *et al* (2000) . It is important to note that, if an adjoint Navier-Stokes solver is available, then it is possible to choose scaling parameters such that the condition $\nabla m_k(c_k) = \nabla f(c_k)$ is also satisfied.

The steps involved in the trust-region augmented variable-fidelity optimization algorithm are summarized in fig.6.1. Note that in Step 5, we reject the step s_k, if it actually leads to an increase in the high-fidelity objective function. The trust-region radius update strategy in Step 5 is based on the following procedure:

Let c_0, δ_o, $0 < \eta_1 < \eta_2 < 1$, and

$0 < \gamma_1 \leq \gamma_2 < 1 \leq \gamma_3$ be given.

Set k = 0.

Step 1: Solve the full-order state equations for flow snapshots corresponding to control input $c_k(t)$ and compute $f(c_k)$.

Step 2: Compute POD Basis, build the reduced-order model and compute $m_k(c_k)$.

Set $\beta_k = f(c_k)/m_k(c_k)$.

Step 3: Compute s_k by minimizing the objective function $\beta_k m_k(c_k + s)$, subject to the trust-region constraint $||s|| \leq \delta_k$

Step 4: Compute $f(c_k + s_k)$ by solving the full-order state equations. Set $\rho_k = \delta f / \delta m_k$; where $\delta f = f(c_k) - f(c_k + s_k)$ and $\delta m_k = m_k(c_k) - m_k(c_k + s_k)$.

Step 5: If convergence criteria is satisfied stop. Else update the trust-region radius to δ_{k+1}.

Set $k = k + 1$.

- If $\rho_k > \eta_1$ set $c_{k+1} = c_k + s_k$ and go to Step 2.
- If $\rho_k \leq \eta_1$ set $c_{k+1} = c_k$ and go to Step 3.

Figure 6.1: Trust-Region Augmented Variable-Fidelity Optimization Algorithm

- If $\rho_k \leq \eta_1 : \delta_{k+1} = \gamma_1 \delta_k$.
- If $\eta_1 < \rho_k < \eta_2 : \delta_{k+1} = \gamma_2 \delta_k$.
- If $\rho_k \geq \eta_2 : \delta_{k+1} = \gamma_3 \delta_k$.

Typical values for η_1 and η_2 are 0.25 and 0.75, respectively. Arian *et al* (2000) suggested that γ_1, γ_2, and γ_3 should be set at 0.5, 0.5, and 2, respectively.

In practice, an approximate solution of the optimization problem in Step 3 is sufficient to achieve convergence to the high-fidelity optima. In the present research, we use a few steps of the Broyden-Fletcher-Goldfarb-Shanno (BFGS) algorithm to compute the optimal value of s_k at each iteration. Further, the trust-region constraint used in the present study is based on the $\mathcal{L}_\infty$ norm. This makes it easier to implement the trust-region framework using existing optimization routines capable of handling bound constraints.

6.2.5 Preliminary results for open-loop flow Control

We have made initial investigations using body forcing as the control input for the reduced model suppressing the flow unsteadiness at Reynolds number, Re = 100. The optimized control input was generated from the reduced model. The control input is parameterized as $c(t) = \sum_{i=1}^{N} c_k \psi_k(t)$ with $\psi_1(t) = 1$, $\psi_{2k}(t) = \cos(2k\pi t/T)$, $\psi_{2k+1}(t) = \sin(2k\pi t/T)$, $k = 1, 2, \ldots 30$, i.e., $N = 30$. The control objective is to achieve steady flow throughout the flow domain, with $v_1 = 1.0$ and $v_2 = 0$. The time window of [0,5] is used for computing the objective function. The initial conditions correspond to fully developed flow. As an initial guess, all the coefficients of the control input are set to be equal to 0. A POD based reduced-order model with 10 modes is used for approximating the full-order objective function. During this preliminary validation study, the optimization algorithm was terminated after three iterations. Around 70% reduction in the flow unsteadiness for the reduced model was observed. For the full model, it was observed that the reduction was around 20% for the objective function. The time history of the optimum control input is shown in fig.6.2. More detailed convergence studies of the optimization scheme will be presented in the future.

In order to study the effects of control input on the flow field, we also examined the flow unsteadiness as a function of time, both before and after control. These trends

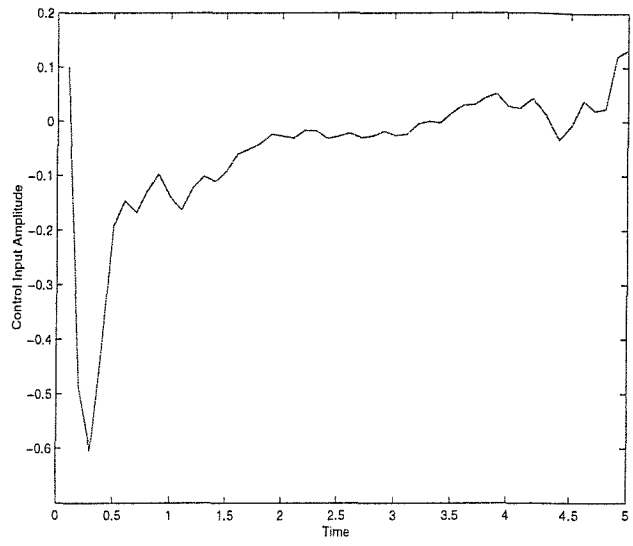

Figure 6.2: Optimum control input.

are shown in figure.6.3. The time-dependent amplitudes of the first four POD modes before and after control are shown in figure.6.5 The uncontrolled velocity field, and the velocity field 5 seconds after applying the control are shown in fig.6.6(a) and fig.6.6(b), respectively.

The change in the kinetic energy of this system defined by Navier-Stokes equation will be dependent on the dissipative or viscous forces as well as the body force. The energy input to the system by the controller is less than the total kinetic energy of the whole system as expected. The energy in the initial fluctuations of the velocity field from the mean energy flux in the fully developed vortex shedding can be observed to be approximately the same magnitude as the input energy from the controller if the assumption is made that the dissipative forces are not existent and the body forcing is used as the control action. As a result the energy input can be expected to be less than that of the fluctuations if the dissipative forces are considered and the control area is confined to the wake street instead of the complete computational domain which will limit the energy consumption. An area confining the vortex street can be sufficient to control the global instability observed in this regime.

If the speculation is made that absolutely unstable region in the cylinder wake flow can be controlled to a certain point by local forcing upstream which influences the rest of the flow field then the strategy can be adopted to a much smaller region than the energy inputs will be lower. This might be possible to a certain degree for low reynolds

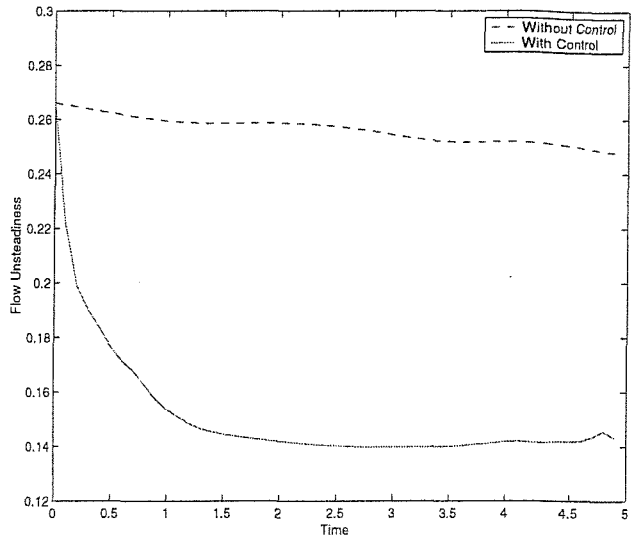

Figure 6.3: Time history of flow unsteadiness with and without control.

numbers and maybe high reynolds numbers. Otherwise high energy inputs might be needed to control absolutely unstable region of full wake flow. This might need a lot of energy but however it might turn out to be a necessity if one decides to control the full vortex regime. The actuating and sensing mechanisms used here are initial ones.

Lastly the number of modes in this regime was relatively limited however, turbulent flows are known to have relatively high dimensions in this framework even at fairly low-Reynolds number,due to their large range of spatial and temporal scales, which makes analysis of these systems difficult as discussed by Keefe *et al* (1992). The higher modes might also be modes with high energy content. Further tests are also reguired to show that approximate system is sufficient to demonstrate the stability of the full system.

6.3 CONCLUSION

In this chapter, we outlined a brief related review of the controller design and trust-region augmented variable-fidelity modeling approach to optimal flow control. A proper orthogonal decomposition technique is used to construct a reduced-order model of the governing equations. The present approach interleaves the full-order governing equations and the reduced-order model in the numerical optimization procedure. Since the move limits in the optimization process are controlled by a trust-region framework, convergence to a local optima can be theoretically guaranteed.

Some preliminary studies were presented for optimal control of flow around a cir-

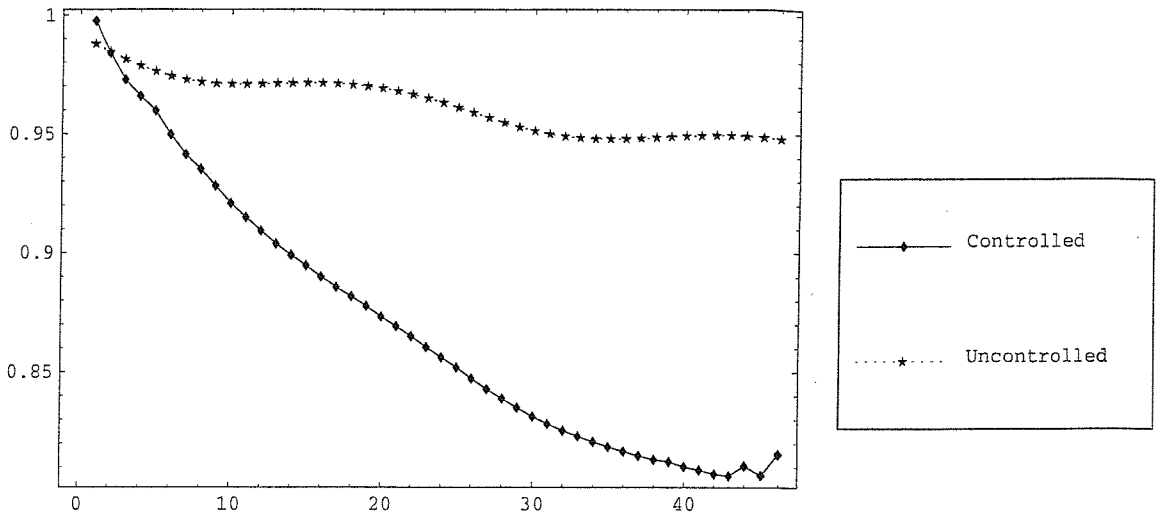

Figure 6.4: Objective function of the controlled and uncontrolled flow. The first five steps are transient.

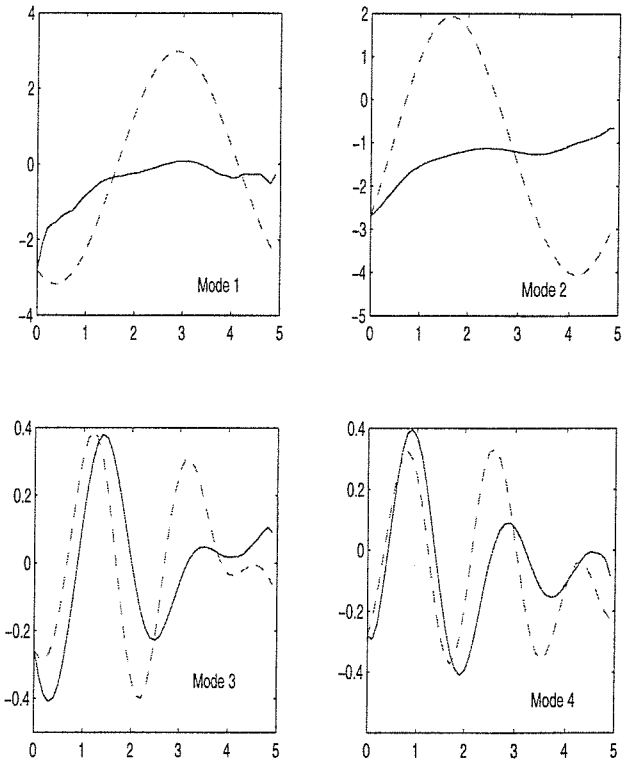

Figure 6.5: Time history of modal amplitudes with and without control.

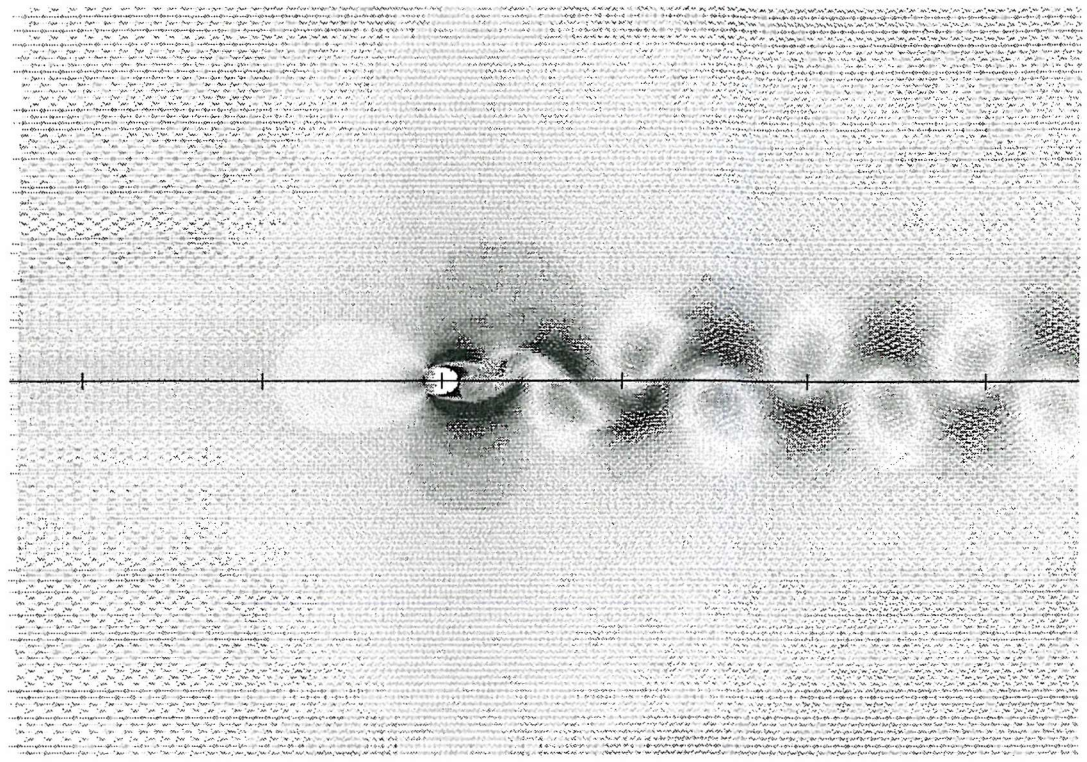

(a)

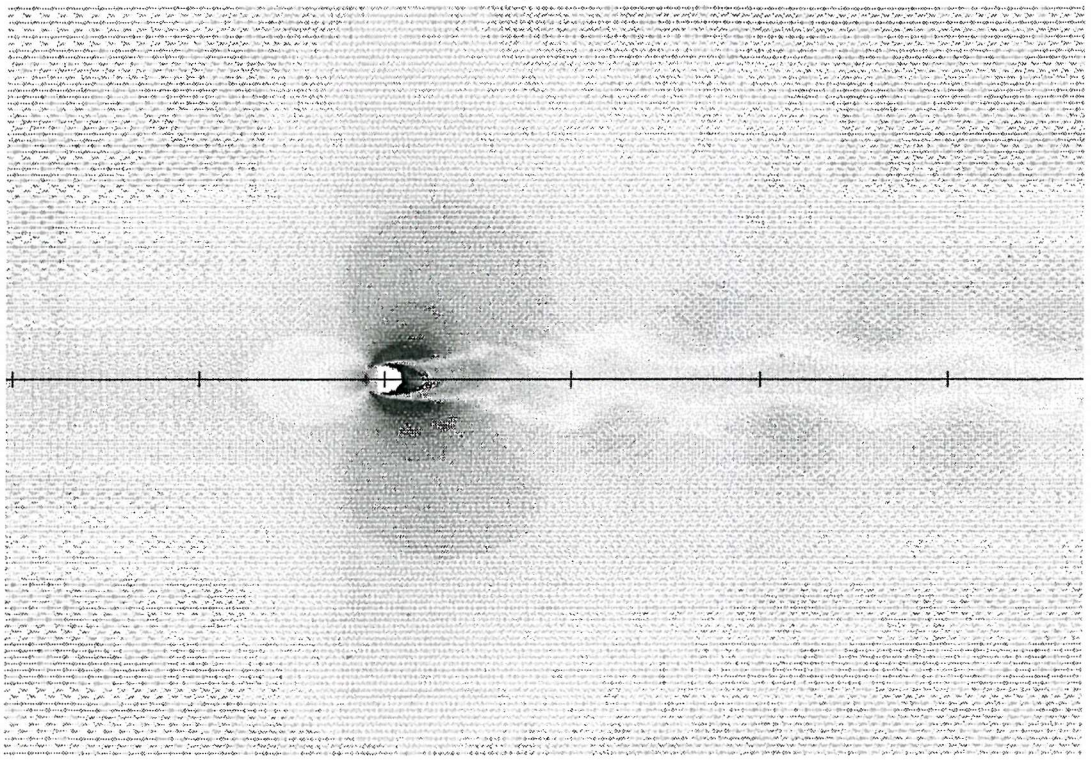

(b)

Figure 6.6: (a) Uncontrolled velocity and (b) Controlled velocity field for a circular cylinder in uniform flow at Re=100.

cular cylinder using body forcing as the control input. It was shown that around 20% reduction for the cost function can be achieved when the control input was applied to the full model. The application of the body forcing to the full model (Boundary element method) proved to be difficult when moderately large inputs were used which must be developed in the future. The oscillation of the cylinder which is an approximation of the body force showed to be a succesful control action even though the approximations involved. The body force can be seen as control input from eletromagnetic Lorentz force (see Nosenchuck (1994)).

The results are encouraging, and suggest the applicability of the present approach to more complex problems.

Chapter 7

CONCLUSION

The cell boundary element method developed by Tan *et al* (1999) and modified herein to study oscillating cylinders or manoeuvring bodies has proved successful, reproducing the detailed characteristics of experimental observations, correlations with theoretical predictions presented by others and experimental measurements of drag and lift coefficients over a range of Re, KC numbers for fixed Stokes parameter $\beta = 35$. This has been achieved by adopting an unstructured mesh to idealise the fluid domain and a primitive-variable formulation to construct a hybrid approach involving boundary element and finite element methods. Through developments of suitable numerical schemes of study associated with the cell boundary element method integrated with the relevant boundary conditions for transversely oscillating cylinders or a cylinder fixed in oscillating flows, the presented computed unsteady flows provide a measure of verification, validation and confidence in the proposed overall approach when compared with other experimental and theoretical findings.

A Proper Orthogonal Decomposition method is used to investigate reduced flow modelling of the vortex shedding wake exhibited behind a circular cylinder. The method is found very effective in creating reduced models to describe vortex shedding processes. The method can also be applied for different Reynolds number cases with modified snapshots or data sets.

A reduced model was also constructed where forcing terms are treated as control actions in the fluid domain and flow simulations with different forcing descriptions have been conducted.

The method discussed herein can also be adopted to the situation when the control action is the forced oscillation of the cylinder. In this case the oscillation of the cylinder is treated as an inertial force term in the Navier-Stokes equations, if the problem is formulated in a body fixed reference system. Although Reynolds number (i.e. $\nu_e = 1/\mathrm{Re}$) is one of the parameters in the reduced model described by equations (4.20–4.23), equation (4.20) cannot be used to model flows at different Reynolds number without modifying the modes involved as well. In some cases, however, the snapshots of flows at different Reynolds numbers may be combined to approximate the snapshots at another Reynolds number which then can be used to produce basis functions in the POD method. As an example, 40 snapshots were collected from each flow simulation at Re=100 and Re=200. New snapshots at other Reynolds numbers (i.e. 100 <Re< 200) were generated by interpolation of these snapshots and this information incorporated in the reduced models to predict shedding frequencies. The results of the calculated Strouhal number are presented in table 4.2 for a series of Reynolds numbers. Also included are data generated by the 'universal' empirical relationship given by Williamson (1988) . The experimentally determined Strouhal values of Williamson have an accuracy claimed 'to the 1% level' and the 'universal' empirical relationship was obtained through interpolation of the observed data.

We outline a trust-region augmented variable-fidelity modeling approach to optimal flow control. A proper orthogonal decomposition technique is used to construct a reduced-order model of the governing equations. The present approach interleaves the full-order governing equations and the reduced-order model in the numerical optimization procedure. Since the move limits in the optimization process are controlled by a trust-region framework, convergence to a local optima can be theoretically guaranteed.

Some preliminary studies were presented for optimal control of flow around a circular cylinder using oscillation of the cylinder as the control input. It was shown that around 70% reduction in the flow unsteadiness can be achieved for this problem for the reduced model. Around 20% reduction was observed for the cost function. The results are encouraging, and suggest the applicability of the present approach to more complex problems.

A brief outline of ongoing research is presented.

- Viscous cell boundary element is investigated systematically for Low-Reynolds number and KC values and the results are further compared with the experimen-

tal data which is available.

- Detailed studies to investigate the benefits of enforcing zero-order and first-order consistency conditions on the reduced-order model for Trust-Region framework. These strategies will be compared with the approach presented in in terms of computational cost and convergence rate.

- A comparison of the effectiveness of using control strategies based on body forcing, cylinder rotation, and cylinder oscillation is invstigated. A comparison analysis will be made. The reduced-order modeling and sensitivity analysis formulation for these cases will be analysed in more detail.

- The body forcing will be further investigated for the full model (Boundary Element).

Bibliography

[1] Abergel, F. and Temam, R. (1990). On some control problems in fluid mechanics. *Theoretical and Computational Fluid Dynamics*, Vol. 1, 303-325.

[2] Alexandrov, N., Dennis, J.E. and Lewis, R.M. (1997) A trust region framework for managing the use of approximation models in optimization. *NASA/CR-1997-201745*, October.

[3] Arian, E., Fahl, M. and Sachs, E.W. (2000) Trust region proper orthogonal decomposition for flow control. *NASA/CR-2000-210124*, May.

[4] Baltrop NDP, Adams AJ. (1991) Dynamics of fixed marine structures. *Butterworth-Heinemann*

[5] Aubry, N., Holmes, P., Lumley, J.L. and Stone, E. (1988) The dynamics of coherent structures in the wall region of turbulent boundary layer. *Journal of Fluid Mechanics*, Vol. 192, pp. 115-173.

[6] Bamieh, B., (1997) The structure of optimal controllers of spatially-invariant distributed parameter systems. *Proceedings of the 36th IEEE Conference on Decision and Control*, Dec 8-12, San Diego.

[7] Baramov L., Tutty O.R. and Rogers E. (2000) Low dimensional robust control of channel flow *Proceedings of IUTAM 2000*

[8] Batchelor, G.K., (1967) Fluid dynamics *Cambridge University Press, Cambridge*

[9] Bearman PW, Downie MJ, Graham JMR, Obasaju ED. (1985) Forces on cylinders in viscous oscillatory flows at low Keulegan-Carpenter numbers. *J. Fluid Mech* 154:337–352.

[10] Berkooz, G., Holmes, P. and Lumley, J.L. (1993) The Proper Orthogonal Decomposition in the analysis of turbulent flows. *Annual Review of Fluid Mechanics*, Vol. 25, pp. 539-575.

[11] Bewley, T.R. and Liu, S. (1998) Optimal and robust control and estimation of linear paths to transition. *Journal of Fluid Mechanics*, Vol. 365, pp. 305-349.

[12] Bewley, T.R. (1999) Linear control and estimation of nonlinear chaotic convection: harnessing the butterfly effect *Physics of Fluids*, Vol. 11, pp. 1169-1186.

[13] Bewley, T.R. (2001) Flow control: New challenges for a new renaissance. *Progress in aerospace science*, To be published

[14] Bishop RED, Hassan AY. (1964) The lift and drag forces on a circular cylinder in a flowing fluid. *Proc. Roy. Soc. Lond. A* 277:51–75.

[15] Borthwick A. (1986) Comparison between two finite–difference schemes for computing the flow around a cylinder. *Int. J. F. Num.Methods in Fluids* 6:275–290.

[16] Brebbia C.A. (1978) The boundary element method for engineers. *Pentech Press, London*

[17] Burcher RK. (1972) Developments in ship manoeuvrability. *Trans RINA* 114:1–32.

[18] Chester W. (1990) A general theory for the motion of a body through a fluid at low Reynolds number. *Proc. Roy. Soc. Lond. A* 430:89–104.

[19] Cho, S.T., Najafi, K., Lowman, CL, and Wise, KD (1989) An ultrasensitive silicon pressure-based flowmeter. *IEDM Technical Digest, 499-502, Dec.*

[20] Choi, H., Moin, P., Kim, J. (1994) Active turbulence control for reduction in wall-bounded flows. *Journal of Fluid Mechanics*, Vol. 262, 503-509.

[21] Cortelezzi, L., Lee, K.H., Kim, J. and Speyer, J.L., (1999) Skin-friction drag reduction via robust reduced-order linear feedback control. *International Journal of Computational Fluid dynamics*, Vol 11, No 1-2, 79-92,1998.

[22] Deane, A.E., Kevrekidis, I.G., Karniadakis, G.E. and Orszag, S.A. (1991) Low-dimensional models for complex geometry flows: application to grooved channels and circular cylinders. *Physics of Fluids A*, Vol. 3, No. 10, Oct., pp. 2337-2354.

[23] Duncan WJ. (1959) The principles of the control and stability of aircraft. *Cambridge University Press*

[24] Dütsch H, Durst F, Becker S, Lienhart H. (1998) Low-Reynolds-number flow around an oscillating circular cylinder at low Keulegan–Carpenter numbers. *J. Fluid Mech.* 360:249–271.

[25] Etkin B. (1972) Dynamics of atmospheric flight. *John Wiley*

[26] Faltinsen MO. (1990) Sea loads on ships and offshore structures. *Cambridge University Press*

[27] Farrant, T., Tan, M. and Price, W.G. (2000) A cell boundary element method applied to laminar vortex shedding from arrays of cylinders in various arrangements. *J. Fluids and Struct.*, Vol. 14(3) pp. 375-402.

[28] Farrant, T., Tan, M. and Price, W.G. (2001) A cell boundary element method applied to laminar vortex shedding from circular cylinders. *Computers & Fluids* (To be published).

[29] Feynman, R. (1959) There is plenty of room at the bottom. *Annual Meeting of The American Physical Society, Dec. 29.*

[30] Garrison C.J. (1990) Drag and inertia forces on a cylinder in harmonic flow. *J. of Waterway, Port, Coastal and Ocean Engin. ASCE* 103(WW2):169–190.

[31] Ghattas, O., and Bark, J.H. (1997) Optimal control of two- and three-dimensional navier-Stokes flows. *Journal of Computational Physics*, Vol. 136, pp. 231-244.

[32] Gillies, E.A. (1998) Low-dimensional control of circular cylinder wake. *Journal of Fluid Mechanics* Vol. 371, pp. 157-178.

[33] Glezer, A., Kadioglu, Z. and Pearlstein, A.J. (1989) Development of an extended proper orthogonal decomposition and its application to a time periodically forced plane mixing layer. *Physics of Fluids A*, Vol. 1, No. 8, Aug., pp. 1363-1373.

[34] Graham, W.R., Peraire, J. and Tang, K.Y. (1999) Optimal control of vortex shedding using low-order models. Part I- Open-loop model development. *International Journal for Numerical Methods in Engineering*, Vol. 44, No. 7, pp. 945-972.

[35] Graham, W.R., Peraire, J. and Tang, K.Y. (1999) Optimal control of vortex shedding using low-order models. Part II- Model based control. *International Journal for Numerical Methods in Engineering*, Vol. 44, No. 7, pp. 973-990.

[36] Hak, G.E. (1996) Modern developments in flow control. *Applied Mechanics Review*, Vol. 49, No. 7. pp. 365-379.

[37] Hak, G.E. (1989) Flow control. *Applied Mechanics Review*, Vol. 42, No. 10.

[38] Hall, P. (1983) The linear development of Gortler Vortices in growing boundary layers. *Journal of Fluid Mechanics*, Vol. 130, pp. 41-58.

[39] Hall P. (1984) On the stability of the unsteady boundary layer on a cylinder oscillating transversely in a viscous fluid. *J. Fluid Mech.* 146:347–367.

[40] Hassan AY. (1962) The effects of vibration on the lift and drag forces on a circular cylinder in a fluid flow. *PhD thesis, University College London, University of London*

[41] Hertz, J., Krogh, A. and Palmer, R.G. (1991) Introduction to the theory of neural computation. *Addison Wesley*

[42] Hirsch (1988) Numerical computation of internal and external flows. *John Wiley and Sons, Chichester, England*

[43] Ho, C.M. and Tai, Y.C. (1996) MEMS and its applications for flow control. *ASME Journal of Fluids Engineering*, Vol. 118, pp. 437-447.

[44] Honji H. (1981) Streaked flow around an oscillating cylinder. *J. Fluid Mech.* 107:509–520.

[45] Huerre, P. and Monkewitz, P.A. (1990) Local and global instabilities in spatially developing flows. *Annual Review of Fluid Mechanics*, Vol. 22, 473-537.

[46] Ionnau, P.A. and Sun, J. (1996) Robust adaptive control. *Prentice Hall*

[47] Ito, K. and Ravindran, S.S. (1998) A reduced-order method for simulation and control of fluid flows. *Journal of Computational Physics*, Vol. 143, pp. 403-425.

[48] Jaecklin, V.P., Linder, C., de Rooji, N.F., Moret, J.M., Bischof, R, and Rudolf, H. (1992) Novel polysilicon comb actuators for xy-stages. *IEEE MEMS Workshop*

[49] Keefe, L.R., Moin, P. and Kim, J. (1992) The dimensions of attractors underlying turbulent Poiseuille flow. *Journal of Fluid Mechanics*, Vol. 242, pp. 1-29

[50] Kelvin, L. (1880) On disturbance in Lord Rayleigh's solution for waves in a plane vortex stratum. *Mathematical and Physical Papers*, Vol. 4, 186-187.

[51] Joshi, S.S., Speyer, J.L. and Kim, J., (1998) A systems theory approach to the feedback stabilization of inifinitemestal and finite-amplitude disturbances in plane Poiseuille flow. *Journal of Fluid Mechanics*, Vol. 332, pp. 157-184.

[52] Justesen P. (1991) A numerical study of oscillating flow around a circular cylinder. *J. Fluid Mech.* 222:157–196.

[53] Knörnschild U. (1994) Experimentelle Unterschungen der Stromungsverhaltnisse um einen oszillierenden Kreiszylinder. *Master's thesis, University of Erlangen-Nurnberg, LSTM, Erlangen.*

[54] Kühtz S. (1996) Experimental investigation of oscillatory flow around circular cylinders at low beta numbers. *PhD Thesis, University of London*

[55] Lall, S., Marsden, J.E. and Glavaski, S. (1999) Empirical model reduction of controlled nonlinear systems. *Proceedings of the IFAC World Congress* Vol. F, July, pp. 473-478.

[56] Lee, C., Kim, J. Babcock, D. and Goodman, R. (1997) Application of neural network to turbulence control for drag reduction. *Physics of Fluids*, Vol. 9, 1740-7

[57] Liepmann, H.W., 1943. Investigation on laminar boundary-layer stability and transition on curved boundaries. *NACA WR W-107*

[58] Lin XW, Bearman PW, Graham JMR. (1996) A numerical study of oscillatory flow about a circular cylinder for low values of beta parameters. *Journal of Fluids and Structures*, No. 10, pp. 501-526

[59] Lumley, J.L. (1971) Stochastic tools in turbulence *Academic Press, New York.*

[60] Lumley, J.L. (1989) Low dimensional models of the wall region of turbulent boundary layer , and the possibility of control. *Proceedings of the Tenth Australasian Fluid Mechanics Conference and Possibility of Control.*

[61] McMichael, J.M. (1996) Prospects and progress for active flow control using MEMS. *AIAA*, Nr. 96-0306

[62] Moin, P. and Bewley, T.R. (1994) Feedback control of turbulence *Applied Mechanics Review*, Vol. 47, (6), part 2, p. S3.

[63] Morison JR, O'Brien MP, Johnson JM, Schaaf SA. (1950) The force exerted by surface waves on piles. *Petrol. Trans. AIME* 1950; 189:149–154.

[64] Maull DJ, Milliner MG. (1978) Sinusoidal flow past a circular cylinder. *Coastal Engineering* 2:149–168.

[65] Nitsche, W., Mirow, P., Szodruch, J. (1989) Piezo-electric foils as means of sensing unsteady surface forces. *Experiments in fluids*, Vol. 7, 111-118.

[66] Nosenchuck, D.M. and Brown, G.L. (1993) Control of turbulent wall shear stress using arrays of TFM tiles. *Bulletin of American Physical Society*, Vol. 38, 12, 21197.

[67] Obasaju ED, Bearman PW, Graham JMR. (1988) A study of forces, circulation and vortex around a circular cylinder in oscillating flow. *J. Fluid Mech.* 196:467–494.

[68] Orr, W.M.F. (1907) The stability or instability of the steady motions of a liquid. Part II: A Viscous Liquid. *Proceedings of Royal Irish Academy*, Vol. XXVII, section A, No. 3, 69-138.

[69] Ott, E.A, Grebogi, C. and Yorke, J.A. (1990) Controlling chaos, *Physics Review Letters*, Vol. 64, No. 11, pp. 1196.

[70] Pearson, K. (1901) On lines and planes of closest fit to systems of points in space. *Philosophical Magazine*, Vol. 2, pp. 559-572.

[71] Peric, M., and Ferziger, J.H. (1996) Computational methods for fluid dynamics. *Springer-Verlag.*

[72] Preisendorfer, R., (1988) Principal component analysis in meteorology and oceanography. *Elsevier, Amsterdam*

[73] Press W.H, Flannery B.P, Teukolsky S.A, Vetterling W.T. (1986) Numerical recipes. *Cambridge University Press*

[74] Price, W.G. and Tan, M. (1992) Fundamental viscous solutions or 'transient oseenlets' associated with a body manoeuvring in a viscous fluid. *Proc. Roy. Soc. Lond.* A438, pp. 447-466.

[75] Price WG, Tan M. (1992) The evaluation of steady fluid forces on single and multiple bodies in low speed flows using viscous boundary elements. In *Proc. Intl. Conf. on the Dynamics of Marine Vehicles and Structures in Waves, 1990* (ed. WG. Price, P. Temarel & AJ. Keane), *Elsevier, 125–133.*

[76] Ravindran, S.S. (1999) The proper orthogonal decomposition in optimal control of fluids. *NASA/TM-1999-209113*, March.

[77] Rayleigh, L. (1879) On the instability of jets. *Scientific Papers*, Vol. 1, Cambridge University Press 361-371.

[78] Rayleigh, L. (1880) On the stability or instability of certain fluid motions. *Proceedings of London Mathematical Society*, Vol. 11, 57-70.

[79] Rayleigh, L. (1887) On the stability or instability of certain fluid motions. *Proceedings of London Mathematical Society*, Vol. 19, 67-74.

[80] Reynolds, O. (1883) An experimental investigation of the circumstances which determine whether the motion of water shall be direct or sinuous, and of the law of resistance in parallel channels. *Philosophical Transactions Royal Society London series A*, Vol. 174, 935-982.

[81] Sarpkaya T (1986) Force on a circular cylinder in viscous oscillatory flows at low Keulegan-Carpenter numbers. *J. Fluid Mech.* 165:61–71.

[82] Sarpkaya T. (1976) Vortex shedding and resistance in harmonic flow about smooth and rough cylinders at high Reynolds number. *Report No. NPS-59SL76021, Naval Postgraduate School, Monterey, California, U.S.A. 1976.*

[83] Sarpkaya T, Isaacson M. (1981) Mechanics of wave forces on offshore structures. *Van Nostrand Reinhold.*

[84] Schlicthing, H. (1932) Concerning the origin of turbulence in a rotating cylinder. *Math.-Phys. Klasse*, no.2, pp. 160-198.

[85] Schubauer, G.B. and Skramstad, H.K. (1947) Laminar boundary layer oscillations and stability of laminar flow. *Journal of Aeronautical Science*, Vol. 14, No. 2, 69-78.

[86] Sirovich, L. (1987) Turbulence and the dynamics of coherent structures. Parts I-III. *Quarterly of Applied Mathematics*, Vol. XLV, No. 3, Oct., pp. 561-590.

[87] Smith, A.M.O., (1955) On the growth of Taylor-Gortler vortices along highly concave walls. *Quarterly Applied Mathematics*, Vol. XXII, No. 3, 233-262.

[88] Smith PA, Stansby PK. (1991) Viscous oscillatory flow around cylindrical bodies at low Keulegan–Carpenter numbers using vortex methods. *J. Fluids Struct.* 5:339–361.

[89] Sommerfeld, A. (1908) Ein beitrag zur Hydrodynamischen Erklaerung der turbulenten fluessigkeits bewegungen. *Atti Int.Congress of Math.*, Vol.3, 116-124, 1908.

[90] Squire, H.B. (1933) On the stability for three-dimensional disturbances of viscous fluid flow between paralel walls. *Proceedings of Royal Society of London Series A*, Vol. CXLII, 621-628.

[91] Stiefel EL. (1963) An introduction to numerical mathematics. *Academic Press*

[92] Stokes GG. (1852) On the effect of the internal friction of fluids on the motion of pendulum. *Trans. Camb. Phil. Soc.* 9:8–106.

[93] Tan M. (1994) A Viscous boundary element approach to fluid flow-structure interaction problems. PhD thesis, University of Southampton.

[94] Tan, M., Farrant, T. and Price, W. G. (1999) A cell boundary element method for viscous laminar flow solutions. *Proc. Roy. Soc. Lond.* A455, pp. 4277-4304.

[95] Tan, M., Uzunoğlu, B. and Price, W.G. (2000) Reduced models for statistically stationary and nonstationary flows. *AIAA*, Nr. 2000-2558, 2000.

[96] Tatsuno M, Bearman PW. (1990) A visual study of the flow around an oscillating circular cylinder at low Keulegan–Carpenter numbers and low Stokes numbers. *J. Fluid Mech.* 211:157–182.

[97] Tollmien, W. (1929) Uber die entstehung der turbulenz. *Math.-Phys. KL.*

[98] Tosaka, N. and Kakuda, K.(1988) The generalized boundary element method for nonlinear problems. Boundary Elements X. Proceedings of the 10th International Cinference Boundary Element Methods, Southampton. *Computational Mechanics Publications.*

[99] Tritton, D.J., (1988) Physical fluid dynamics *Oxford University Press, Oxford*

[100] Uzunoğlu, B., Tan, M. and Price, W.G. (1999) Oscillating circular cylinders' force coefficients determined by a cell viscous boundary element method. *Proc. BEM-XXI, Oxford, UK*, Vol. 6, Ch. 70, 1999, pp. 443-452.

[101] Uzunoğlu, B., Tan, M. and Price, W.G. (2001) Low-Reynolds-number flow around an oscillating circular cylinder using a viscous cell boundary element method. *International Journal for Numerical Methods in Engineering* Vol.50, pp. 2317-2338.

[102] Uzunoğlu, B., Nair, P.B., Price, W.G., Rogers, E. (2001) Optimal flow control using trust-region augmented variable-fidelity modeling. (To appear).

[103] Villemagne, C. and Skelton, R. (1988) Model reductions using a projection formulation. *International Journal of Control*, Vol. 46, 2141-2169

[104] Wang C.Y. (1968) On high-frequency oscillatory viscous flows. *J. Fluid Mech.* 32:55–68.

[105] Wang CY, Dalton C. (1991) Oscillating flow past a rigid circular cylinder: A finite difference calculation. *Trans. ASME J: J. Fluids Engng*; 113:377–383.

[106] Williams, D.R. and Amoto C.W. Unsteady pulsing of cylinder wakes. *in Frontiers in Experimental Fluid Mechanics, Lectures Notes in Engineering* , Vol. 46, 337-364, Springer-Verlag, Berlin.

[107] Williamson, C.H.K. (1988) Defining a universal and continuous Strouhal-Reynolds number relationship for the laminar vortex shedding of a circular cylinder. *Phys. Fluids*, Vol. 31, No. 10, Oct., pp. 2742-2744

[108] Williamson C.H.K. (1985) Sinusoidal flow relative to circular cylinders. *J. Fluid Mech.* 155:141–174.

[109] Williamson CHK. (1991) 2-D and 3-D aspects of the wake of a cylinder, and their relation to wake computations. *Lectures in Applied Mathematics* 28:719–751.

[110] Wise, K.D. (1991) Integrated microelectromechanical systems: a perspective on MEMS in the 90s. *Proc 1991 IEEE MEMS Workshop 33-38*

[111] Wortmann, F.X. (1969) Visualization of transition. *Journal of Fluid Mechanics*, Vol. 38, Pt. 3, 473-480.

[112] Zhang H.L, Zhang X. (1997) Flow structure analysis around an oscillating circular cylinder at low KC number: a numerical study. *Computers and Fluids* 26:83–106.

[113] Zhou, K., Doyle, J.C. and Glover, K. (1996) Robust and optimal Control. *Prentice Hall*

[114] Zienkiewicz OC. (1977) The finite element method. *Mc Graw-Hill*